Numerical study for some nonlinear differential systems

By

Mair Khan

Supervised By

Prof. Dr. Muhammad Yousaf Malik

Department of Mathematics
Quaid-I-Azam University
Islamabad, Pakistan
2020

Numerical study for some nonlinear differential systems

By

Mair Khan

Supervised By

Prof. Dr. Muhammad Yousaf Malik

Department of Mathematics
Quaid-I-Azam University
Islamabad, Pakistan
2020

Numerical study for some nonlinear differential systems

By

Mair Khan

A THESIS SUBMITTED IN THE PARTIAL FULFILLMENT OF THE REQUIREMENT FOR

THE DEGREE OF

DOCTOR OF PHILOSOPHY

IN

MATHEMATICS

Supervised By

Prof. Dr. Muhammad Yousaf Malik

Department of Mathematics
Quaid-I-Azam University
Islamabad, Pakistan
2020

Author's Declaration

I, **_Mair Khan_**, hereby state that my PhD thesis titled **_Numerical study for some nonlinear differential systems_** is my own work and has not been submitted previously by me for taking any degree from Quaid-I-Azam University Islamabad, Pakistan or anywhere else in country/world.

At any time, if my statement is found to be incorrect even after my graduation the university has the right to withdraw my PhD degree.
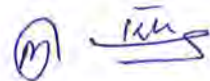
Name of student: Mair Khan

Dated: 17/ 02/ 2020

Plagiarism Undertaking

I solemnly declare that research work presented in the thesis titled "***Numerical study for some nonlinear differential systems***" is solely my research work with no significant contribution from any other person. Small contribution/help wherever taken has been duly acknowledged and that complete thesis has been written by me.

I understand the zero-tolerance policy of the HEC and Quaid-i-Azam University towards plagiarism. Therefore, I as an Author of the above titled thesis declare that no portion of my thesis has been plagiarized and any material used as reference is properly referred/cited.

I undertake that if I am found guilty of any formal plagiarism in the above titled thesis even afterward of PhD degree, the University reserves the rights to withdraw/revoke my PhD degree and that HEC and the University has the right to publish my name on the HEC/University Website on which names of students are placed who submitted plagiarized thesis.

Student/Author Signature

Name: Mair Khan

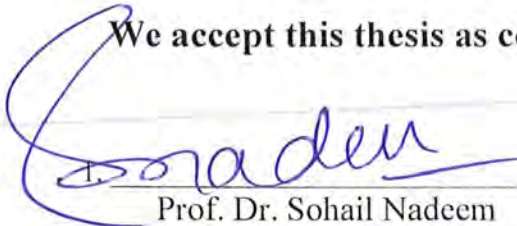# Numerical study for some nonlinear differential systems
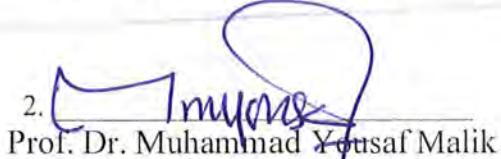
By

Mair Khan

CERTIFICATE

A THESIS SUBMITTED IN THE PARTIAL FULFILLMENT OF THE
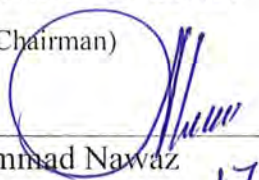REQUIREMENTS FOR THE DEGREE OF THE DOCTOR OF
PHILOSOPHY

We accept this thesis as conforming to the required standard

1. _____
Prof. Dr. Sohail Nadeem
(Chairman)

2. _____
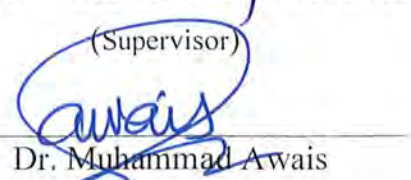Prof. Dr. Muhammad Yousaf Malik
(Supervisor)

3. _____
Dr. Muhammad Nawaz   17-02-2020

Department of Applied Mathematics
and Statistics Institute of Space
Technology Near Rawat Tool Plaza,
Islamabad.
(External Examiner)

4. _____
Dr. Muhammad Awais

Department of Mathematics
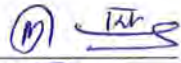COMSATS University
Islamabad, Attock
Campus.
(External Examiner)

Department of Mathematics
Quaid-I-Azam University
Islamabad, Pakistan
2020

Certificate of Approval

This is to certify that the research work presented in this thesis entitled ***Numerical study for some nonlinear differential systems*** was conducted by ***Mr. Mair Khan*** under the kind supervision of ***Prof. Dr. Muhammad Yousaf Malik***. No part of this thesis has been submitted anywhere else for any other degree. This thesis is submitted to the Department of Mathematics, Quaid-i-Azam University, Islamabad in partial fulfillment of the requirements for the degree of Doctor of Philosophy in field of Mathematics from Department of Mathematics, Quaid-I-Azam University Islamabad, Pakistan.

Student Name: **Mair Khan**   Signature:_____

External committee:

a) **External Examiner 1**:   Signature:_____

    Name: **Dr. Muhammad Nawaz**

    Designation: Associate Professor

    Office Address: Department of Mathematics and Statistics Institute of Space Technology (IST), Near Rawat Toll Plaza, Islamabad.
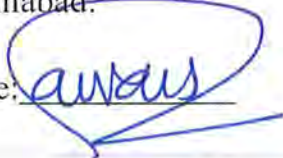
b) **External Examiner 2**:   Signature:_____

    Name: **Dr. Muhammad Awais**

    Designation: Assistant Professor

    Office Address: Department of Mathematics COMSATS University Islamabad Attock Campus.

c) **Internal Examiner**   Signature:_____

    Name: **Prof. Dr. Muhammad Yousaf Malik**

    Designation: Professor

    Office Address: Department of Mathematics, QAU Islamabad.

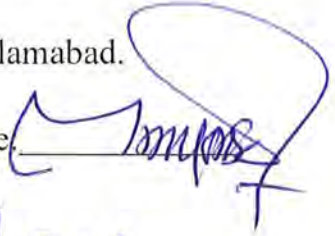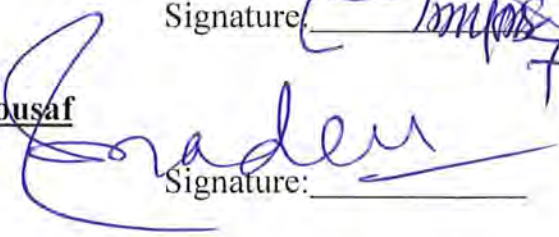**Supervisor Name:**   Signature:_____

Prof. Dr. Muhammad Malik Yousaf

Name of Dean/ HOD   Signature:_____
Prof. Dr. Sohail Nadeem

This thesis is dedicated to my grandfather

Khan Shir

And

my uncle

M. Karnial

Acknowledgments

Frist and foremost I would like to thank Professor Muhammad Yousaf Malik for his advice, guidance and the namouras opportunities he has afforded me. I am indebted to him for his willingness to take me on as a Ph.D. student. I must also thank Dr. Taimoor Salahuddin for the excellent guidance I received during the initial stages of my studies. I also say thanks my IRSP supervisor Professor Sharon Stephen for his guidance and expertise to prolong my research at foreign institute and his love care during my stay at Australia.   Additionally, I would like to acknowledge my senior lap fellows Dr. Farzana, Dr. Balil, Dr. Arif Hussain, Dr. Awias, Dr. Imad, Dr. Khalil, for the many useful discussion relating to this work, secondly, Dr. Nasser, Dr. Usman without his suggestions large part of this thesis my never have materialized, thirdly I would also thanks my teachers thought me able to overcome all the challenges, particularly Professor M. Ayub, Professor Tasawar Hayat, Professor Masood Khan and Professor Sohail Nadeem fourthly Dr. Ijaz Khan, Dr. Waleed, Dr. Fasial Shah, Salman, Dr. Waqas, Dr. Shahid, Dr. Nadeem, Dr. Masood, Nasir Jamal, Noor Shad Ali, Waheed Orakzai, Dr. Manzoor, Dr. Amir, Dr. Zeeshan, Safadar, for guiding me towards a my life career in academia.

I am extremely grateful for the continued support of my parents, brother, cousin and uncle, without which I wouldn't be in the position I find myself now. Hajr I appreciated the important life lessons you have taught me, not forgetting to mention 'the only equations I will ever need'...

Buy Oranges (50 PKR) + Sell Oranges ($1) = Profit,

I have no doubt that remembering this will prove useful, especially in the unlikely event that I one day open a greengrocers.

Lastly, I would like to thank my partner Hajr without her my years as a Ph.D. student would not have been so enjoyable.

Abstract

The study of nonlinear fluid flows (having complex geometries) has many applications in industrial engineering e.g. construction of, paper production, polymer sheet, glass fabric, hot rolling and petroleum production. Focus of present study is on mathematical modelling for boundary layer flow having different geometries in a non-Newtonian viscosity model. This study involves four models namely (Carreau, Carreau-Yasuda, Williamson and Maxwell models). Our main concern will be the analysis of non-Newtonian fluids within the boundary layer. For fluids with share-rate dependent viscosity the base flow has no longer analytic solutions for the Naiver-Stoke equations. However, for a large value of Reynolds number the flow inside the boundary layer can be determined via a similarity solution. The solution of the modelled differential equations is computed by using moderate and well-known numerical technique namely shooting method. The different governing physical parameter are utilized to control the motion of fluid. Skin friction coefficient, Nusselt number and Sherwood number are calculated in order to examine the flow behavior near the surface of the sheet, rotating surface and disk. A comparison has been made with the previous published literature in order to check the accuracy of the method. Conclusion is drawn based on entire study.

This thesis comprises 9 chapters by including introduction as zero chapter. Research background and the objectives are stated at the end of this chapter.

Chapter 1 is dedicated to investigating the effects of variable viscosity on MHD Carreau nanofluid flow along a nonlinear stretching surface in the presence of thermal stratified medium. Generalized Fourier's and Fick's laws are used in order to examine the heat and mass transport phenomena. Near the surface of the plate mass flux is assumed to be zero. The contents of this paper are published in the **Journal of the Brazilian Society of Mechanical Sciences and Engineering. (2018) 40: 457. https://doi.org/10.1007/s40430-018-1371-6**.

Chapter 2 is devoted to acquiring non-similar solutions for the behavior of slip conditions on steady MHD Carreau-Yasuda fluid flow over a rotating disk. In order to examine the heat transfer phenomena superior form of Fourier's law is used and the conductivity of the fluid is assumed to be changeable. The contents of this chapter are published in **Journal of the Brazilian Society of Mechanical Sciences and Engineering, 412(2019):78**.

Chapter 3 deal with transient MHD Carreau-Yasuda nanofluid flow produced by impulsively started rotating disk in the occurrence of Darcy-Forchheimer and chemical reactive species considering conventional Fourier's and Fick's laws. The findings are accepted in **Canadian journal of Physics, 97(2019) 670-677.**

Variable viscosity and inclined Lorentz force effects on Williamson nanofluid over a stretching sheet with variable thickness is addressed in chapter 4. Variable viscosity is assumed to vary as a linear function of temperature. The contents of chapter 4 are published in **Results in Physics, 8(2018) 862-868.**

Chapter 5 is presented to elaborate the effects of temperature dependent viscosity and double stratification is also assumed by taking Williamson fluid model. The contents of this chapter are published in **International Journal of Heat and Mass Transfer, 126(2018) 941-948.**

Change in internal energy of thermal diffusion stagnation point Maxwell nanofluid flow along with solar radiation and thermal conductivity is discussed in chapter 6. After boundary layer approximation, the governing equations are achieved (namely Maxwell upper convected material derivative, thermal and concentration diffusions). The contents of this chapter are accepted in **Chinese Journal of Chemical Engineering, (2019) doi.org/10.1016/j.cjche.2018.12.023.**

Chapter 7 is written to analysis the behavior of transformed internal energy change in magnetohydrodynamic Maxwell nanofluid flow over a stretching sheet along with Arrhenius activation energy and chemical reaction. The contents this chapter are accepted in **European Physical Journal of Plus, (2019) 134: 198. doi.org/10.1140/epjp/i2019-12563-8.**

Chapter 8 addresses the heat and mass diffusion (Cattaeno-Christov model) upper convected Maxwell nanomaterials passed by a linear stretched surface (slip surface) near the stagnation point region. Improved form of Fourier's and Fick's laws are employed to investigate heat and mass diffusion phenomena. The contents of this chapter are accepted in **Journal of the Brazilian Society of Mechanical Sciences and Engineering, (2019) 41: 138. doi.org/10.1007/s40430-019-1620-3.**

Nomenclature

List of symbols	
$\mathbf{V}$	Velocity field
$\mathbf{S}$	extra stress tensor
τ	Cauchy stress tensor
u, v, w	velocity component
x, y, z	space coordinates
r, θ, z	cylindrical space coordinates
u_r, v_θ, w_z	cylindrical space coordinates
$\mathbf{q}_r$	radiative heat flux
$\mathbf{j}$	mass flux
ρ_f	density of liquid
p	pressure
I	identity tensor
C_p	specific heat
τ	heat capacity ratio
$(\rho c)_p$	effective heat capacity of nanoparticles
$(\rho c)_f$	heat capacity of fluid
D_B	Brownian diffusion coefficient
D_T	thermophoresis diffusion coefficient
ρ	density

m	Stretching index
Γ	time constant
σ	electrical conductivity of the fluid
$\mu(T)$	temperature dependent viscosity
T_w	temperature at the wall
C_w	concentration at the wall
T	fluid temperature
C	fluid concentration
T_∞	free stream temperature
C_∞	free concentration
ξ	independent similarity variable
η	similarity variable
St	thermal stratification
Sc	solutal stratifications
Ha^2	Hartmann number
We^2	Weissenberg number
Pr	Prandtl number
N_b	Brownian mutation parameter
N_t	Thermophoresis parameter
ς	temperature dependent viscosity
ς_1	concentration dependent viscosity
δ_t	thermal buoyance
δ_c	concentration buoyancy
α	Wall thickness parameter

ψ	Stream function
ν	kinematic viscosity
μ	dynamic viscosity
a, b	constant
μ_0	zero shear rate viscosity
μ_∞	infinity shear rate viscosity
∇	differential operator
$\overset{o}{\gamma}$	second order invariant tensor
d	fluid parameter
k_f	thermal conductivity
∇T	temperature gradient
∇C	concentration gardened
$H_0(x)$	non-uniform magnetic field
H_0	magnetic field strength
λ_1	slip parameter
λ_2	tangential slip parameter
λ	porosity parameter
λ_m	fluid relaxation parameter
$K(T)$	temperature dependent thermal conductivity
ε	thermal conductivity parameter
Ω	angular velocity
K	chemical reaction parameter

Gr_x	Local Grashof number due to thermal
Gr_x^*	Local Grashof number due to counteraction
b_1	temperature dependent viscous parameter
b_2	temperature dependent thermal conductivity parameter
T_0	reference temperature
C_0	reference concentration
R	radiation parameter
Ec	Eckert number
$\mathbf{J}$	current density
q_r	heat flux
A	ratio parameter
k^o	absorption constant $\left(\frac{k^{-w}}{\sec}\right)$
k	8.61×10^{-5} Boltz-mann constant
α^o	Stefan Boltz-mann constant
Ea	activation energy
μ_e	magnetic permeability
$\mathbf{C}_f$	Skin friction coefficient
Nu	Nusselt number
Sh	Sherwood number
Re_x	Reynolds number
f	reduce stream function

F_c	inertia factor
γ	inclined angle
θ	dimensionless temperature
ϕ	dimensionless concentration
Le	Lewis number
n	power law index
τ_w	wall shear stress
q_w	heat surface flux
J_w	mass flux
β_C	mass diffusion
β_T	thermal diffusion
g	magnitude of the gravity
r	thermal propriety of fluid
δ	location of viscosity
θ_r	variable viscosity

Contents

Chapter 0

Introduction

0.1 Overview

This work pertains the theoretical and numerical study of nonlinear differential equations for Newtonian and non-Newtonian fluids. This chapter provides an overview of different physical aspects along with different fluid models.

0.2 Research background

The differential equations of non-Newtonian fluids are generally of higher order and difficult to solve. Since these are highly non-linear as compare to Navier-Stokes equations. The non-Newtonian power law viscosity model has some limitations, i.e. it cannot predict sufficient information about the viscosity at low or very high shear rates. To overcome this defficiency another viscosity model (for large and very small shear rates) was presented by Carreau [1]. Present model was very accurate to predict the pseudoplastic and dilatant characteristics of fluids by utilizing the different values of power law exponents. Due to its huge applications, the Carreau fluid model has got great interest of various investigators and engineers during the last few years. Bush and Phan-Thien [2] and Chhapra and Uhlherr [3] analyzed the flow of Carreau fluid on sphere. Vajravelu et al. [4] examined the peristatic flow of Carreau fluid in a non-uniform channel with heat and mass assignment. Akbar and Nadeem [5] discussed the blood flow study of Carreau fluid model in tapered artery with stenosis. Analytical results were

calculated for resistance impedance, velocity, shear stress and wall shear stress at the stenosis. The blood flow as Carreau fluid in a two dimensional straight tube was presented by Tabakova et al. [6]. Hayat et al. [7] studied the stagnation point flow for Carreau fluid persuaded by movement of stretching surface. The Carreau fluid model for different geometries and physical aspects was considered by many scholars (see refs. [8-10]).

Carreau-Yasuda model is well known rheological model utilized to approximate the steady viscosity in non-Newtonian models (named by Carreau-Yasuda [11]). This model predicts the shear thinning and thickening behavior. In present problems, usually it is assume that infinite shear rate viscosity is equal to zero. It is worth revealing here that this model is converted into Carreau fluid model when the value of the fluid parameter is taken as two and for time constant equals to zero or power law index equals to one. It will behave like Newtonian fluid. Pseudoplastic is a concept utilized to refer the viscosity reduction due to raise in deformation rate. It is attributed to the Caurreau Yasuda model proposed in literature [12-15]. Khechiba et al. [16] deliberated the effects of Carreau-Yasuda rheological parameters on free convection horizontal permeable cavity. Salahuddin et al. [17] discussed the numerical and theoretical study of free stream squeezed flow of Carreau Yasuda fluid flow due to a sensor surface under the magnetic field. Tanveer et al. [18] discussed the force and free convection for peristalses of Caurreu Yasuda nanofluid saturating by permeable space in cured channel. Khan et al. [19] scrutinized the significance of chemical reaction against hydromagnetic Carreau Yasuda nanofluid flow due to nonlinear stretching surface under the zero normal flux. Kefayati and Tang [20] discussed the thermosolutal free convection and entropy generation of non-Newtonian Caureau Yasuda fluid and solved the problem via Lattice Boltzmann technique.

Williamson fluid is one of the type of non-Newtonian fluids having pseudoplastic property. This model was introduce by Williamson [21]. Thin layer of the Williamson fluid due to inclined solid surface along with gravitational field was presented by Lyubimov and Perminov [22]. Nadeem et al. [23] considered the two dimensional flow of Williamson fluid flow due to a stretched surface. Kothandapani and Prakash [24] designated the theoretical examination of peristaltic flow of Williamson nanoliquid in tapered asymmetric channel under the action of solar radiation. The electro-osmotic flow of Williamson ionic nanofluid in occurrence of peristaltic propulsion was examined by Prakash and Tripathi [25]. Khan et al. [26] analyzed the change in

5

viscosity of Williamson fluid flow induced by a nonlinear stretching surface. Variable viscosity was assumed to be temperature dependent and due to stratified medium, variable viscosity also depends upon thermal diffusion. Lyubimove et al. [27] analyzed the linear polarized high frequency trembling on the quasi-equilibrium municipal stability of an infinite layer of Williamson fluid flow between two rigid parallel plates. Khan et al. [28] scrutinized the computational aspect of chemical response on Williamson nanofluid flow over a variable thicked surface.

The dynamics of material having characteristics of viscosity and elasticity when undertaken deformation is a fundamental area in fluid dynamics. This kind of fluid (Maxwell fluid) has gained attention of numerous researchers due to its number of industrial and technical applications. James Clerk Maxwell initiated Maxwell fluid in 1867 and the knowledge was familiarized by James Oldroyd few years later (see Christopher [29]). Adegbie et al. [30] scrutinized the numerical solution of Maxwell fluid induced by a stretching surface along with temperature dependent viscosity and thermal stratified medium. Mahsud et al. [31] investigated the unsteady two dimensional boundary layer flow of frictional derivative Maxwell fluid. Liu and Liu [32] investigated the boundary layer flow of upper convected fractional Maxwell fluid flow due to stretching surface with variable thickness. A numerical L1- technique was assumed to solve nonlinear differential system of the boundary values problem. Poungthong et al. [33] discussed the analytic solution for the comparative strength of mth harmonics Maxwell fluid flow. Khan et al. [34] illustrated the thermal diffusion stagnation point flow of Maxwell fluid over a linear stretching surface with solar radiation. Na et al. [35] presented the concept of finite element time domain Maxwell solver for the study of revolving geometries.

Fourier [36] verified the formula to visualize the mechanism of heat transference known as "Fourier's law of heat conduction". This clearly specifies that an initial disturbance would instantaneously affect the coordinated flow. Cattaneo [37] extended the Fourier relation of heat conduction by considering the additional parameter known as relaxation time. Christov [38] created amendment in Cattaneo theory by utilizing the time Oldroyd's upper convective time derivation formula. Khan et al. [39] scrutinized the inspection of boundary layer heat and mass transfer (Cattaneo-Christov model) due to inclined stretching surface under the magnetic field. Ibrahim et al. [40] numerically explored the boundary layer flow of a rotating Eyring-Powell nanofluid. Khan et al. [41] analyzed the problem of Cattaneo-Chirstov mass and heat flux

6

model along with thermal and solutal stratification on Carreau fluid flow due to a stretching surface under the variable viscosity effect.

The nanofluids consist of small particles of diameter sized from 1 to 100 nm and these particles include oxides, metals, non-metals and carbides (see [42]). The phenomenon of thermal conductivity improvement due to nanofluid has been presented by Masuda et al. [43]. Bia et al. [44] analyzed the stagnation point flow of the Maxwell nanofluid induced by a stretching surface under the convective boundary conditions. Viscous dissipation as well as thermal radiation in the Maxwell nanofluid flow was presented by Nayak [45]. Shen at al. [46] proposed a new mathematical model of heat diffusion MHD Maxwell nanofluid flow due to a vertical plate. Li et al. [47] numerically investigated the heat transfer characteristics of free convection in variable thermal nanofluid.

The word activation energy was firstly proposed by Swedish scientist Svante Arrhenius in 1889. Activation energy can also be presented as the smallest energy to create a chemical reaction. This energy is mostly convenient in the areas related to oil reservoir engineering, water emulsions and geothermal engineering. Boundary layer flow with chemical reaction was published by Bestman [48]. Awad et al. [49] designated the spectral relaxation method to solve the highly nonlinear coupled differential equations of unsteady rotating viscous fluids along with Arrhenius activation energy and binary chemical reaction. Hsiao [50] discussed the activation energy, viscous dissipation and free convention of a viscoelastic Carreau nanofluid flow near the stagnation point. Hamied et al. [51] exemplified the effects of activation energy and heat absorption on unsteady Williamson fluid flow produced by stretching cylinder in the presence of nanomaterials.

The behavior of fluid motion close to stagnation region of solid surface arises in both situations of fixed and movable body. The researchers have paid strong attention due to its several applications in industry like flows over a submarines and tips of aircraft. Hiemenz [52] firstly characterized the stagnation point flow of steady incompressible viscous fluid and subsequently initiated exact solutions. Homann [53] further improved this work [54] for axisymmetric case. Merkin and Pop [55] deliberated the stagnation point flow of stretching/shrinking surface with exothermic surface reaction. Mahapatra and Sidui [56] exemplified the unsteady non-axisymmetric stagnation point flow due to a stretching/shirking surface. Tuner and Wedman

7

[57] considered the problem of two impinging Howarth stagnation point regions.

Thermal conductivity and fluid viscosity were supposed to be constant throughout the boundary layer problems. Although, it is found that the physical characteristics of the fluid changes with temperature significantly . The intensifications of temperature leads to a local improve in the transport phenomena by decreasing the viscosity across the momentum boundary and so the heat transport rate at the wall is also affected. High shear rate leads to the high temperature that is produced within the fluid. Anyakoha [58] analysed that in fluid dynamics, the property in which temperature increases is thermal conductivity and viscosity presented. Xun et al. [59] obtained the numerical solutions of bioconvection rotating system between two rotating plates occupied by nanofluid with temperature dependent thermal conductivity and viscosity. Hayat et al. [60] discussed the thermal conductivity and temperature dependent viscosity in the force and free convention flow of viscous fluid over an exponentially stretching sheet with heat transport. Kameyama and Yamamoto [61] used the improved numerical experiments of thermal convention compressible fluid flow by systematically varying thermal conductivity and viscosity. The temperature dependent variables i.e. viscosity and thermal conductivity of graphene quantum dots nanometers were presented by Sedaghat and Yousefi [62]. Sunil et al. [63] discussed the couple stress fluid saturating permeable sheet with pressure and temperature dependent viscosity.

Stratification is an essential aspect in temperature and concentration diffusions and it has been analyzed by different researchers. It arises in flow field induced by temperature difference, concentration variation or fluid with different densities. Robert and Lackey [64] mathematically exemplified how to exclude thermal stratification in oceans through compressed air system. Sohut et al. [65] elaborated the double stratification influence of boundary layer flow towards a stretching cylinder with chemical reaction and heat generation. Daniel et al. [66] discussed the solar radiation and Joule heating impact on MHD nanofluid flow due to nonlinear stretching surface with thermal and solutal stratifications. Kandasamy et al. [67] deduced that thermal and solutal stratifications changes heat and mass diffusions induced due to nanomaterials over a permeable vertical plate.

Magnetohydrodynamic flow of an electrical conducting fluid generated by the deformation of wall surface are quite prominent and motivating in modern metal work and in metallurgy.

8

In addition, such kind of fluids are advented in industrial apparatus like MHD creator, cooling of nuclear reactor, gas turbines, petroleum industries, pumps, crystal growth, power generator, etc. Khan et al. [68] explored the numerical solution of the temperature dependent viscosity and inclined force impact on Williamson nanofluid flow due to stretching surface. Rana et al. [69] exemplified the analytical approach to examine the dual solutions of Jeffery fluid with Ohmic heating, magnetic field and viscous dissipation. Sheikhoeslami [70] designated the magnetic force on non-Newtonian nanofluid flow. Alamri et al. [71] illustrated the magnetohydrodynamic effect of heat transfer on second grade fluid flow associated with the mass transfer. Hosseini et al. [72] examined the entropy phenomena on MHD fluid flow with heat generation.

Viscous dissipation and solar radiation modification in temperature distribution play a significant role in many energy sources. The influence of viscous dissipation depends upon weather the plate is being heated or cooled. Many researchers examined heat transfer fluid flow over an expanded surface in the presence of solar radiation and viscous dissipation. Nayak [73] reported three dimensional MHD flow of heat transfer analysis along with solar radiation as well as viscous dissipation over a shirking sheet. Pandey and Kumar [74] illustrated the solar radiation on MHD flow of Cu-water nanomaterials past a wedge along with viscous dissipation and chemical reaction. The solar radiation and viscous dissipation effects on unsteady magnetodyrodynamic two dimensional boundary layer flow were presented by Devi and Kumari [75]. Kumar et al. [76] discussed the combine effects of thermal radiation and viscous dissipation on MHD three dimensional Oldroyd B nanoliquid.

0.3 Objectives

The objectives of this thesis are:

- to develop mathematical models representing different fluids flow.
- to solve the boundary layer related flow problems with different physical geometries.
- to compute these problems numerically by employing different numerical methods.

9

Chapter 1

An immediate change in viscosity of Carreau nanofluid due to double stratified medium: Application of Fouries's and Fick's Laws

This chapter extends the effect of variable viscosity and thermal diffusion on MHD Carreau nanofluid flow along a nonlinear stretching surface in the presence of thermal stratified medium. Generalized Fourier's and Fick's laws are used in order to examine the heat and mass transport phenomena. Near the surface of the plate, mass flux is assumed to be zero. The governing boundary layer equations are modelled and renovated into nonlinear ODE's by using similarity transformation and numerical solution is calculated via shooting method (coefficients upgraded by Cash and Carp). Plots and tables representing friction factor, velocity distribution, temperature and concentration distributions are discussed. Conclusions are made on the basis of entire examinations and it is found that the velocity profile enhances on enhancing values of Weissenberg number and thermal buoyancy parameter while thermal buoyancy shows opposite behavior for temperature distribution. Moreover, concentration profile diminishes for enhancing values of solutal stratification parameter and concentration buoyancy parameter.

1.1 Mathematical analysis

1.1.1 Flow analysis

Consider a mathematical model for two dimensional boundary layer Carreau nanofluid flow over a continuously nonlinear stretching sheet with variable thickness. The velocity of stretched plate is denoted by $U_w = U_0(x+b)^{m-1}$, here m is the stretching index, b is the dimensionless constant and U_0 is reference stretching rate. Suppose that the thickness of sheet is $y = A(x+b)^{\frac{1-m}{2}}$. It is further assumed that $m \neq 1$, because for $m = 1$, the problem reduces to a flat sheet. Magnetic field of strength H_0 is applied normal to the sheet (as illustrated in Fig. 1.1).
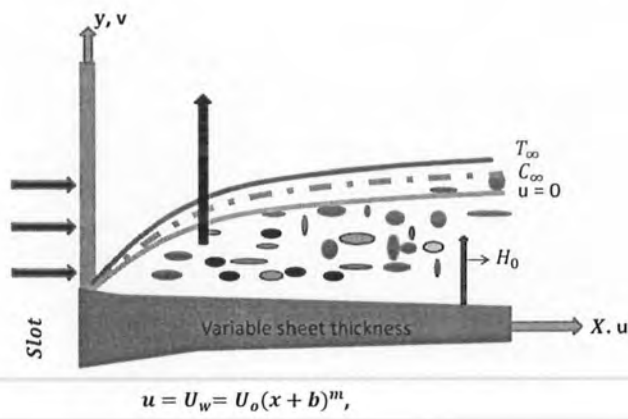

Fig. 1.1. Geometrical illustration of the model.

Under the above assumptions and boundary layer approximations the main governing equations (Carreau fluid model, energy and concentration) are given as:

Continuity Equation

$$\partial_x u + \partial_y v = 0. \tag{1.1}$$

Momentum Equation

$$u\partial_x u + v\partial_y u = \frac{1}{\rho}\partial_y \left[\mu(T) \left(\partial_y u + \Gamma^2 \frac{(n-1)}{2} (\partial_y u)^3 \right) \right] - u\frac{\sigma H_0^2}{\rho}. \tag{1.2}$$

11

Energy and Concentration equations

The Cattaneo-Christov model has been used to deliberate the impact of thermal and concentration diffusions as the relaxation mass and heat flux respectively. By using extended form of Fourier's and Fick's laws, the nanofluid equations take the following form:

$$\mathbf{q} + \lambda_T \left[\partial_t \mathbf{q} + \mathbf{V}.\left(\boldsymbol{\nabla}\mathbf{q}\right) - \mathbf{q}.\left(\boldsymbol{\nabla}\mathbf{V}\right) + \left(\boldsymbol{\nabla}.\mathbf{V}\right)\mathbf{q} \right] = -k_f \boldsymbol{\nabla} T, \tag{1.3}$$

$$\mathbf{J} + \lambda_c \left[\partial_t \mathbf{J} + \mathbf{V}.\left(\boldsymbol{\nabla}\mathbf{J}\right) - \mathbf{J}.\left(\boldsymbol{\nabla}\mathbf{V}\right) + \left(\boldsymbol{\nabla}.\mathbf{V}\right)\mathbf{J} \right] = -D_B \boldsymbol{\nabla} C. \tag{1.4}$$

If $\boldsymbol{\nabla}.\mathbf{q} = 0$, $\boldsymbol{\nabla}.\mathbf{J} = 0$; and for steady state model $\frac{\partial \mathbf{q}}{\partial t} = 0$, $\frac{\partial \mathbf{J}}{\partial t} = 0$. The new equations are:

$$\mathbf{q} + \lambda_T \left[\mathbf{V}.\boldsymbol{\nabla}\mathbf{q} - \mathbf{q}.\boldsymbol{\nabla}\mathbf{V} \right] = -k_f \boldsymbol{\nabla} T, \tag{1.5}$$

$$\mathbf{J} + \lambda_C \left[\mathbf{V}.\boldsymbol{\nabla}\mathbf{J} - \mathbf{q}.\boldsymbol{\nabla}\mathbf{J} \right] = -D_B \boldsymbol{\nabla} C. \tag{1.6}$$

For two dimensional flow, the energy and concentration eqs. (1.5) and (1.6) takes the following form

$$u\partial_x T + v\partial_y T + \lambda_T \left[\partial_x T \left(u\partial_x u + v\partial_y u\right) + \partial_y T \left(u\partial_x v + v\partial_y v\right) + u^2\partial_{xx}T + v^2\partial_{yy}T + 2uv\partial_{xy}T \right]$$
$$= \alpha\partial_{yy}T + \tau\left\{ D_B \left(\partial_y T \partial_y C\right) + \frac{D_T}{T\infty}\left(\partial_y T\right)^2 \right\}, \tag{1.7}$$

$$u\partial_x C + v\partial_y C + \lambda_C \left[\partial_x C \left(u\partial_x u + v\partial_y u\right) + \partial_y C \left(u\partial_x v + v\partial_y v\right) + u^2\partial_{xx}C + v^2\partial_{yy}C + 2uv\partial_{xy}C \right]$$
$$= D_B\partial_{yy}T + \frac{D_T}{T\infty}\partial_{yy}T. \tag{1.8}$$

The specified boundary conditions of the present problem takes the form

$$u(x,y) \quad = \quad U_w(x) = U_0(x+b)^m, \ v(x,y) = 0, \ T(x,y) = T_w \ , \ D_B \partial_y C + \frac{D_T}{T_\infty} \partial_y T = 0 \text{ at } y = A(x+b)^{\frac{1-m}{2}},$$

$$u(x,y) \quad \to \quad 0, \ T(x,y) \to T_\infty, \ C(x,y) \to C_\infty \text{ as } y \to \infty. \tag{1.9}$$

Here $(u,\ v)$ are the velocity components along the $(x,\ y)$ directions respectively, Γ is the time constant, ρ is the fluid density, U_0 is the stretching velocity rate, σ is the electrical conductivity of the fluid, $\mu(T)$ is the temperature dependent viscosity, $T_w(x,y)$ is known as temperature at the wall, $C_w(x,y)$ is known as ambient concentration at the wall, T and C are the temperature and concentration respectively, C_p is the specific heat, D_B is the mass diffusivity, T_∞ is the free temperature and D_T is known as thermophoresis diffusivity. In order to justify the variation in viscosity due to inside friction between fluid particles and the stretching surface, temperature dependent viscosity model used by Ajayi et al. [78] and [79] is implemented to sort out the problem.

$$\mu(T) = \mu_0[a_{1+}b_1(T_w - T)], \tag{1.10}$$

$$\Theta(\eta) = \frac{T - T_\infty}{T_w - T_0}, \quad \Phi(\eta) = \frac{C - C_\infty}{C_w - C_0}. \tag{1.11}$$

Due to double stratifications T_w and C_w take the form

$$\begin{aligned}
T_w &= T_0 + m_1(x+b)^{\frac{1-m}{2}}, \quad T_\infty = T_0 + m_2(x+b)^{\frac{1-m}{2}}, \\
C_w &= C_0 + m_3(x+b)^{\frac{1-m}{2}}, \quad C_\infty = C_0 + m_4(x+b)^{\frac{1-m}{2}}.
\end{aligned} \tag{1.12}$$

Using Eq. (1.12), Eq. (1.11) becomes

$$\begin{aligned}
T_w - T &= (1 - \Theta(\eta))(T_w - T_0) - m_2(x+b)^{\frac{1-m}{2}}, \\
C_w - C &= (1 - \Phi(\eta))(C_w - C_0) - m_4(x+b)^{\frac{1-m}{2}}.
\end{aligned} \tag{1.13}$$

From double stultifications, valid relation can easily be achieved as

13

$$b_1\left(T_w - T_0\right) = b_1 m_1 (x+b)^{\frac{1-m}{2}}, \quad b_1\left(T_\infty - T_0\right) = b_1 m_2 (x+b)^{\frac{1-m}{2}},$$

$$b_2\left(C_w - C_0\right) = b_2 m_3 (x+b)^{\frac{1-m}{2}}, \quad b_2\left(C_\infty - C_0\right) = b_2 m_4 (x+b)^{\frac{1-m}{2}}, \quad (1.14)$$

here T_0 and C_0 are known as reference temperature and concentration. A significant two differences in $(T_w - T_0)$, $(T_\infty - T_0)$, $(C_w - C_0)$ and $(C_\infty - C_0)$ can easily be calculated from above equations. In view of this, it is usable to define temperature dependent viscous parameter ξ by considering in Eq. (1.14). The ratio of the two terms in Eq. (1.14) produce the stratification parameters S_t and Sc.

$$b_1\left(T_w - T_0\right) = \zeta, \quad b_1\left(T_\infty - T_0\right) = \zeta S_t, \quad S_t = \frac{m_2}{m_1},$$

$$b_2\left(C_w - C_0\right) = \zeta_1 \quad b_2\left(C_\infty - C_0\right) = \zeta Sc, \quad Sc = \frac{m_4}{m_3}. \quad (1.15)$$

The similarity variable can be speculated in the following form

$$\eta = y\sqrt{\frac{(m+1)U_0}{2\nu}}(x+b)^{\frac{m-1}{2}}, \quad \psi = \left[\sqrt{\frac{2\nu U_0}{m+1}}F(\eta)\right](x+b)^{\frac{m-1}{2}},$$

$$u = U_0(x+b)^m F'(\eta), \quad v = -\left(\frac{(m+1)\nu U_0}{2}\right)^{\frac{1}{2}}\left[F(\eta) + \eta\frac{m-1}{m+1}F'\right](x+b)^{\frac{m-1}{2}}. \quad (1.16)$$

Eq. (1.1) is identically satisfied. After substituting Eq. (1.16) into (1.2), (1.7) and (1.8) one can obtain the following system of nonlinear differential equations:

$$(a+\zeta-\zeta\Theta-S_t\zeta)\left(1+3\frac{(n-1)}{2}We^2F''\right)F''' - \frac{2m}{m+1}\left(F'\right)^2 - \zeta\left(1+We^2\frac{(n-1)}{2}\left(F''\right)^2\right)\Theta'F''$$

$$+F'F'' - \frac{2Ha^2}{m+1}F' = 0, \quad (1.17)$$

14

$$\Theta'' + \Pr\left[\left(N_b\Phi'\Theta' + \Theta'F(\eta) + N_t(\Theta')^2\right) + \delta t\left(\frac{(n-3)}{2}F'F(\eta) - \frac{(n-1)}{2}F^2(\eta)\Theta''\right)\right]$$

$$-\Pr\left(\frac{1-m}{1+m}\right)F'S_t = 0, \tag{1.18}$$

$$\Phi'' + \frac{N_t}{N_b}\Theta'' + \Pr\left[Le\Phi'F(\eta) - Le\left(\frac{1-m}{1+m}\right)F'Sc + \delta c\left(\frac{(n-3)}{2}F'F(\eta) - \frac{(n-1)}{2}F^2(\eta)\Phi''\right)\right] = 0. \tag{1.19}$$

Using (1.16), the associated boundary conditions are

$$
\begin{aligned}
F' &= 1,\ F(\alpha) = \frac{(m-1)}{(1+m)}\alpha,\ \Theta(\alpha) = 1,\ N_b\Phi' + N_t\Theta' = 0,\ \text{at } \eta = \alpha,\\
F' &\to 0,\ \Theta \to 0,\ \Phi \to 0,\ \text{as } \eta = \alpha \to \infty.
\end{aligned} \tag{1.20}
$$

Here wall thickness parameter $\alpha = A\sqrt{\left(\frac{U_0(m+1)}{2v}\right)}$. In order to transform the required equations and Neumann boundary conditions, define $F(\eta) = f(\xi - \alpha) = f(\xi)$, $\theta(\xi) = \theta(\xi - \alpha) = \Theta(\eta)$ and $\phi(\xi) = \phi(\xi - \alpha) = \Phi(\eta)$ which gives

$$(a + \zeta - \zeta\theta - S_t\zeta)\left(1 + 3\frac{(n-1)}{2}We^2f''\right)f''' - \frac{2m}{m+1}\left(f'\right)^2 - \xi\left(1 + We^2\frac{(n-1)}{2}\left(f''\right)^2\right)\theta'f''$$

$$+ f'f'' - \frac{2Ha^2}{m+1}f' = 0, \tag{1.21}$$

15

$$\theta'' + \Pr\left[N_b\phi'\theta' + \theta'f(\eta) + N_t\left(\theta'\right)^2 + \delta t\left(\frac{(n-3)}{2}f'f(\eta) - \frac{(n-1)}{2}f^2(\eta)\theta''\right)\right]$$

$$-\Pr\left(\frac{1-m}{1+m}\right)f'St = 0, \tag{1.22}$$

$$\phi'' + \frac{N_t}{N_b}\theta'' + \Pr\left[Le\phi'f(\eta) - Le\left(\frac{1-m}{1+m}\right)f'Sc + \delta c\left(\frac{(n-3)}{2}f'f(\eta) - \frac{(n-1)}{2}f^2(\eta)\phi''\right)\right] = 0, \tag{1.23}$$

$$\begin{aligned}
f(\eta) &= \frac{\alpha(m-1)}{(1+m)}, \ f' = 1, \ \theta(\eta) = 1, \ N_b\phi' + N_t\theta' = 0, \ \text{at } \eta = 0, \\
f' &\to 0, \ \theta \to 0, \ \phi \to 0 \text{ as } \eta = \infty,
\end{aligned} \tag{1.24}$$

where $\zeta = b_1\left(T_w - T_0\right)$ is temperature dependent viscosity, $\zeta_1 = b_2\left(C_w(x, y) - C_0\right)$ concentration dependent viscosity, $St = \frac{m_2}{m_1}$ is thermal stratification, $Sc = \frac{m_4}{m_3}$ is solutal stratification parameter, $Ha^2 = \frac{\sigma H_0^2}{\rho U_0(x+b)^{m-1}}$ is Hartmann number, $\delta_c = \lambda_c U_0(x+b)^{m-1}$ concentration buoyancy parameter, $We^2 = \sqrt{\frac{(m+1)U_o^3(x+b)^{3m-1}}{2\nu}}$ is Weissenberg number, $\Pr = \frac{\mu c_p}{k}$ is Prandtl number, $\delta_t = \lambda_t U_0(x+b)^{m-1}$ thermal buoyancy parameter, $N_t = \frac{\tau D_t(T_w - T_0)}{T_\infty \nu}$ is thermophoresis parameter, $Le = \frac{\nu}{D_B}$ is Lewis number and $N_b = \frac{\tau D_B(C_w - C_0)}{\nu}$ is Brownian motion parameter.

1.1.2 Physical quantity of interest

Physical quantity near the wall i.e the friction factor coefficient (C_f) is defined via the following relation:

$$C_f = \frac{\tau_w}{\rho\sqrt{\frac{m+1}{2}}}, \tag{1.25}$$

here τ_w denotes the shear stress which is defined as:

$$\tau_w = \mu \left[\partial_y u + \frac{\Gamma^2(n-1)}{2} (\partial_y u)^3 \right]_{y=A(x+b)^{\frac{1-m}{2}}} . \tag{1.26}$$

The dimensionless fraction factor coefficient (C_f) is given by

$$C_f \left(\frac{\text{Re}_x^{\frac{1}{2}}}{2} \right) = \sqrt{\frac{(m+1)}{2}} (a + \xi - \xi\theta - S_t\xi) \left[f'' + \left(\frac{n-1}{2} \right) We^2 (f'')^3 \right]_{\xi=0}, \tag{1.27}$$

where $Re_x = \sqrt{\frac{U_0(x+b)^{m-1}}{\nu}}$ denotes local Reynolds number.

1.2 Numerical Procedure

In this section, an effective computational scheme Runge-Kutta Fehlberg method has been implemented to calculate the solution of eqs. (1.21)-(1.23) subject to the Neumann boundary conditions (1.24). The differential equations are of 3rd order in $f(\xi)$, 2nd order in $\theta(\xi)$ and $\phi(\xi)$. First converte into a system of simultaneous first order ordinary differential equations. In order to solve this system by utilizing Runge-Kutta Fehlberg method, we need three more missed initial conditions. However, the values of $f'(\xi)$, $\theta(\xi)$ and $\phi(\xi)$ are known when $\xi \to \infty$. These end conditions are utilized in order to achieve unknown initial conditions at $\xi = 0$. The most important step of this technique is to choose the suitable finite values far field boundary conditions. The convergent criteria and step size are taken to be 0.00001 and 10^{-6} respectively.

1.3 Results and discussion

Shooting technique is used to solve the ODEs for Carreau nanofluid over a nonlinear stretching sheet by using Cattaneo-Christov heat and mass flux models. The related physical parameters like wall thickness parameter, temperature dependent fluid dynamic viscosity, power law index, Weissenberg number, Prandtl number, Brownian motion, Hartmann number, Lewis number, thermal stratification parameter, thermophoretic parameter, solutal concentration parameter and stretching index parameter are computationally deliberated in this section. Fig. 1.2 depicts the vibration in Hartman number Ha^2 on horizontal velocity profile. It is obvious that by

17

enhancing the vertical velocity profile, reduction near the wall and quickly intensifications close to the stretching sheet is noticed. Lorentz force which acts as a retarding force tends to increase the frictional resistance that causes decrease in boundary layer thickness. In case of variable thickness, the momentum boundary layer rises. Fig. 1.3 illustrates the variations in wall thickness parameter α on vertical velocity profile for $m > 1$ and $m < 1$. It is clear that the velocity close to plate increases as thickness parameter α increases for $m < 1$ and reverse behavior is noticed for $m > 1$. Also, increase in wall thickness α causes increase in thermal boundary layer. Fig. 1.4 shows the variation in horizontal velocity profile for different values of temperature dependent plastic dynamic viscosity ξ. It is obvious that for large values of ξ, transverse vertical velocity profile close to free stream and the horizontal velocity distribution near the surface increases. Fig. 1.5 designates the physical behavior of power law index (nonlinearity index) n on velocity profile. Large values of power law index n results an intensification in vertical velocity profile. In this case the flow moves away from the stretchable surface in the velocity field. Fig. 1.6 is designed to demonstrates the impact of Weissenberg number We^2 on vertical velocity profile. This graph obviously shows that for shear thickening fluid, velocity profile rises monotonically with improved values of Weissenberg number We^2.
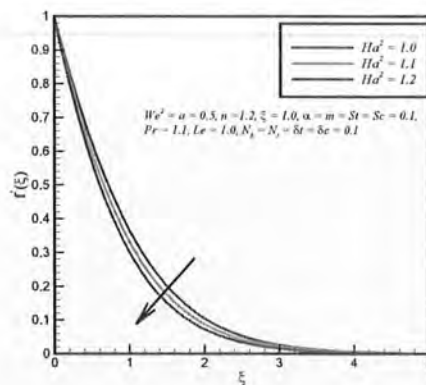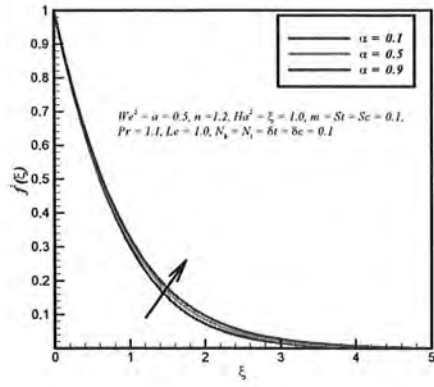

Fig. 1.2. Influence of Ha^2 on $f'(\xi)$.

18

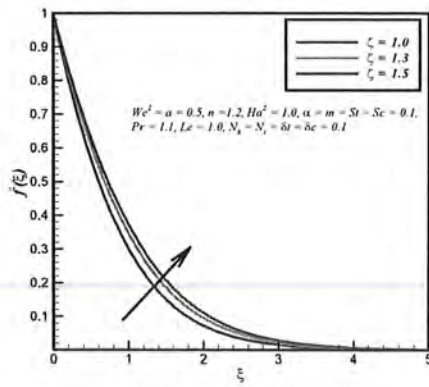Fig. 1.3. Influence of α on $f'(\xi)$.

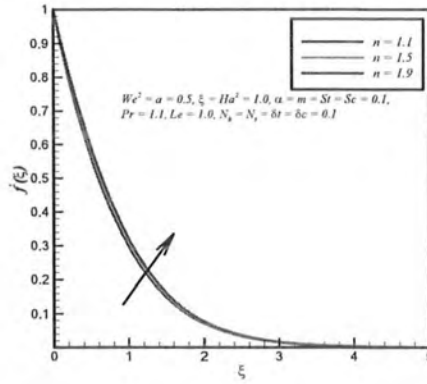Fig. 1.4. Influence of ζ on $f'(\xi)$.

19

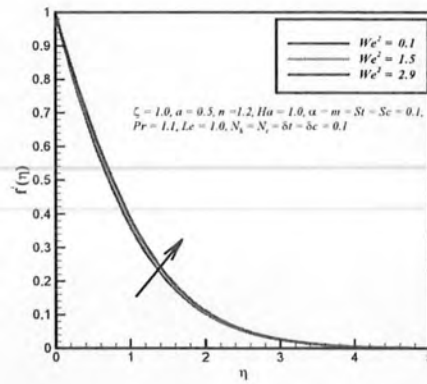Fig. 1.5. Influence of n on $f'(\xi)$.

Fig. 1.6. Influence of We^2 on $f'(\xi)$.

In Fig. 1.7 depicts the variation in Prandtl number Pr on temperature profile. The graph shows that by increasing Pr the thermal boundary layer thickness becomes greater than boundary layer thickness. Figs. 1.8 and 1.9 are plotted to observe the behavior of Brownian motion N_b and thermophoresis N_t on temperature profile. It is seen that for large values of N_b and N_t the temperature distribution increases i.e. strong Brownian motion N_b and thermophoretic N_t diffusion leads to intensification in temperature. Fig. 1.10 is plotted to scrutinize the

20

variations in temperature field for various values of thermal stratifications St. The convective potential that coincides with nonlinear stretching sheet and temperature profile that reduces by enhancing St. In view of this, both thermal boundary layer thickness and temperature profile decreases for large values of St. Fig. 1.11 shows that for large values of δt temperature profile reduces. Physically, for large values of δt, particles reflect non-conducting act i.e. particles need additional time to transfer heat which responses with decrease in temperature profile. It is noticed that the temperature diminishes for large values of δt, so the viscosity of the fluid slightly enhances.
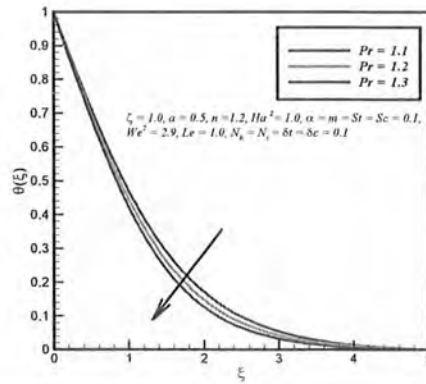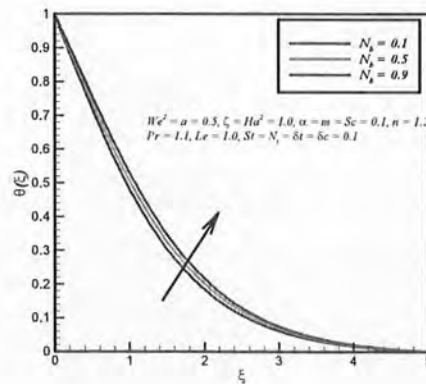

Fig. 1.7. Influence of Pr on $\theta\left(\xi\right)$.
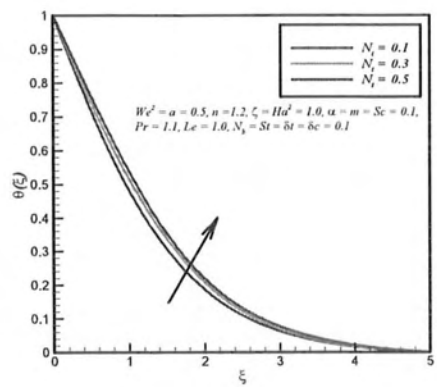

Fig. 1.8. Influence of N_b on $\theta\left(\xi\right)$.

21

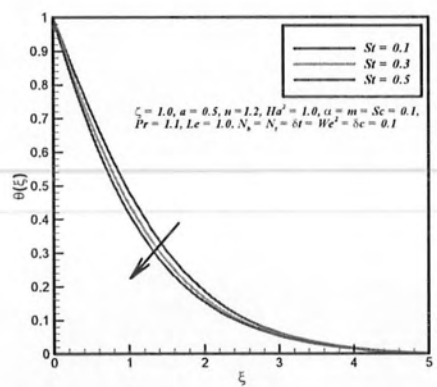Fig. 1.9. Influence of N_t on $\theta(\xi)$.

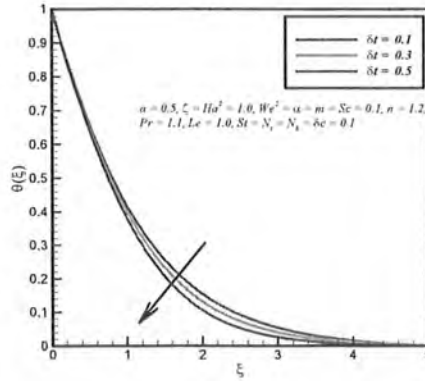Fig. 1.10. Influence of δ_t on $\theta(\xi)$.

22

Fig. 1.11. Influence of δt on $\theta(\xi)$.

In Fig. 1.12 shows that the nanoparticle concentration profile decreases significantly for large values of Lewis number Le. Enhanced values of Lewis number Le reduces Brownian motion diffusion coefficient. The concentration profile enhances for large values of Lewis number Le. Fig. 1.13 examines the variation in solutal stratification parameter Sc on concentration profile. It is noticed that concentration decreases with an increase in solutal stratification parameter Sc. Fig. 1.14 examines the variation of δc on concentration profile. Higher disturbance is observed for $\delta c = 0.0$. Fig. 1.15 shows the variation of Ha^2 and We^2 on $C_f \, \mathrm{Re}_x^{\frac{1}{2}}$. For large values of Hartmann number Ha^2, $C_f \, \mathrm{Re}_x^{\frac{1}{2}}$ increases. **Table 1.1** displays the variation of friction factor in tabulated form for unlike values Hartmann number, thermal stratification parameter, temperature dependent viscosity and Weissenberg number. Comparison of present results with pervious literature of Acharya et al. [80] and Khan and Pop [81] has been shown in **Table 1.2.**
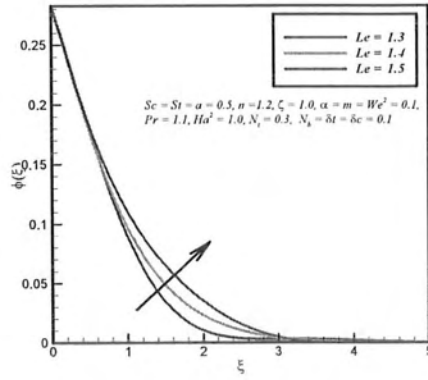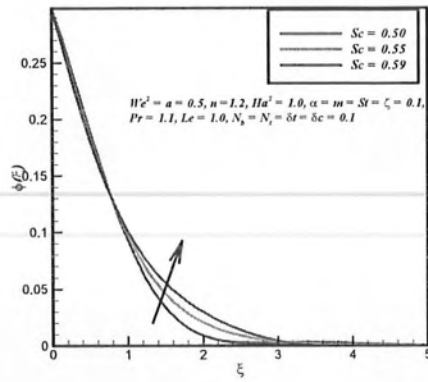
23

Fig. 1.12. Influence of Le on $\phi(\xi)$.

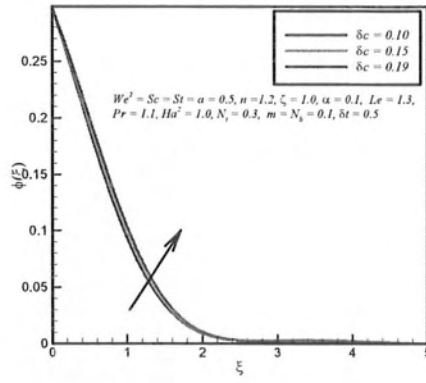

Fig. 1.13. Influence of Sc on $\phi(\xi)$.
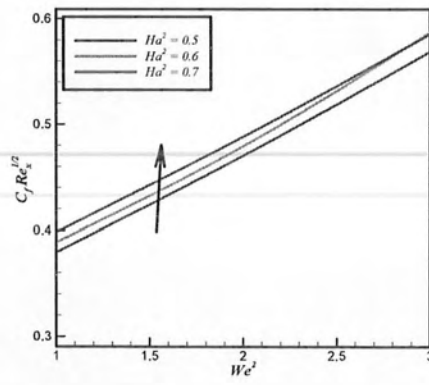
24

Fig. 1.14. Influence of δc on $\phi(\xi)$.

Fig. 1.15. Skin friction coefficient for various values of We^2 and Ha^2.

25

Table 1.1. Computational results of $C_f \operatorname{Re}_x^{\frac{-1}{2}}$ for different values of Ha^2, ζ, St and We^2 When $a = 0.5$, $m = 0.1$, $n = 1.2$ and $\alpha = 0.9$.

Ha^2	ζ	St	We^2	$C_f \operatorname{Re}_x^{\frac{-1}{2}}$
0.1	1.0	1.2	0.5	1.8811
0.2				2.1020
0.3				2.3199
0.1	1.0	1.2	0.5	1.8811
	1.1			1.7860
	1.2			1.6988
0.1	1.0	1.2	0.5	1.8811
		1.3		1.9001
		1.4		1.9200
0.1	1.0	1.2	0.5	1.8811
			0.6	1.8886
			0.7	1.8963

Table 1.2. Comparison of $-\theta'(0)$ and $-\phi'(0)$ with pervious literature when $We^2 = \xi = 0.5$, $\alpha = m = N_b = N_t = St = 0.1$, $\delta t = \delta c = 0.0$. and $Le = \Pr = 1.0$.

N_t	Acharyaa et al. [80] $-\theta'(0)$	Acharyaa et al. [80] $-\phi'(0)$	Khan et al. [81] $-\theta'(0)$	Khan et al. [81] $-\phi'(0)$	Present results $-\theta'(0)$	Present results $-\phi'(0)$
0.1	0.952432	2.129474	0.9524	2.1294	0.9527	2.1296
0.2	0.693211	2.273201	0.6932	2.2732	0.6928	2.1786
0.3	0.520147	2.528633	0.5201	2.5286	0.5221	2.5286
0.4	0.402631	2.795216	0.4026	2.7952	0.4031	2.7887
0.5	0.321149	3.035100	0.3211	3.0351	0.3529	3.0363

26

Chapter 2

Impact of enhancing diffusion on Carreau-Yasuda fluid flow over a rotating disk with slip conditions

A non-similar solutions to study the behavior of slip conditions for a steady MHD Carreau-Yasuda fluid flow over a rotating disk are presented in this chapter. In order to examine the heat transfer phenomena superior form of Fourier's law is used and the conductivity of the fluid is assumed to be changeable. The non-linear partial differential equations representing fluid flow and the related thermal field are written in the non-dimensional ordinary differential form by using suitable transformations. The non-dimensional set of coupled ordinary differential equations is solved through RK method. The impact of various nondimensional physical parameters on velocity and temperature fields is explored. The numerical results of resistant force in terms of the skin friction coefficient are revealed graphically for various physical parameters involved in the model.

2.1 Mathematical formulation

2.1.1 Flow analysis

The physical model for steady three dimensional axisymmetric flow of Carreau-Yusuda fluid due to a rotating disk in the presence of a uniform magnetic field applied along z positive directions is shown in Fig. 2.1. Heat transport characteristics are examined by taking variable thermal conductivity and by using Cattaneo-Charistov heat flux model. The governed equations are in cylindrical coordinate form.
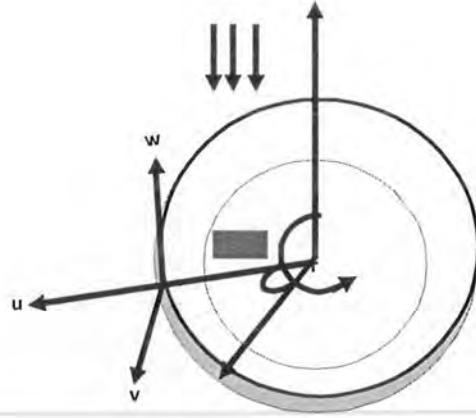

Fig. 2.1. Physical schematic diagram.

The extra stress tensor for Carreau-Yasuda fluid model is:

$$\tau = \left[\mu_\infty + (\mu_0 - \mu_\infty) \left(1 + (\Gamma \dot{\gamma})^d \right)^{\frac{1-n}{d}} \right] \mathbf{A}_1, \qquad (2.1)$$

here τ, μ_0 and μ_∞ denotes extra stress tensor, zero and infininte coeficient viscosity respectively. Γ^d is time constant, d is fluid parameter, n is the power law index, $\mathbf{A}_1 = L + L^t = (\nabla \mathbf{V}) + (\nabla \mathbf{V})^t$ is the kinematical tensor, ∇ differential operator and $\dot{\gamma} = \sqrt{\frac{1}{2} tr A_1^2}$ is second order invariant symmetric part of the velocity gradient. Suppose that the infinite shear rate viscosity $\mu_\infty = 0$ and by using first order Binomial series approximation eq. (2.1) reduces to

28

$$\tau = \left[u_0 \left(1 + \frac{1-n}{d} (\Gamma \dot{\gamma})^d \right) \right] \mathbf{A}_1, \tag{2.2}$$

under the above assumptions, the governing equations for Carreau-Yasuda fluid model in Cylinderical polar coordinates are given as

$$\begin{aligned}
\boldsymbol{\tau}_{rr} &= 2\mu_0 \left(1 + \frac{1-n}{d} (\Gamma \dot{\gamma})^d \right) \partial_r u, \; \boldsymbol{\tau}_{r\theta} = \boldsymbol{\tau}_{\theta r} = \mu_0 \left[\left(1 + \frac{1-n}{d} (\Gamma \dot{\gamma})^d \right) \left(\frac{1}{r} \partial_\theta u + \partial_r v - \frac{v}{r} \right) \right], \\
\boldsymbol{\tau}_{\theta\theta} &= 2 \left[\mu_0 \left(1 + \frac{1-n}{d} (\Gamma \dot{\gamma})^d \right) \left(\frac{1}{r} \partial_\theta v + \frac{u}{r} \right) \right], \; \boldsymbol{\tau}_{rz} = \boldsymbol{\tau}_{zr} = \mu_0 \left[\left(1 + \frac{1-n}{d} (\Gamma \dot{\gamma})^d \right) (\partial_z u + \partial_r u) \right], \\
\boldsymbol{\tau}_{zz} &= 2 \left[\mu_0 \left(1 + \frac{1-n}{d} (\Gamma \dot{\gamma})^d \right) \partial_z w \right], \; \boldsymbol{\tau}_{\theta z} = \boldsymbol{\tau}_{z\theta} = \mu_0 \left[\left(1 + \frac{1-n}{d} (\Gamma \dot{\gamma})^d \right) \left(\frac{1}{r} \partial_\theta w + \partial_z v \right) \right], \tag{2.3}
\end{aligned}$$

here

$$\dot{\gamma} = \sqrt{2 (\partial_r u)^2 + \left(\frac{1}{r} \partial_\theta u + \partial_r v - \frac{v}{r} \right)^2 + \left(\frac{1}{r} \partial_\theta v + \frac{u}{r} \right)^2 + (\partial_z u + \partial_r u)^2 + 2 (\partial_z u)^2}. \tag{2.4}$$

The governing continuity, momentum (Carreau-Yasuda model) and heat equations are

$$\partial_r u + \frac{u}{r} + \partial_z w = 0, \tag{2.5}$$

$$\rho \left(u \partial_r u - \frac{v^2}{r} + w \partial_z u \right) = -\partial_r p + \partial_r \boldsymbol{\tau}_{rr} + \partial_z \boldsymbol{\tau}_{zr} + \frac{\boldsymbol{\tau}_{rr} - \boldsymbol{\tau}_{\theta\theta}}{r} - u\sigma H_0^2, \tag{2.6}$$

$$\rho \left(u \partial_r v + \frac{vu}{r} + w \partial_z v \right) = \partial_r \boldsymbol{\tau}_{r\theta} + \partial_z \boldsymbol{\tau}_{z\theta} + 2 \frac{\boldsymbol{\tau}_{r\theta}}{r} - v\sigma H_0^2, \tag{2.7}$$

$$\rho \left(u \partial_r w + w \partial_z w \right) = -\partial_z p + \partial_r \boldsymbol{\tau}_{rz} + \partial_z \boldsymbol{\tau}_{zz} + \frac{\boldsymbol{\tau}_{rz}}{r}, \tag{2.8}$$

here velocity vectors $\mathbf{V} = [u, \; v, \; w]$ are in r, θ and z directions, respectively ν is the kinematic viscosity, n is the power law index, Γ is the time constant and ρ is the density.

The new version of Fourier's law is

$$\mathbf{q} + \lambda_T \left[\partial_t \mathbf{q} + \mathbf{V}.(\nabla \mathbf{q}) - \mathbf{q}.(\nabla \mathbf{V}) + (\nabla.\mathbf{V})\mathbf{q} \right] = -k_f \nabla T, \tag{2.9}$$

Fourier first proposed (see Winterton [82]) the heat conduction model based on the temperature distribution, by implimenting the above assumptions we have $\nabla.\mathbf{q} = 0$ and $\frac{\partial \mathbf{q}}{\partial t} = 0$, the above equation reduces to

$$\mathbf{q} + \lambda_T \left[\mathbf{V}.\nabla \mathbf{q} - \mathbf{q}.\nabla \mathbf{V} \right] = -k_f \nabla T, \tag{2.10}$$

where α is temperature based thermal conductivity, k_f is generally supposed to be constant. Now, the energy equation in cyliderical coordinates will be

$$u\partial_r T + w\partial_z T + \lambda_T \left[(u\partial_r u + w\partial_z u)\partial_r T + (u\partial_r w + w\partial_z w)\partial_z T + u^2 \partial_{rr} T + w^2 \partial_{zz} T + 2uw\partial_{rz} T \right]$$
$$= \frac{1}{r}\partial_r (rk(T)\partial_r T) + \partial_z (\alpha\partial_z T), \tag{2.11}$$

the boundary conditions for adopted problem are

$$u = K_1 \tau_{rz}, \ v = \Omega r, +K_2 \tau_{r\theta}, \ w = -w_0, \ T = T_w, \ \text{at} \ z = 0.$$
$$v \rightarrow 0, \ u \rightarrow 0, \ T \rightarrow T_\infty, \ P \rightarrow P_\infty, \ \text{as} \ z \rightarrow \infty.$$

Applying transformations:

$$\eta = \sqrt{2\frac{\Omega}{\nu}}, \ u = r\Omega f'(\eta), \ v = r\Omega g(\eta), \ z = -\sqrt{2\Omega\nu} f(\eta), \ k(T) = k_\infty \left(1 + \varepsilon \frac{T - T_\infty}{T_w - T_\infty} \right),$$

$$T - T_\infty, = (T_w - T_\infty)\theta(\eta). \tag{2.12}$$

30

Using the above similarity transformations the governing equations are converted into the following form:

$$2f''' + \left\{ f''' \frac{1}{\Omega^2} + \left(\dot{\gamma}\right)^{-2} \left[14\left(f''\right)^2 \frac{df}{d\eta} + 2\left(g'\right)^2 f' + \operatorname{Re}2\left(\left(f''\right)^2 f''' + g'g''f''\right)\right]\right\}$$

$$\times \left(2\frac{(n-1)}{d}\left(\dot{\gamma}\right)^d We^d(1+d)\right) - \left(f'\right)^2 - g^2 + 2ff'' - Ha^2 f' = 0, \qquad (2.13)$$

$$2g'' + \left\{ \frac{1}{\Omega^2}g'' + \left(\dot{\gamma}\right)^{-2} \left[12\left(f''\right)^2 f'g' + \operatorname{Re}2\left(\left(f''\right)^2 f'''g' + \left(g'\right)^2 g''\right)\right]\right\}$$

$$\times \left(2\frac{(n-1)}{d} We^d \left(\dot{\gamma}\right)^d (1+d)\right) - Ha^2 g = 0, \qquad (2.14)$$

$$(1 + \varepsilon\theta)\theta'' + \operatorname{Pr} f\theta' + \varepsilon\left(\theta'\right)^2 - 2\delta_t\left(f\theta'f' + f^2\theta''\right) = 0, \qquad (2.15)$$

and the boundary conditions will be

$$
\begin{aligned}
f(0) &= s, \ f' = f'' \left[1 + \frac{(n-1)}{d} We^d [12\left(f'\right)^2 + 2\operatorname{Re}\left(\left(f''\right)^2\left(g'\right)^2\right)\lambda_1\right], \\
g(0) &= 1 + g' \left[1 + \frac{(n-1)}{d} We^d [12\left(f'\right)^2 + 2\operatorname{Re}\left(\left(f''\right)^2\left(g'\right)^2\right)\right]\lambda_2, \ \theta(0) = 1, \ \text{at } \eta = 0, \\
f' &\rightarrow 0, \ \theta \rightarrow 0, \ P \rightarrow \infty, \ \text{as } \eta \rightarrow \infty.
\end{aligned}
\qquad (2.16)
$$

Where, velocity slip parameter $\lambda_1 = K_1\mu_0\sqrt{\frac{2\Omega}{v}}$, Hartmann number $Ha^2 = \frac{\sigma H_0^2}{\rho\Omega}$, tangential slip parameter $\lambda_2 = K_2\mu_0\sqrt{\frac{2\Omega}{v}}$, Weissenberg number $We^d = (\Omega\Gamma)^d$, Reynolds number $\operatorname{Re} = \frac{\Omega r^2}{v}$, Prandtl number $\operatorname{Pr} = \frac{\mu c_p}{k}$ and thermal relaxtion parameter $\delta_t = \lambda_t\Omega$.

The pressure can be initiated from eq. (2.8) as given by

31

$$p' = \left\{ \frac{1}{\Omega^2} f'' + \left(\dot{\gamma} \right)^{-2} \left[48 \left(f'' \right) f' + \mathrm{Re} \left(4 \left(f'' \right) f''' + 4 \left(g' \right) g'' \right) - \left(f'' \right)^2 - \left(g' \right)^2 \right] \right\}$$

$$\times \left(\left(\frac{n-1}{d} \right) (1+d) \, W e^d \right) + 2 f f' + 2 f''. \tag{2.17}$$

It is observed that the pressure do not depends upon r and θ. Generally speaking, there is no solutions available for above transformed equations (see Ref. [83]).

The essential physical quantity of interest i.e. reaction factor coefficients (C_f, C_g) in dimensionless form can be written as

$$C_f \, \mathrm{Re}_x^{\frac{-1}{2}} = \sqrt{2} f'' \left[1 + W e^d \frac{(n-1)}{d} \sqrt{12 \left(f' \right)^2 + 2 \mathrm{Re} \left(\left(f'' \right)^2 + \left(g' \right)^2 \right)} \right]_{\eta=0}, \tag{2.18}$$

$$C_g \, \mathrm{Re}_x^{\frac{-1}{2}} = \sqrt{2} g' \left[1 + W e^d \frac{(n-1)}{d} \sqrt{12 \left(f' \right)^2 + 2 \mathrm{Re} \left(\left(f'' \right)^2 + \left(g' \right)^2 \right)} \right]_{\eta=0}, \tag{2.19}$$

where $\mathrm{Re}_x = \sqrt{\frac{\Omega r^2}{v}}$.

2.2 Numerical Procedure

The PDEs are renovated into ODEs by using suitable similarity transformations. These transformed eqs. (2.14) to (2.16) are nonlinear differential equations. Therefore, the system of equations is difficult to solve analytically. Thus, eqs. (2.14) to (2.16) along with the boundary condtions (2.17) are solved numerically by using upgraded form of Fehlberg method (Cash and Karp).

2.3 Results and discussion

The set of dimensionless non-linear ODEs [i.e. eqs. (2.14) to (2.16)] under the boundary conditions (2.17) are solved numerically by using shooting method. Fig. 2.2 presents the

32

influence of Hartmann number Ha^2 on velocity profile. A Lorentz force that was named drag-like force is generated normal to the flow. It is clear that the velocity profile moderates by increasing Hartmann number Ha^2. It is important to mention that by increasing resistance on the material causes the heat to be created in the fluid. Fig. 2.3 describes the influence of Weissenberg number We^d on the velocity profile. It is clear from this figure that enhancement in Weissenberg number We^d tends to reduce velocity profile. Fig. 2.4 illuminates a very important effect of radial slip parameter λ on velocity profile. It is noticed that the velocity fluid enhances by enhancing radial slip parameter λ. Fig. 2.5 presents the variation of nonlinear stretching index n on velocity profile. It is also observed that by enhancing nonlinear stretching index n rises the velocity profile. Fig. 2.6. illustrates the variation of the fluid parameter d on velocity profile. It is found that the fluid parameter d increases by increasing velocity profile.
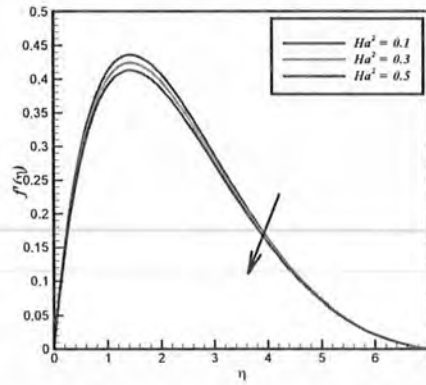

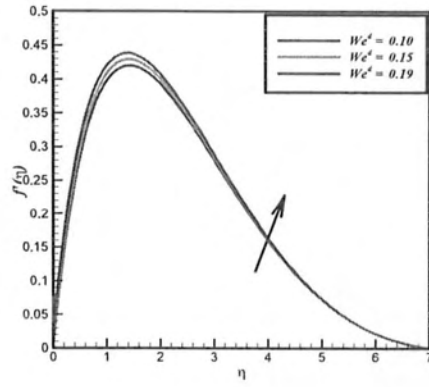Fig. 2.2. Variation of Ha^2 number on $f'(\eta)$.
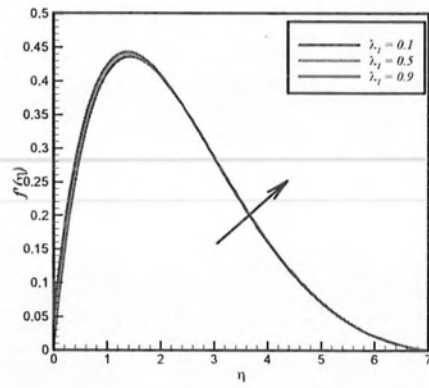
Fig. 2.3. Variation of We^2 number on $f'(\eta)$.

Fig. 2.4. Variation of λ_1 on $f'(\eta)$.
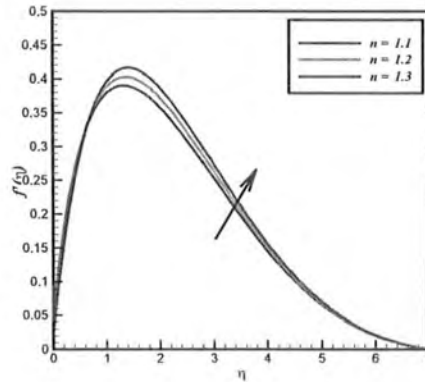
34

Fig. 2.5. Variation of power law index n on $f'(\eta)$.
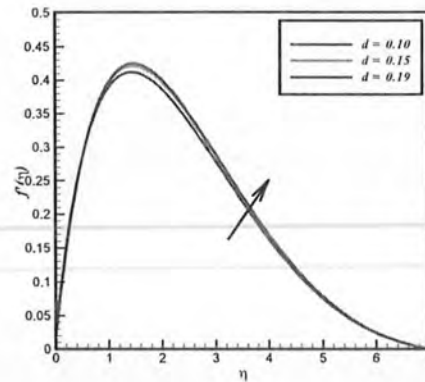

Fig. 2.6. Variation of d on $f'(\eta)$.

Fig. 2.7 indicates the influence of relaxation parameter δ_t on temperature distribution. It is observed from this figure that by increasing the values of relaxation parameter δ_t, heat assignment reduces, as a results rotating thermal boundary layer and temperature profile reduces. From fig. 2.8 it is seen that for larger values of Prandtl number Pr, temperature distribution diminishes. An increase in Prandtl number Pr reduces the thermal diffusivity and thus temperature of the fluid reduces. Fig. 2.9. shows the behavior of thermal conductivity ε in temperature distribution. It is found that the thermal conductivity parameter ε enhances by increasing temperature profile. **Table 2.1** shows the behavior of friction factor $(C_f,\ C_g)$ respec-

35

tively for different numerical values of physical parameters. For validation of current numerical scheme, the results are compared with Lin and Lin [84]. The outcomes of the current numerical results are in better agreement with previous results (shown in **Table 2.2**).
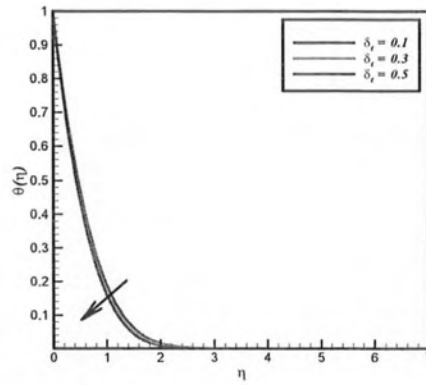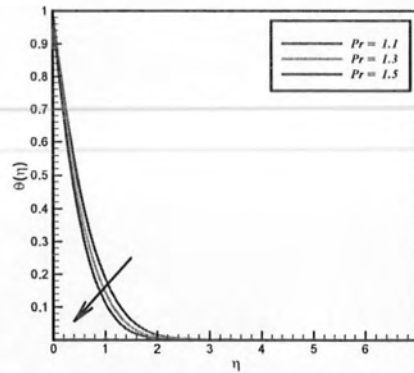

Fig. 2.7. Variation of δ_t on $\theta\left(\eta\right)$.
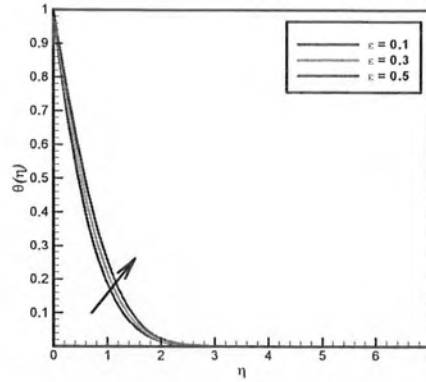

Fig. 2.8. Variation of Pr number on $\theta\left(\eta\right)$

Fig. 2.9. Variation of ε on $\theta(\eta)$

Table 2.1: Numerical values of $C_f \operatorname{Re}_x^{\frac{\varepsilon}{2}}$ for physical parameters We^d, Re and n while keeping $d = 0.1$.

We^d	Re	n	$C_f \operatorname{Re}_x^{\frac{1}{2}}$	$C_g \operatorname{Re}_x^{\frac{1}{2}}$
0.1	0.1	1.1	0.0081	1.1100
0.2			1.2725	1.2512
0.3			2.1018	1.4128
0.1	0.2	1.1	4.5677	2.6116
	0.4		6.0158	2.6179
	0.6		8.5781	2.6279
0.1	0.1	1.2	0.0825	2.8721
		1.3	0.1218	3.1326
		1.4	0.2465	3.3931

Tables 2.2: Comparsion of Prandtl number with Lie et al. [84] when $We^d = n = d = \delta_t = \lambda_1 = \lambda_2 = Ha = 0$ and $\varepsilon = 0.5$.

Pr	Lin et al. [84]	Present results
0.001	0.88600	0.88690
0.01	0.87658	0.87662
0.1	0.81614	0.81625
0.72	0.65512	0.65521
1.0	0.62902	0.62913
10	0.56095	0.56170

Chapter 3

Implementation of Darcy-Forchheimer effect on magnetohydrodynamic Carreau Yasuda nanofluid flow: Application of Von Kármán

This chapter configures the problem on MHD flow in Carreau-Yasuda nanofluid produced by impulsively started rotating disk in the occurrence of Darcy-Forchheimer and chemical reactive specie by employing conventional Fourier's and Fick's laws. Fourier introduced a model that relates heat transfer mechanism, but its major drawback is that it creates a parabolic heat equation which means that initial disturbance is felt through the entire scheme. The theory is constructed by adding time relaxation term to Fourier's law of heat conduction which permits the transferences of thermal in the form of heat waves with finite speed. Christov utilized Oldroyed's upper convective derivative in contrast of time derivative in Maxwell-Cattaneo's model in order to employ the material invariant analysis. Appropriate transformations are used to renovate the constitutive equations into nonlinear ODEs and then worked out by using improved form of Ruge-Kutta method. The deviation in flow field due to velocity, friction

factor, temperature, heat diffusion rate, nanoparticle concentration and mass transfer rate is analyzed subsequent for various ambient parameters appearing in the problem. The results of the study reveal that Weissenberg number appearing in the equations lead to decelerate the radial and tangential velocities while the power law index tends to accelerate the radial and tangential velocities.

3.1 Formulation and solutions of the problem

3.1.1 Flow fourmulation

Consider the steady 3-D axisymmetric Carreau-Yasuda nanofluid flow over a rotating disk with Cattaneo-Christov mass and heat flux models. The flow is generated via disk rotating with constant angular velocity Ω. An external magnetic field H_0 is applied normal to the plan disk. A schematic diagram of the physical configuration is shown in Fig. 3.1. Uniform concentration C_w and temperature T_w is presumed at the surface of rotating disk. The free stream temperature and ambient concentration are assumed to be T_∞ and C_∞.
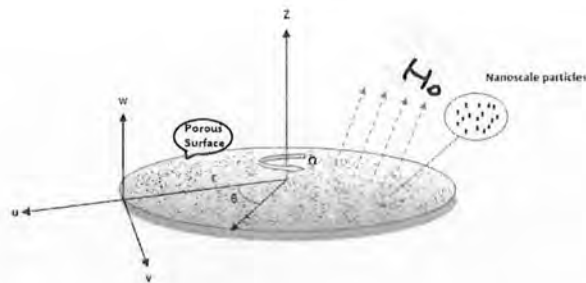

Fig. 3.1. Schematic diagram of physical model .

3.1.2 Rheological model for Carreau yasuda

The Cauchy stress tensor of Carreau-Yasuda rheological model is

$$\tau = \left[\mu_\infty + (\mu_0 - \mu_\infty) \left(1 + (\Gamma\dot{\gamma})^d \right)^{\frac{1-n}{d}} \right] \mathbf{A}_1, \tag{3.1}$$

here τ, μ_∞ and μ_0 denotes extra stress tensor, infinite and zero shear rate viscosities respectively. d is fluid parameter, Γ^d is the materials parameter, n is the power law index, $\mathbf{A}_1 = L + L^t = (\boldsymbol{\nabla V}) + (\boldsymbol{\nabla V})^t$ is the ratio of the strain tensor, ∇ differential operator and $\dot{\gamma} = \sqrt{\frac{1}{2}tr(\mathbf{A}_1^2)}$ is second order invariant strain tensor. Moreover, it is worth mentioning that this model reduces to Carreau fluid model when $d = 2$ and in similar way reduces to viscous fluid model when $n = 1$ or $\Gamma = 0$. Suppose that the infinite shear rate, viscosity is zero ($\mu_\infty = 0$) and by using binomial series eq. (3.1) becomes

$$\tau = \left[\mu_0 \left(1 + \frac{1-n}{d}(\Gamma\dot{\gamma})^d \right) \right] \mathbf{A}_1, \tag{3.2}$$

Carreau-Yasuda fluid model in Cylinderical polar coordinates become

$$\tau_{rr} = 2\mu_0\partial_r u \left(1 + \frac{1-n}{d}(\Gamma\dot{\gamma})^d \right), \quad \tau_{\theta r} = \tau_{r\theta} = \mu_0 \left[\left(1 + \frac{1-n}{d}(\Gamma\dot{\gamma})^d \right) \left(\frac{1}{r}\partial_\theta u + \partial_r v - \frac{v}{r} \right) \right],$$

$$\tau_{\theta\theta} = 2 \left[\mu_0 \left(\frac{1}{r}\partial_\theta v + \frac{u}{r} \right) \left(1 + \frac{1-n}{d}(\Gamma\dot{\gamma})^d \right) \right], \quad \tau_{zr} = \tau_{rz} = \mu_0 \left[\left(1 + \frac{1-n}{d}(\Gamma\dot{\gamma})^d \right) (\partial_z u + \partial_r u) \right],$$

$$\tau_{zz} = 2 \left[\mu_0\partial_z w \left(1 + \frac{1-n}{d}(\Gamma\dot{\gamma})^d \right) \right], \quad \tau_{z\theta} = \tau_{\theta z} = \mu_0 \left[\left(\frac{1}{r}\partial_\theta w + \partial_z v \right) \left(1 + \frac{1-n}{d}(\Gamma\dot{\gamma})^d \right) \right], \tag{3.3}$$

where

$$\dot{\gamma} = \sqrt{\left(\frac{1}{r}\partial_\theta u + \partial_r v - \frac{v}{r} \right)^2 + 2\left(\partial_r u\right)^2 + \left(\frac{1}{r}\partial_\theta v + \frac{u}{r} \right)^2 + 2\left(\partial_z w\right)^2 + \left(\partial_z u + \partial_r u\right)^2}. \tag{3.4}$$

The continuity and momentum equations are

$$\partial_r u + \frac{u}{r} + \partial_z w = 0, \tag{3.5}$$

41

$$\rho\left(u\partial_r u - \frac{v^2}{r} + w\partial_z u\right) = \partial_r P - \partial_r \tau_{rr} + \frac{\tau_{rr} - \tau_{\theta\theta}}{r} + \partial_z \tau_{zr} - \frac{\mu F_s}{K^*} u - \rho \frac{F_s}{\sqrt{K^*}} u^2 - \sigma u H_0^2, \quad (3.6)$$

$$\rho\left(u\partial_r v + \frac{vu}{r} + w\partial_z v\right) = \partial_r \tau_{r\theta} + 2\frac{\tau_{r\theta}}{r} + \partial_z \tau_{\theta z} - \frac{\mu F_s}{K^*} - \rho \frac{F_s}{\sqrt{K^*}} v^2 - \sigma \nu H_0^2, \quad (3.7)$$

$$\rho\left(u\frac{\partial w}{\partial r} + w\frac{\partial w}{\partial z}\right) = \partial_z P - \partial_r \tau_{rz} + \frac{\tau_{rz}}{r} + \partial_z \tau_{zz} - w\frac{\mu F_s}{K^*} - \rho \frac{F_s}{\sqrt{K^*}} w^2. \quad (3.8)$$

Here velocity field $\mathbf{V} = [u, v, w]$ is in r, θ and z directions, respectively. $\frac{\rho F_s}{\sqrt{K^*}}$ is the interial factor, ν is the kinematic viscosity and ρ is density. The extended Fourier's and Fick's laws take the following form:

$$\mathbf{q} + \lambda_T \left[\partial_t \mathbf{q} + \mathbf{V}.\left(\nabla \mathbf{q}\right) - \mathbf{q}.\left(\nabla \mathbf{V}\right) + \left(\nabla.\mathbf{V}\right)\mathbf{q}\right] = -k_f \nabla T, \quad (3.9)$$

$$\mathbf{J} + \lambda_c \left[\partial_t \mathbf{J} + \mathbf{V}.\left(\nabla \mathbf{J}\right) - \mathbf{J}.\left(\nabla \mathbf{V}\right) + \left(\nabla.\mathbf{V}\right)\mathbf{J}\right] = -D_B \nabla C. \quad (3.10)$$

By implimenting $\nabla.\mathbf{q} = 0$, $\nabla.\mathbf{J} = 0$, $\frac{\partial \mathbf{q}}{\partial t} = 0$ and $\frac{\partial \mathbf{J}}{\partial t} = 0$, the above equations become

$$\mathbf{q} + \lambda_T \left[\mathbf{V}.\nabla \mathbf{q} - \mathbf{q}.\nabla \mathbf{V}\right] = -k_f \nabla T, \quad (3.11)$$

$$\mathbf{J} + \lambda_C \left[\mathbf{V}.\nabla \mathbf{J} - \mathbf{q}.\nabla \mathbf{J}\right] = -D_B \nabla C. \quad (3.12)$$

Now the energy and concentration equations in cylindrical coordinates become

$$u\partial_r T + w\partial_z T + \lambda_T \left[(u\partial_r u + w\partial_z u)\partial_r T + (u\partial_r w + w\partial_z w)\partial_z T + w^2 \partial_{zz} T + u^2 \partial_{rr} T + 2uw\partial_{rz} T\right]$$
$$= \alpha\left(\partial_{rr} T + \frac{1}{r}\partial_r T + \partial_{zz} T\right) + \tau\left[D_B\left(\partial_r T\partial_r C + \partial_z T\partial_z C\right) + \frac{D_T}{T\infty}\left((\partial_r T)^2 + (\partial_z T)^2\right)\right], \quad (3.13)$$

42

$$u\partial_r C + w\partial_z C + \lambda_T \left[(u\partial_r u + w\partial_z u)\,\partial_r C + (u\partial_r w + w\partial_z w)\,\partial_z C + w^2\partial_{zz}C + u^2\partial_{rr}C + 2uw\partial_{rz}C\right]$$

$$= D_B\left(\partial_{rr}C + \frac{1}{r}\partial_r C + \partial_{zz}C\right) + \frac{D_T}{T\infty}\left[\left(\partial_{rr}T + \frac{1}{r}\partial_r T + \partial_{zz}T\right)\right] - k_r(C - C_\infty). \tag{3.14}$$

Here $\sigma = \frac{k}{\rho C_p}$ is the thermal diffusion, D_T is the thermophoresis diffusivity, C_p is the specific heat, D_B is the molecular diffusivity and $\tau = \frac{(\rho c)_s}{(\rho c)_f}$ is the nanoparticles heat capacity.

The transformations are

$$\eta = \sqrt{2\frac{\Omega}{\nu}},\ u = r\Omega f',\ v = r\Omega g(\eta),\ z = -\sqrt{2\Omega\nu}f(\eta),$$

$$T - T_\infty = (T_w - T_\infty)\,\Theta\,(\eta)\,,\ C - C_\infty = (C_w - C_\infty)\,\phi\,(\eta)\,. \tag{3.15}$$

Using the above similarty transformations the governing equations are converted into the following form:

$$2f''' + \left\{f'''\frac{1}{\Omega^2} + \left(\dot\gamma\right)^{-2}\left[14\left(f''\right)^2 f' + 2\left(g'\right)^2 f' + \mathrm{Re}\left(\left(f''\right)^2 f''' + g'g''f''\right)\right]\right\}$$

$$\times\left(2\frac{(n-1)}{d}\dot\gamma^d We^d(1+d)\right) + g^2 - \left(f'\right)^2 - f'\lambda + 2f'f - Ha^2 f' - F_c\left(f'\right)^2 = 0, \tag{3.16}$$

$$2g'' + \left\{\frac{1}{\Omega^2}g'' + \left(\dot\gamma\right)^{-2}\left[12f'\left(f''\right)^2 g' + \mathrm{Re}\left(\left(f''\right)^2 f'''g' + \left(g'\right)^2 g''\right)\right]\right\}$$

$$\times\left(2\frac{(n-1)}{d}We^d\left(\dot\gamma\right)^d(1+d)\right) - \lambda g - F_c g^2 - Ha^2 g = 0, \tag{3.17}$$

$$\theta'' + \Pr\left[f\theta' + N_b\phi'\theta' + N_t\left(\theta'\right)^2 - \delta_t\left(ff'\theta' + f^2\theta''\right)\right] = 0, \tag{3.18}$$

$$\phi'' + \frac{N_t}{N_b}\theta'' + \Pr Le\left[\phi' f - K\phi - \delta_c\left(f f'\phi' + f^2\phi''\right)\right] = 0, \tag{3.19}$$

the boundary conditions will be

$$f(0) = s, \ f' = 0, \ g(0) = 1, \ \theta(0) = 1, \ \phi(0) = 1, \ at \ \eta = 0,$$

$$f' \to 0, \ \theta \to 0, \ \phi \to 0, \ P \to \infty, \ as \ \eta \to \infty. \tag{3.20}$$

Where the dimensionless parameters are Hartmann number $Ha^2 = \frac{\sigma H_0^2}{\rho\Omega}$, porosity parameter $\lambda = \frac{\nu F_s}{K^*\Omega}$, inertia parameter $F_c = \frac{Fs}{\sqrt{K^*}}r$, Weissenberg number $We^d = (\Omega\Gamma)^d$, Brownian moment parameter $N_b = \frac{\tau D_B(C_w - C_\infty)}{\nu}$, Reynolds number $Re = \frac{\Omega r^2}{\nu}$, concentration buoyancy parameter $\delta_c = \lambda_c\Omega$, Prandtl number $\Pr = \frac{\mu c_p}{k}$, thermal buoyancy parameter $\delta_t = \lambda_t\Omega$, chemical reactive specie $K = \frac{k_r}{2\Omega}$, Lewis number $Le = \frac{\nu}{D_B}$ and thermophoresis parameter $N_t = \frac{\tau D_t(T_w - T_\infty)}{\nu T_\infty}$.

The pressure can be calculated from eq. (3.8), which gives

$$p' = +\left\{\frac{1}{\Omega^2}f'' + \left(\dot{\gamma}\right)^{-2}\left[48\left(f''\right)f' + Re\left(4\left(f''\right)f''' + 4\left(g'\right)g''\right) - \left(g'\right)^2 - \left(f''\right)^2\right]\right\}$$

$$\times\left(\left(\frac{n-1}{d}\right)(1+d)We^d\right) - f\left(\lambda + f F_c\right) + 2\left(f'' + f f'\right). \tag{3.21}$$

The essential physical quantities of interest i.e. reaction factor coefficient (C_f, C_g) in dimensionless form can be written as

$$C_f \, Re_x^{\frac{-1}{2}} = \sqrt{2}f''\left[1 + We^d\frac{(n-1)}{d}\sqrt{(f')^2 + Re\left(f'' + g'\right)}\right]_{\eta=0},$$

$$C_g \, Re_x^{\frac{-1}{2}} = \sqrt{2}g'\left[1 + We^d\frac{(n-1)}{d}\sqrt{(f')^2 + Re\left(f'' + g'\right)}\right]_{\eta=0}, \tag{3.22}$$

where $Re_x = \sqrt{\frac{\Omega r^2}{v}}$.

44

3.2 Numerical Procedure

To solve the eqs. (3.17)-(3.19) associated with Neumann boundary conditions (3.20), upgraded form of Runge-Kutta method (Cash and Karp) is implemented. Firstly, the boundary value problem is transformed into system of initial value problems. Then, fifth order Runge-Kutta technique is implemented to solve the corresponding initial value problems. The accuracy in numerical solution is controlled by assuming that tolerance error must be less than 10^{-6}.

3.3 Results and discussion

The solutions of the dimensionless eqs. (3.17)-(3.19) along with boundary conditions (3.20) are calculated by manipulating shooting procedure (Cash and Carp). Consequence of different flow governing parameters on velocity $f'(\eta)$, temperature $\theta(\eta)$ and concentration $\phi(\eta)$ has been calculated. The values of engineering concern i.e. local friction factor has been calculated for different regulatory parameters of a flow field. Figs. (3.2) and (3.3) display the graphical behavior of Hartmann number Ha^2 on $f'(\eta)$ and $g(\eta)$. It is observed that by enhancing Hartman number Ha^2, $f'(\eta)$ and $g(\eta)$ reduces. Lorentz force produces a retarding force which tends to strengthen the frictional resistance of fluid particles, causing reduction in $f'(\eta)$ and $g(\eta)$. Fig. 3.4 depicts that velocity profile enhances on increasing Weissenberg number We^d. Here for greater Weissenberg number We^d, the radial velocity increases close to disk that allow additional fluid particles to pass through. As a result velocity profile $f'(\eta)$ increases. Fig. 3.5 examines the behavior of Weissenberg number We^d on tangential velocity $g(\eta)$. It is seen that by enhancing Weissenberg number We^d tangential velocity, $g(\eta)$ reduces. Fig. 3.6 portrays the influence of power law index n on $f'(\eta)$. To strengthen values of power law index n, velocity profile magnifies. It is clear from sketch that velocity profile enhances by enhancing power law index n. Fig. 3.7 illustrates the variation on velocity profile $f'(\eta)$ for different values of inertia factor F_c. For higher values of inertia factor F_c, the velocity profile $f'(\eta)$ reduces. Fig. 3.8 illustrates the variation of fluid parameter d on velocity profile. For higher values of fluid parameter d, the velocity distribution increases. Fig. 3.9 illustrates the variation of local porosity parameter λ on velocity distribution $f'(\eta)$. It is observed that for higher values of the local porosity parameter λ, the velocity profile declines near the disk. Fig. 3.10 examines

45

the nature of Prandtl number Pr on temperature distributions. Prandtl number Pr is the ratio of momentum to thermal diffusivity. It is clear that for improved values of Prandtl number Pr temperature profile reduces. Figs. 3.11 and 3.12 represent the behavior of N_b and N_t on temperature profile. It is evident that strong values of N_b and N_t lead to enhance the temperature profiles. Fig. 3.13 shows that enhancement in δt causes reduction in temperature profile. Physically, this clarifies that as we increase δt, particles esteem non-conducting act i.e. particles take essential extra time to create heat among material which is responsible for reduction in temperature profile $\theta(\eta)$. Fig. 3.14 shows that nanoparticle concentration $\phi(\eta)$ diminishes for large values of Lewis number Le. Fig. 3.15 reveals the influence of K on concentration $\phi(\eta)$. It is seen that by enhancing chemical rection K the concentration profile diminishes. Fig. 3.16 represents the variation of δ_c on concentration profile. Higher distribution is observed for $\delta_c = 0.0$. i.e. classical Fick's law of diffusion. A comparison of current task with pervious published work is presented in **Table 3.1**. It can be seen that the present numerical values show outstanding match with Acharya et al. [80]. Using numerical calculations, local friction factor coefficient results are presented in a tabular form (see **Table 3.2**).
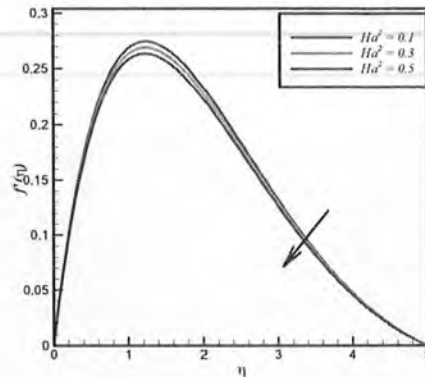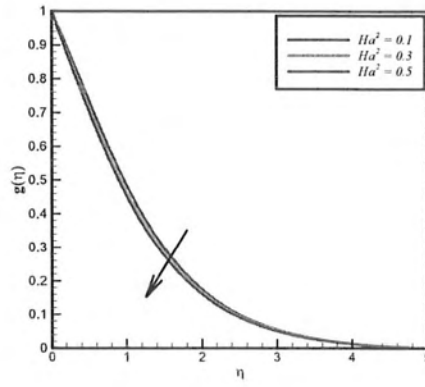

Fig. 3.2. Variation of Ha^2 on $f'(\eta)$
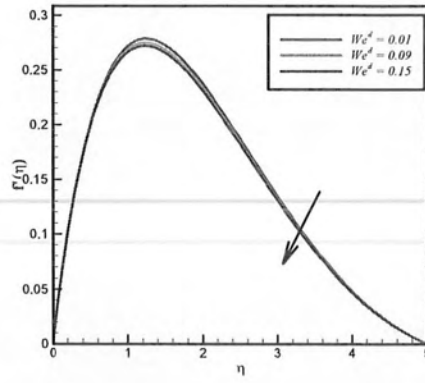
46

Fig. 3.3. Variation of Ha^2 number on $g(\eta)$

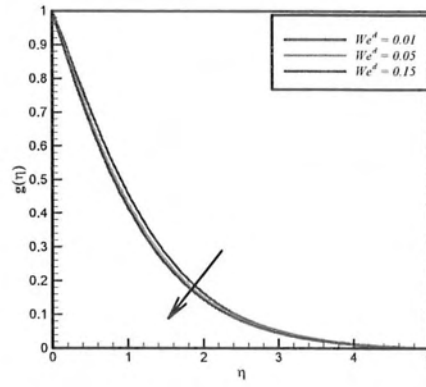Fig. 3.4. Variation of We^d on $f'(\eta)$.

47

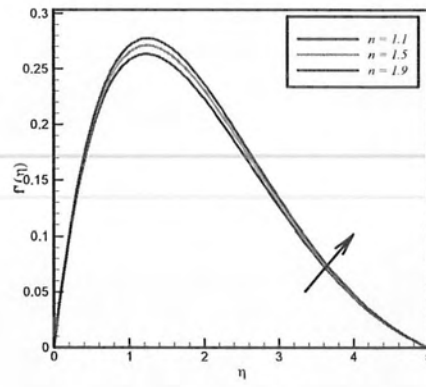Fig. 3.5. Variation of We^d number on $g(\eta)$.

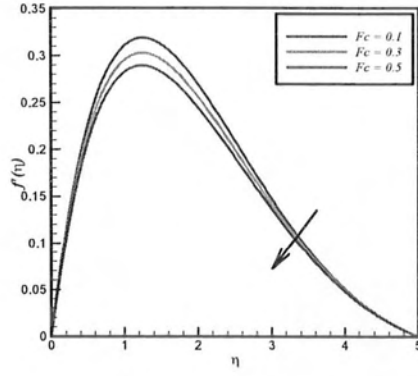Fig. 3.6. Variation of power law index n on $f'(\eta)$.
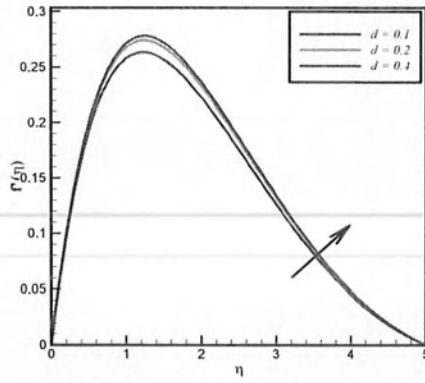
48

Fig. 3.7. Variation of inertia factor Fc on $f'(\eta)$.
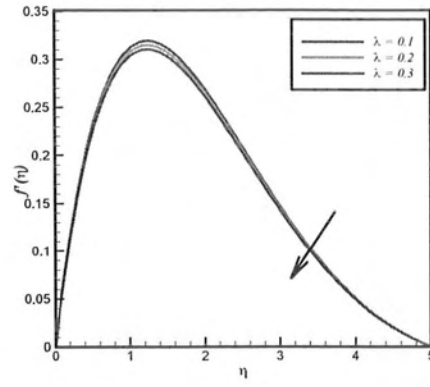

Fig. 3.8. Variation of fluid parameter d on $f'(\eta)$.

49

Fig. 3.9. Variation of porosity parameter λ on $f'(\eta)$.
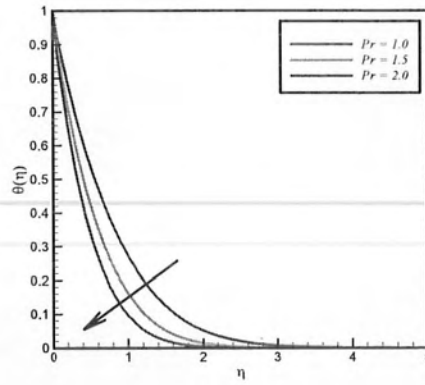

Fig. 3.10. Variation of Prandtl number Pr on $\theta(\eta)$.

50
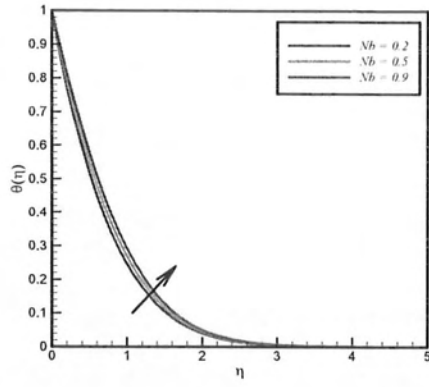
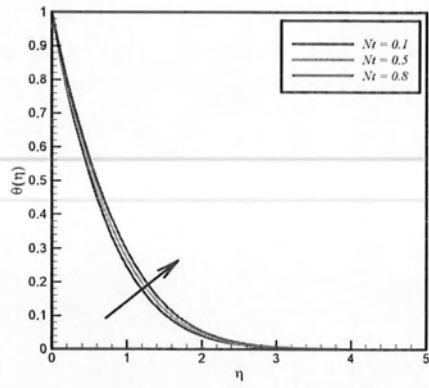Fig. 3.11. Variation of N_b on $\theta(\eta)$.

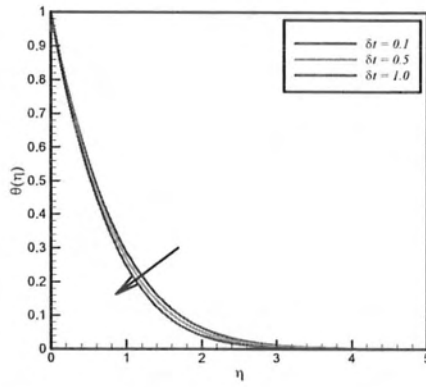Fig. 3.12. Variation of N_t on $\theta(\eta)$.
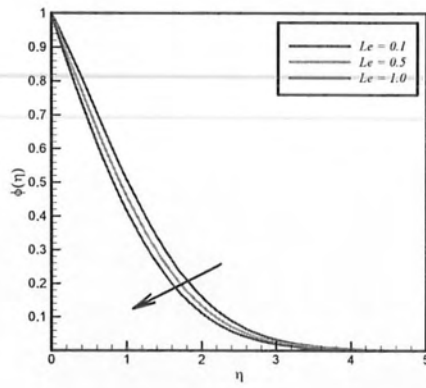
51

Fig. 3.13. Variation of δt on $\theta(\eta)$.
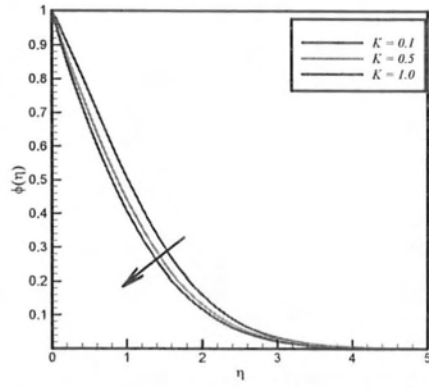

Fig. 3.14. Variation of Le on $\phi(\eta)$.

52

Fig. 3.15. Variation of K on $\phi(\eta)$.
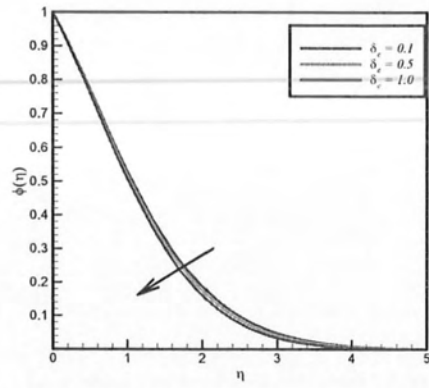
Fig. 3.16. Variation of δc on $\phi(\eta)$.

53

Table 3.1: Comparison of the current results with previous studies when $N_t = d = 0.1$, $\mathrm{Re} = F_c = We^d = K = n = Le = 0.0$ and $\mathrm{Pr} = 1.0$.

N_t	Acharya et al. [80]	Present work
0.1	0.9524	0.9524
0.2	0.6932	0.6938
0.3	0.2501	0.2511
0.5	0.4026	0.4026
0.6	0.3211	0.3231

Table 3.2: Numerical values of $f''(0)$ and $g'(0)$ when $N_t = Nb = \mathrm{Re} = F_c = We^d = K = 0.1$, $\mathrm{Pr} = 1.0$, $Le = 0.8$ and $n = 1.1$.

Ha^2	d	λ	$C_f \mathrm{Re}_x^{-\frac{1}{2}}$	$C_g \mathrm{Re}_x^{-\frac{1}{2}}$
0.5	0.1	0.1	05369	0.2769
0.6			0.5415	0.2654
0.7			0.5439	0.2565
0.5	0.1	0.1	0.5369	0.2769
	0.2		0.5888	0.2231
	0.3		0.6026	0.2092
0.5	0.1	0.1	0.5369	0.2769
		0.4	0.5449	0.2495
		0.7	0.5424	0.2353

Chapter 4

Heat and mass transfer of Williamson nanofluid flow yield by an inclined Lorentz force over a nonlinear stretching sheet

This chapter focus to explore the computational solution of variable viscosity and inclined Lorentz force effects on Williamson nanofluid over a stretching sheet. The Williamson model is nearly equal to blood as it almost describes the nature of blood flow. Variable viscosity is assumed to vary as a linear function of temperature. The basic mathematical modelled problem i.e. system of PDE's is converted into nonlinear ODE's by applying suitable transformations. To compute numerical solution of the problem an efficient numerical technique shooting is employed. Characteristics of controlling different parameters are plotted to visualize various physical constraints. Additionally, friction factor coefficient, Nusselt number and Sherwood number are presented in the form of graphs and tables.

4.1 Mathematical formulation

Let us consider a mathematical model for two dimensional boundary layer flow of Williamson nanofluid over a continuously nonlinear stretching sheet with variable viscosity. The plate is stretched with velocity $U_w = U_0(x + b)^{m-1}$, where U_0 is reference stretching rate, m is the stretching velocity index and b is the dimensionless constant. The sheet is considered at $y = A(x + b)^{\frac{1-m}{2}}$, where A is very small constant. Further, it is assumed that the model must be satisfied only for $m \neq 1$, because for $m = 1$, it reduces to flat sheet. Magnetic field of strength $H_0(x)$ is applied along normal direction of flow at an angle γ from sheet (as shown in Fig. 4.1).
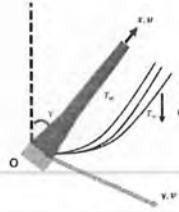
Fig. 4.1. Schematic representation of the problem.

4.1.1 Rheological formation of Williamson model

The Cauchy stress tensor for Williamson fluid model is defined as

$$\mathbf{S} = -P\mathbf{I} + \boldsymbol{\tau}, \tag{4.1}$$

$$\boldsymbol{\tau} = \left(\mu_\infty + \frac{\mu_0 - \mu_\infty}{1 - \Gamma\dot{\gamma}} \right) \mathbf{A}_1, \tag{4.2}$$

where

$$\dot{\gamma} = \sqrt{\frac{1}{2}\pi}, \ \pi = trace\left(\mathbf{A}_1^2 \right), \tag{4.3}$$

56

in which $\mathbf{S}$ is the extra tensor, $\mathbf{I}$ is the identity tensor, P is the Hydrostatic pressure, τ is the Cauchy tensor, μ_0 denotes limiting viscosity at zero shear rate, μ_∞ represents shear rate at infinite, $\Gamma > 0$ is a time constant, $\mathbf{A}_1 = (\nabla \mathbf{V}) + (\nabla \mathbf{V})^t = L + L^t$ is the first Rivlin-Ericksen tensor.

Where, we have assumed the case for which $\mu_\infty = 0$ and $\Gamma \overset{o}{\gamma} < 1$. Eq. (4.2) becomes

$$\tau = \left(\frac{\mu_0}{1 - \Gamma \overset{o}{\gamma}} \right) \mathbf{A}_1, \tag{4.4}$$

using binomial expansion, we get

$$\tau = \mu_0 \left(1 + \Gamma \overset{o}{\gamma} \right) \mathbf{A}_1, \tag{4.5}$$

4.1.2 Problem formulation

Under these assumptions and boundary layer approximations the governing equations i.e. Williamson nanofluid momentum, energy and concentration equation becomes:

$$\partial_x u + \partial_y v = 0, \tag{4.6}$$

$$
\begin{aligned}
u\partial_x u + v\partial_y u \;=\; & \frac{1}{\rho}\partial_y \left(\mu(T)\partial_y u \right) + \frac{\Gamma\sqrt{2}}{\rho} \left[\partial_y \left(\mu(T)\partial_y u \right) \partial_y u \right] \\
& + g\beta_T \left(T - T_\infty \right) + g\beta_C \left(C - C_\infty \right) - \sin^2(\gamma)u\frac{\sigma H_0^2}{\rho},
\end{aligned}
\tag{4.7}
$$

$$u\partial_x T + v\partial_y T = \tau \left\{ D_B \left(\partial_y C \right) \partial_y T + \left(\frac{D_T}{T_\infty} \right) \left(\partial_y T \right)^2 \right\} + \alpha \left(\partial_{yy} T \right), \tag{4.8}$$

$$u\partial_x C + v\partial_y C = -k_r (C - C_\infty) + \left[D_B \left(\partial_{yy} C \right) + \left(\frac{D_T}{T_B} \right) \partial_{yy} T \right], \tag{4.9}$$

57

the specified boundary conditions are assumed at variable thicked stretching sheet

$$u(x + A(x+b)^{\frac{1-m}{2}}) \quad = \quad U_w(x) = U_0(x+b)^m, \ v(x + A(x+b)^{\frac{1-m}{2}}) = 0, \ T = T_w, \ C = C_w, \text{ at } y = A(x +$$

$$u \quad \rightarrow \quad 0, T \rightarrow T_\infty, C \rightarrow C_\infty, \text{ as } y \rightarrow \infty.$$

Here (u, v) are the velocity components along (x, y) directions respectively, $\mu(T)$ is the variable viscosity, ρ is the density, β_C and β_T are the coefficients of mass and thermal diffusion, γ is the inclined angle, σ is the electric conductivity, H_0 is the magnetic field strength, g is the magnitude of the gravity, C and T are the fluid concentration and temperature, T_w and T_∞ are the surface and ambient temperature respectively, C_w and C_∞ are the fluid concentration near and for away the surface and k_r is the chemical reaction. The temperature dependent variable viscosity is define as (see Ref. [85])

$$\frac{1}{\mu(T)} = \frac{1}{\mu_\infty}[1 + r[T - T_\infty], \tag{4.11}$$

or

$$\frac{1}{\mu} = \delta(T - T_r), \tag{4.12}$$

here $T_r = T_\infty - \frac{1}{r}$ and $\delta = \frac{r}{\mu_\infty}$ are constants and these values depend on the location state, μ_∞ is the dynamic viscosity of the free stream and r is the thermal property of the fluid. Generally $\delta > 0$ for a liquid and for gases $\delta < 0$.

The governing equations (PDE's) are converted into ODE's with the help of following transformations (see Ref. [86])

$$\eta \quad = \quad y\sqrt{\frac{(m+1)U_0}{2\nu}}(x+b)^{\frac{m-1}{2}}, \quad \psi = \left[\sqrt{\frac{2\nu U_0}{m+1}}F(\eta)\right](x+b)^{\frac{m-1}{2}},$$

$$u \quad = \quad U_0(x+b)^m F'(\eta), \ v = -\left(\frac{(m+1)\nu U_0}{2}\right)^{\frac{1}{2}}\left[F(\eta) + \eta\frac{m-1}{m+1}F'(\eta)\right](x+b)^{\frac{m-1}{2}},$$

$$\Theta(\eta) \quad = \quad \frac{T - T_\infty}{T_w - T_\infty}, \ \Phi(\eta) = \frac{C - C_\infty}{C_w - C_\infty}. \tag{4.13}$$

58

Eq. (4.6) is identically satisfied, now via substituting eq. (4.13), eqs. (4.7)-(4.9) gives the following nonlinear differential equations:

$$\left(\frac{\Theta_r}{\Theta_r - \Theta}\right)(1 + 2We^2 F'')F''' - \frac{2m}{m+1}(F')^2 + FF'' + (1 + F''We)$$

$$\times \frac{\Theta_r}{(\Theta_r - \Theta)^2}\Theta' F'' + \lambda_C(\Theta + \lambda_T \Phi) - \sin^2(\gamma)Ha^2 F' = 0, \tag{4.14}$$

$$\Theta'' + \Pr\left(N_b \Phi' \Theta' + \Theta' F + N_t(\Theta')^2\right) = 0, \tag{4.15}$$

$$\Phi'' + \frac{N_t}{N_b}\Theta'' + \Pr Le\Phi' F - Le\Pr K\Phi = 0. \tag{4.16}$$

Using eq. (4.10), the associated boundary conditions are transformed to

$$
\begin{aligned}
F' &= 1, \ F(\alpha) = \frac{(1-m)}{(1+m)}\alpha, \ \Theta(\alpha) = 1, \ \Phi(\alpha) = 1, \ \text{at } \alpha = 0, \\
F' &= 0, \ \Theta(\alpha) = 0, \ \Phi(\alpha) = 0, \ \text{as } \alpha \to \infty.
\end{aligned} \tag{4.17}
$$

Here $\alpha = A\sqrt{\frac{U_0(x+b)(m+1)}{2v}}$ is wall thickness parameter. In order to transform the required equations and Neumann boundary conditions a new set of variables is defined as $F(\eta) = f(\xi - \alpha) = f(\xi)$, $\Theta(\eta) = \theta(\xi - \alpha) = \theta(\xi)$ and $\Phi(\eta) = \phi(\xi - \alpha) = \phi(\xi)$ which gives

$$\left(\frac{\theta_r}{\theta_r - \theta}\right)(1 + 2We^2 f'')f''' - \frac{2m}{m+1}(f')^2 + ff'' + (1 + f''We)\frac{\theta_r}{(\theta_r - \theta)^2}\theta' f'' + \frac{2}{m+1}\left(\lambda_C(\theta + \lambda_T \phi) - \sin^2(\gamma)Ha\right.$$

$$\tag{4.18}$$

$$\theta'' + \Pr\left[\theta' f + N_b \phi' \theta' + N_t(\theta')^2\right] = 0, \tag{4.19}$$

59

$$\phi'' + \frac{N_t}{N_b}\theta'' + \Pr Le \left[f\phi' - K\phi\right] = 0, \qquad (4.20)$$

$$\begin{aligned} f &= \frac{\alpha(1-m)}{(1+m)}, \ f' = 1, \ \theta(\eta) = 1, \ \phi(\eta) = 1, \ \text{at } \xi = 0, \\ f' &\rightarrow 0, \ \Theta(\eta) \rightarrow 0, \ \phi(\eta) \rightarrow 0, \ \text{as } \xi = \infty, \end{aligned} \qquad (4.21)$$

where $\theta_r = \frac{T_r - T_\infty}{T_W - T_\infty} = \frac{-1}{r(T_W - T_\infty)}$ is the variable viscosity parameter, $Ha^2 = \frac{\sigma H_0^2}{\rho U_0 (x+b)^{m-1}}$ is the Hartmann number, $We^2 = \sqrt{\frac{(m+1)U_o^3(x+b)^{3m-1}}{2\nu}}$ is the Weissenberg number, $Gr_x = \left(g\beta_T \frac{(T-T_0)}{U_0^2(x+b)^{2m-1}}\right)$ is the local Grashof number, $\lambda_T = \frac{Gr_x}{R^2 e_x}$ the mixed convection parameter, $G^*r_x = \frac{g\beta_T(C-C_0)}{U_0^2(x+b)^{2m-1}}$ is the local Grashof number due to concentration, $\lambda_C = \frac{G^*r_x}{Gr_x}$ is the ratio of thermal to concentration buoyancy force, $K = \frac{2K_r}{(m+1)U_0(x+b)^{m-1}}$ is the chemical reactive species, $\Pr = \frac{\mu c_p}{k}$ is the Prandtl number, $N_t = \frac{D_t(T_w - T_\infty)\tau}{\nu}$ is the thermophoresis parameter, $Le = \frac{\nu}{D_B}$ is the Lewis number and $N_b = \frac{D_B(C_w - C_\infty)\tau}{\nu T_\infty}$ is the Brownian motion parameter.

For physical quantities near the wall i.e. the friction factor coefficient, rate of heat and mass transfer are given by

$$C_f \left(\frac{\text{Re}_x^{\frac{1}{2}}}{2}\right) = \left\{\frac{\theta_r}{\theta_r - \theta}\left[f''(\eta) + We^2\left(f''(\eta)\right)^2\right]\sqrt{\frac{(m+1)}{2}}\right\}_{\eta=0}, \qquad (4.22)$$

$$Nu \, \text{Re}_x^{\frac{-1}{2}} = -\sqrt{\frac{(m+1)}{2}}\theta'(0), \ Sh \, \text{Re}_x^{\frac{-1}{2}} = -\sqrt{\frac{(m+1)}{2}}\phi'(0). \qquad (4.23)$$

Here $\text{Re}_x = \left(\frac{U_0(x+b)^{m-1}}{\nu}\right)^{\frac{1}{2}}$.

4.2 Numerical procedure

Numerical solutions of highly nonlinear differential system i.e. Eqs. (4.18)-(4.20) along with Neumann boundary conditions (4.21) are solved via shooting technique. Among some other numerical scheme, the shooting method is more flexible for the reason that the initial guesses control the convergence criteria. The main steps to achieve the computational solution via shooting method are as follows:

60

1.   Reduce eqs. (4.18)-(4.20) to a system of 1st order ordinary differential equations.

2.   Insert the three missing initial approximations.

3.   Finally, solve the reduced system of first order equations via Rung-Kutta method.

4.   Compute boundary residuals (difference between given and computed values at the end point boundary conditions), if these residuals are less than the error tolerance i.e. 10^{-6}, then we get the solutions, on the other hand modify the initial guesses with Newtons method.

5.   Repeat these steps, unless computed solutions satisfy the convergence criteria.

4.3   Results and discussion

The major focus of this chapter is to scrutinize the impact of double stratification and inclined Lorentz force on Williamson nanofluid flow past a nonlinear stretching sheet with variable thickness. The governing equations i.e. eqs. (4.18)-(4.20) together with Neumann boundary conditions (4.21) are solved numerically via shooting scheme. Fig. 4.2 represents the behavior of inclined angle γ on velocity distribution. It is observed that inclined angle γ declines the velocity profile. Fig. 4.3 illustrates the variation of wall thickness parameter α on velocity distribution. It is seen that on increasing values of wall thickness parameter α, fluid velocity diminishes . Because it is observed that for higher values of α, viscoelastic impact increases over stretchable surface (which repels layer thickness) and then velocity distribution decreases. Fig. 4.4 examines the influence of Hartmann number Ha^2 on velocity. It is clear that the velocity reduces with increase in the Hartmann number Ha^2. Since the claim of transverse magnetic field produces a drag-like force (Lorentz force), which opposes the fluid motion and velocity gradient. Fig. 4.5 deliberates the influence of variable viscosity θ_r on velocity distribution. From fig 4.5, it is seen that the velocity profile reduces with enhancement in variable viscosity parameter θ_r. It could be seen that the enhancement in variable viscosity parameter causes reduction in boundary layer thickness. Fig. 4.6 illustrates the impact of Weissenberg number We^2 on velocity distribution. It is noticed that the velocity gradient enhances by changing the values of Weissenberg number We^2. Fig. 4.7 examines the influence of mixed convection parameter λ_T on velocity profile. This figure exhibits that the velocity distribution and boundary layer thickness enhances by enhancing λ_T. Because large values of λ_T provide a strong buoyance

61

force which leads to enhance the velocity. Fig. 4.8 illustrates that the velocity profile enhances against λ_C. Because λ_C is the ratio between thermal and concentration buoyancy forces. The thermal buoyancy ratio parameter enhances as a result velocity profile growup.
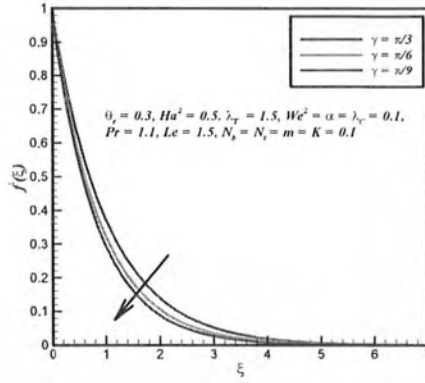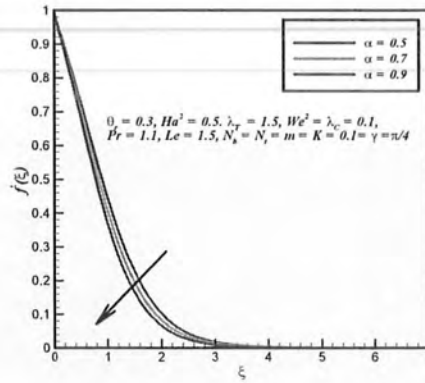

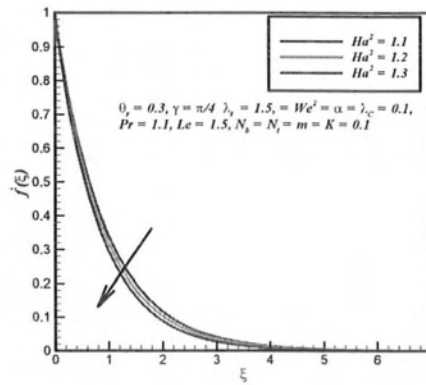Fig. 4.2. Influence of inclined angle γ on $f'(\xi)$.

Fig. 4.3. Influence of α on $f'(\xi)$.
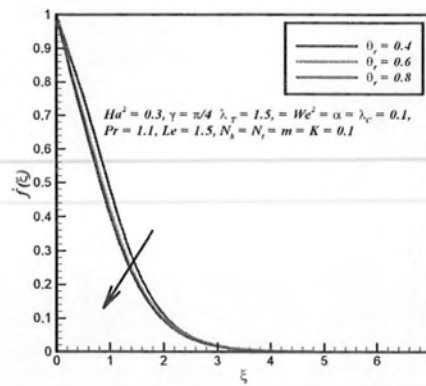
Fig. 4.4. Infuence of Ha^2 number $f'(\xi)$.

Fig. 4.5. Influence of θ_r on $f'(\xi)$.

63
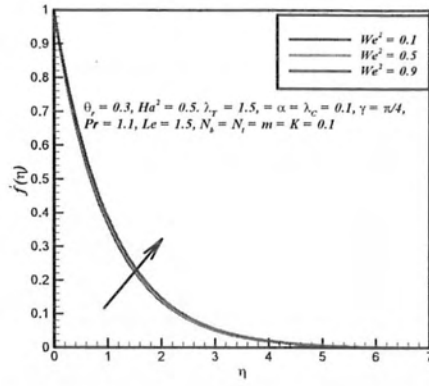
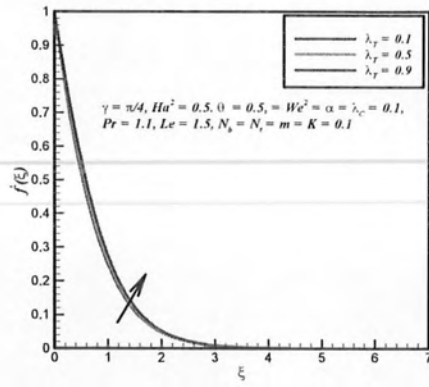Fig. 4.6. Influence of We^2 number on $f'(\xi)$.

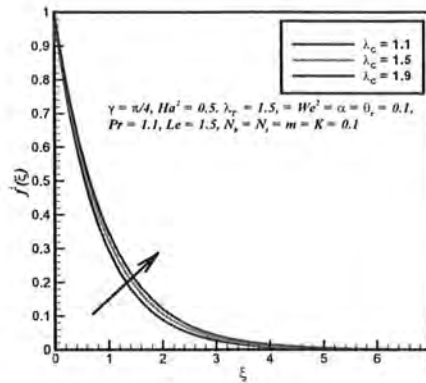Fig. 4.7. Influence of λ_T on $f'(\xi)$.

64

Fig. 4.8. Influence of λ_C on $f'(\xi)$.

Fig. 4.9 scrutinizes the effect of Prandtl number Pr on fluid temperature. Since Prandtl number is related to the momentum diffusion and thermal diffusion in the boundery layer regime. Thus the thermal boundary layer in the temperature distribution reduces by enhancing the values of Prandtl number Pr. Fig. 4.10 characterizes the effect of Brownian motion N_b on temperature profile. Temperature constantly reduces against increasing values of Brownian motion parameter N_b. Fig. 4.11 illustrates the variation of thermophoretic parameter N_t on temperature profile. It is validates the fact that the thermophoretic parameter enhances the temperature profile. Because thermophoretic phenomenon transferred nanoparticles from hot

65

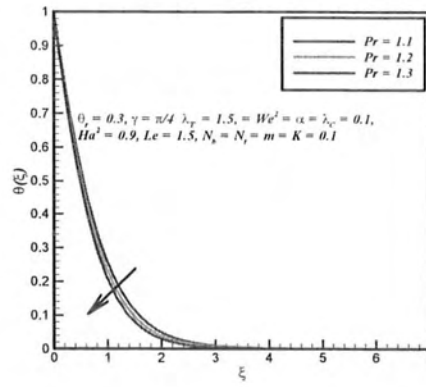surface to cold region due to this temperature of the fluid enhances.
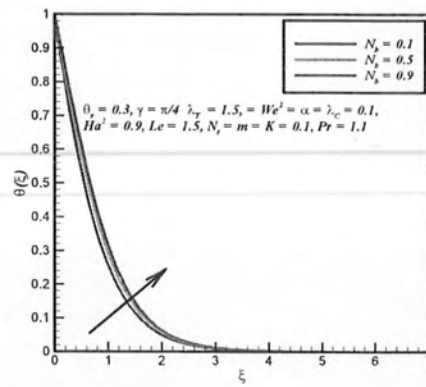

Fig. 4.9. Influence of Pr number on $\theta\left(\xi\right)$.

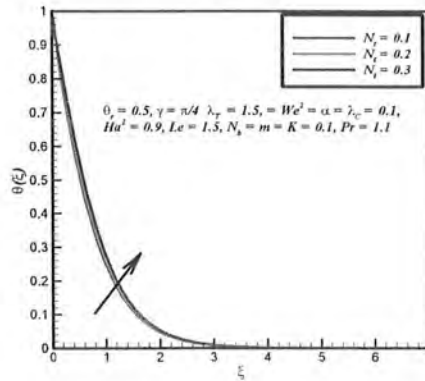Fig. 4.10. Influence of N_b on $\theta\left(\xi\right)$.

66

Fig. 4.11. Influence of N_t on $\theta(\xi)$.

Fig. 4.12 gives the variation in concentration distribution for several values of Lewis number Le. It is seen that the Lewis number Le reduces the concentration profile substantially. Because by enhancing the Lewis number Le, it reduces the concentration rate diffusivity and hence concentration profile. Fig. 4.13 exemplifies the fluid concentration profile for different values of chemical reactive species parameter K. It is found that the chemical reactive species parameter K enhances the concentration profile. Fig. 4.14 displays that the wall friction factor decreases for enhancing values of Weissenberg number We^2 while it increases with increase in Hartmann number Ha^2. Fig. 4.15 examines the heat transfer rate for distinct values of Prandtl number Pr and thermophoresis parameter N_t. It is found that the heat transfer rate increases for large values of Prandtl number Pr on the other hand thermophoresis parameter N_t declines it. **Tables 4.1-4.3** demonstrate the local friction factor coefficient, heat and mass transfer rates for various values of Hartmann number, Weissenberg number, Prandtl number, thermophoretic parameter, Lewis number and chemical reactive species parameter. The behavior of different physical parameters is demonstrated from these tables.
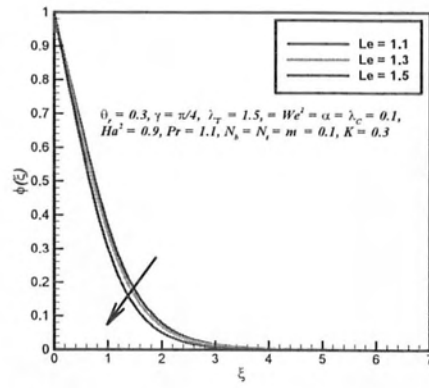
Fig. 4.12. Influence of Le on $\phi(\xi)$.
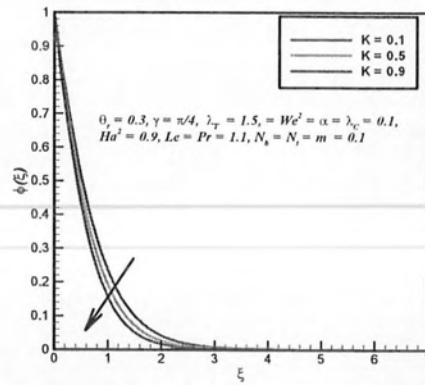
Fig. 4.13. Influence of K on $\phi(\xi)$.

68
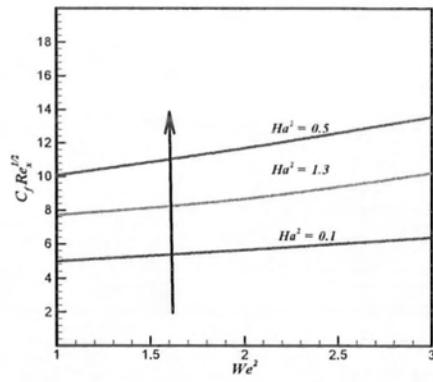
Fig. 4.14. Influence of Ha^2 and We^2 on friction factor.
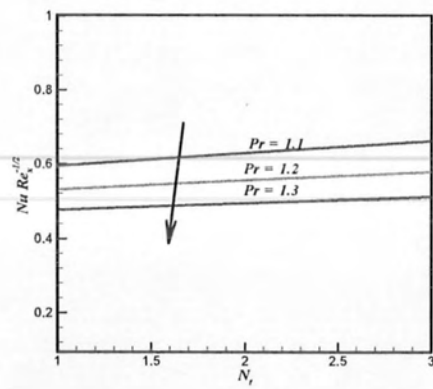
Fig. 4.15. Influence of Pr and N_t on Nusselt number.

69

Table 4.1: Numerical values of wall friction factor for different values of We^2 and Ha^2 when $\theta_r = 0.3$, $\lambda_C = 1.5$, $m = K = N_t = N_t = 0.1$, $\Pr = 1.5$, $\gamma = \frac{\pi}{4}$ and $\alpha = 0.9$.

Ha^2	We^2	$C_f \, Re_x^{\frac{1}{2}}$
0.1	0.1	0.4263
0.2		0.4322
0.3		0.4430
0.1	0.2	0.4062
0.2		0.4119
0.3		0.4207
0.1	0.3	0.3883
0.2		0.3869
0.3		0.3883

Table 4.2: Computational values of heat transfer rate i.e. $\left(-Nu \, Re_x^{\frac{-1}{2}} \right)$ for different values of N_t and $\Pr$.

N_t	$\Pr$	$-NuRe_x^{\frac{-1}{2}}$
0.1	1.1	0.8348
	1.2	0.7767
	1.3	0.7227
0.2	1.1	0.8871
	1.2	0.7905
	1.3	0.7292
0.3	1.1	0.8348
	1.2	0.7767
	1.3	0.7227

Table 4.3: Numerical values of mass transfer rate i.e. $(-\phi'(0))$ against unlike values of K and Le.

K	Le	$-ShRe_x^{\frac{-1}{2}}$
0.1	1.1	1.3442
0.2		1.3800
0.3		1.4153
0.1	1.2	1.3585
0.2		1.3949
0.3		1.4310
0.1	1.3	1.3750
0.2		1.4122
0.3		1.4490

Chapter 5

Change in viscosity of Williamson nanofluid flow due to thermal and solutal stratifications

This chapter deliberates the computational aspects of variable viscosity on Williamson nanofluid over a non-linear stretching sheet. Viscosity is a basic property of fluids that plays improtant role in different ways like printing and coating, petroleum, beverages and food, industiral chemisty, power, organic chemsity, environment, etc. In rheological science viscosity is clasp as a function of either pressure or temperature. In this chapter viscosity of the fluid is assumed to be dependent on temperature and due to thermal stratification, viscosity of the fluid also depends upon thermal diffusion. The basic mathematical problem (system of PDEs) is converted into non-linear ODEs via suitable trasformations. Computational solutions of the problem are achieved through efficient numerical approach (shooting method). Characteristics of controlling parameters are plotted for concentration, velocity and temperature gradients. Furthermore, friction factor coefficient, heat and mass diffusion rates are presented through graphs and tables. Conclusions are made on the basis of entire investigation and it is seen that velocity profile reduces for large values of variable viscosity and thermal stratification parameters while thermal stratification parameter shows opposite behavior for temperature profile. Moreover, concentration profile is expected to reduce on enhancing values of Lewis number and increases for large values

72

of stretching velocity parameter.

5.1   Mathematical analysis

Let us consider a mathematical model for two dimensional boundary layer flow of Williamson nanofluid flow over a continuously nonlinear stretching surface with variable dynamic viscosity. The plate is stretched with velocity $U_w = U_0(x+b)^{m-1}$. The surface is taken at $y = A(x+b)^{\frac{1-m}{2}}$, where A is very small constant, m is the stretching index, U_0 is the stretching rate and b is the dimensionless constant. Further it is assumed that the model must be fulfilled only for $m \neq 1$, because for $m = 1$, it reduces to flat surface. A uniform external magnetic field H_0 is applied in normal direction of flow, vertical to the sheet (as illustrated in Fig. 5.1)

Under these assumptions and boundary layer approximations the governing equations (Williamson nanofluid model, energy and concentration equations) become:
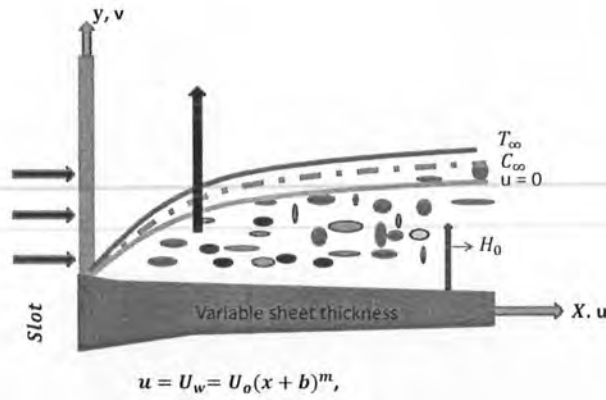

Fig. 5.1. Geometry of the problem.

$$\partial_x u + \partial_y v = 0, \tag{5.1}$$

$$u\partial_x u + v\partial_y u = \frac{1}{\rho}\partial_y\left(\mu(T)\partial_y u\right) + \frac{\Gamma\sqrt{2}}{\rho}\left[\partial_y\left(\mu(T)\partial_y u\right)\partial_y u\right] - u\frac{\sigma H_0^2}{\rho}, \tag{5.2}$$

73

$$u\partial_x T + v\partial_y T = \tau \left\{ (D_B \partial_y C) \, \partial_y T + \frac{D_T}{T_\infty} (\partial_y T)^2 \right\} + \frac{k}{\rho c_p} (\partial_{yy} T), \tag{5.3}$$

$$u\partial_x C + v\partial_y C = \left[D_B (\partial_{yy} C) + \left(\frac{D_T}{T_\infty} \right) \partial_{yy} T \right], \tag{5.4}$$

the specified boundary conditions are

$$u(x+y) = U_w(x) = U_0(x+b)^m, \ v(x+y) = 0, \ T(x,y) = T_w, C(x,y) = C_w \ \text{at} \ y = A(x+b)^{\frac{1-m}{2}},$$

$$u(x,y) \to 0, \ T(x,y) \to T_\infty, \ C(x,y) \to C_\infty \ \text{as} \ y \to \infty. \tag{5.5}$$

Here $(u, \ v)$ are the components of velocity in radial and axial directions respectively, μ_∞ is the infinite shear viscosity, μ is the temperature based dynamic viscosity, ρ is the density, T_w is denotes the temperature of wall, σ is electrical conductivity of the liquid, C_w is known as ambient concentration at the wall, C and T are the concentration and temperature respectively, c_p is the specific heat, D_B is the mass diffusivity, T_∞ is the free temperature and D_T is known as thermophoresis diffusivity. In order to justify the nature of viscosity due to inside friction between particles and the stretching surface, consider a mathematical model in which viscosity depends on temperature (used by Ajayi et al. [78]) with appropriate similarity variables defined as

$$\mu(T) = \mu_0[a_1 + b_1(T_w - T)], \tag{5.6}$$

and

$$\Theta(\xi) = \frac{T - T_\infty}{T_w - T_0}, \quad \Phi(\xi) = \frac{C - C_\infty}{C_w - C_0}. \tag{5.7}$$

The main PDEs are reduced into ODEs by using following transformations

$$\begin{aligned} T_w &= T_0 + m_1(x+b)^{\frac{1-m}{2}}, & T_\infty &= T_0 + m_2(x+b)^{\frac{1-m}{2}}, \\ C_w &= C_0 + m_3(x+b)^{\frac{1-m}{2}}, & C_\infty &= C_0 + m_4(x+b)^{\frac{1-m}{2}}. \end{aligned} \tag{5.8}$$

74

Using Eq. (5.8) we get

$$
\begin{aligned}
T_w - T &= (1 - \Theta)(T_w - T_0) - m_2(x + b)^{\frac{1-m}{2}}, \\
C_w - C &= (1 - \Phi)(C_w - C_0) - m_4(x + b)^{\frac{1-m}{2}}.
\end{aligned}
\tag{5.9}
$$

From thermal stratification model, the valid relation can easily be achieved as

$$
\begin{aligned}
b_1 (T_w - T_0) &= b_1 m_1 (x + b)^{\frac{1-m}{2}}, \quad b_1 (T_\infty - T_0) = b_1 m_2 (x + b)^{\frac{1-m}{2}}, \\
b_2 (C_w - C_0) &= m_3 (x + b)^{\frac{1-m}{2}}, \quad b_2 (C_\infty - C_0) = m_4 (x + b)^{\frac{1-m}{2}}.
\end{aligned}
\tag{5.10}
$$

Here T_0 and C_0 are known as reference temperature and concentration.

From Eq. (5.10) we get

$$
\begin{aligned}
b_1 (T_w - T_0) &= \zeta, \quad b_1 (T_\infty - T_0) = \zeta S_t, \quad St = \frac{m_2}{m_1}, \\
b_2 (C_w - C_0) &= \zeta, \quad b_2 (C_\infty - C_0) = \zeta Sc, \quad Sc = \frac{m_4}{m_3}.
\end{aligned}
\tag{5.11}
$$

By using the following similarity variables

$$
\eta = y \sqrt{\frac{(m + 1)U_0}{2\nu}} (x + b)^{\frac{m-1}{2}}, \quad \psi = \left[\sqrt{\frac{2\nu U_0}{m + 1}} F(\eta) \right] (x + b)^{\frac{m-1}{2}}, u = U_0 (x + b)^m F'(\eta),
$$

$$
v = -\left(\frac{(m + 1)\nu U_0}{2} \right)^{\frac{1}{2}} \left[F(\eta) + \eta \frac{m - 1}{m + 1} F'(\eta) \right] (x + b)^{\frac{m-1}{2}}.
\tag{5.12}
$$

The continuity eq. (5.1) is identically satisfied, now by substituting eq. (5.9) into eqs. (5.2)-(5.4) we get the transformed ODEs

75

$$(a+\zeta-\zeta\Theta-S_t\zeta)(1+2We^2F'')F''' - \frac{2m}{m+1}\left(F'\right)^2 + FF'' - \zeta\left(1+We^2F''\right)\Theta'F'' - \frac{2Ha^2}{m+1}F' = 0,$$

$$(5.13)$$

$$\Theta'' + \Pr\left[N_b\Phi'\Theta' + \Theta'F + N_t(\Theta')^2 - \left(\frac{1-m}{1+m}\right)F'St\right] = 0,\qquad(5.14)$$

$$\Phi'' + \frac{N_t}{N_b}\Theta'' + \left[\Pr Le\Phi'F - Le\left(\frac{1-m}{1+m}\right)F'Sc\right] = 0,\qquad(5.15)$$

using eq. (5.5), the boundary conditions will be

$$\begin{aligned}
F'(\alpha) &= 1,\ F(\alpha) = \frac{(m-1)}{(1+m)}\alpha,\ \Theta(\alpha)=1,\ \Phi(\alpha)=1,\ \text{at } \alpha=0,\\
F'(\alpha) &= 0,\ \Theta(\alpha)=0,\ \Phi(\alpha)=0,\ as\ \alpha\to\infty.
\end{aligned}\qquad(5.16)$$

In order to convert the required differential equations and Neumann boundary, put $F(\eta) = f(\eta-\alpha) = f(\xi)$, $\Theta(\eta) = \Theta(\xi-\alpha) = \theta(\xi)$ and $\Phi(\eta) = \Phi(\xi-\alpha) = h(\xi)$, we get

$$((a+\zeta-\zeta\theta-S_t\zeta))(1+2We^2f'')f''' - \frac{2m}{m+1}\left(f'\right)^2 + ff'' - \zeta(1+f''We^2)\theta'f'' - \frac{2}{m+1}Ha^2f' = 0,$$

$$(5.17)$$

$$\theta'' + \Pr\left[\theta'f + N_b\phi'\theta' - \left(\frac{1-m}{1+m}\right)f'St + N_t(\theta')^2\right] = 0,\qquad(5.18)$$

$$\phi'' + \frac{N_t}{N_b}\theta + \Pr\left[Lef\phi' + '' - Le\left(\frac{1-m}{1+m}\right)f'Sc\right] = 0,\qquad(5.19)$$

$$\begin{aligned}
f(\eta) &= \frac{\alpha(m-1)}{(1+m)},\ f'=1,\ \theta(\eta)=1,\ \phi(\eta)=1,\ \text{at } \xi=0,\\
f' &\to 0,\ \theta(\eta)=0,\ \phi(\eta)=0,\ as\ \eta=\infty,
\end{aligned}\qquad(5.20)$$

76

where $b_1(T_w - T_0) = \zeta$ is temperature dependent viscosity, $\alpha = A\left(\frac{U_0(m+1)}{2v}\right)^{0.5}$ is wall thickness parameter, $N_b = \frac{\tau D_B(C_w - C_0)}{\nu}$ is Brownian motion parameter, $Ha^2 = \frac{\sigma H_0^2}{\rho U_0(x+b)^{m-1}}$ is Hartmann number, $\mathrm{Pr} = \frac{uc_p}{k}$ is Prandtl number, $We^2 = \sqrt{\frac{(m+1)U_o^3(x+b)^{3m-1}}{2\nu}}$ is Weissenberg number, $N_t = \frac{\tau D_t(T_w - T_0)}{T_\infty \nu}$ is thermophoresis parameter and $Le = \frac{\nu}{D_B}$ is Lewis number.

To obtain physical interests near the wall i.e. the friction factor coefficient, heat and mass diffusion rates, the following relations are used:

$$C_f = \frac{\tau_w}{\rho\sqrt{\frac{m+1}{2}}}, \quad Nu = \frac{(x+b)q_w}{\rho\sqrt{\frac{m+1}{2}}}, \quad Su = \frac{(x+b)J_w}{\rho\sqrt{\frac{m+1}{2}}}. \tag{5.21}$$

Here τ_w denotes the shear stress or skin friction, q_w and J_w denotes the heat and mass diffusions near the wall, where τ_w, q_w and J_w are defined as:

$$\tau_w = \mu\left[\partial_y u + \frac{\Gamma}{2}(\partial_y u)^2\right]_{y=A(x+b)^{\frac{1-m}{2}}}, \quad q_w = -k\left[\partial_y T\right]_{y=A(x+b)^{\frac{1-m}{2}}}, \quad J_w = -D_b\left[\partial_y C\right]_{y=A(x+b)^{\frac{1-m}{2}}}. \tag{5.22}$$

After using the scaling variables, friction factor, Nusselt and Sherwood numbers transformed into:

$$C_f\left(\mathrm{Re}_x^{\frac{1}{2}}\right) = (a + \zeta - \zeta\Theta - S_t\zeta)\left[f''(\eta) + We^2\left(f''(\eta)\right)^2\right]_{\eta=0}, \tag{5.23}$$

$$Nu\,\mathrm{Re}_x^{\frac{-1}{2}} = -\theta'(0), \quad Sh\,\mathrm{Re}_x^{\frac{-1}{2}} = -\phi'(0). \tag{5.24}$$

Where $\mathrm{Re}_x = \left(\frac{U_0(x+b)^{m-1}}{\nu}\right)^{\frac{1}{2}}$.

5.2 Numerical procedure

Numerical solutions for nonlinear self-similar differential system i.e. eqs. (5.17)-5.19) along with boundary conditions (5.20) are solved numerically by utilizing RK-4 procedure in conjunction with shooting technique. Among some other numerical techniques, shooting method is more adaptable because initial guesses control the convergence criteria. The main steps to achieve the numerical solutions by shooting technique are as follows:

77

1. Convert eqs. (5.17)-(5.19) into a system of 1st order ordinary differential equations.

2. Use the end conditions to generate three unknowns.

3. Finally, solve the first order system via Runge-Kutta method.

4. Calculate the boundary layer residuals, if these residuals are less than error tolerances i.e. 10^{-6}, than solution will be achieved, otherwise we modify initial guesses with Newton's method.

5. This procedure is repeated until it satisfies the convergence criteria i.e. 0.0001.

5.3   Results and discussion

This section describes the impact of different emerging parameters i.e, thermal stratification St, Weissenberg number We^2, Prandtl number Pr, viscosity parameter ζ, thermophoretic parameter N_b, Hartmann number Ha^2 and Lewis number Le on velocity profile, skin friction, Sherwood number, temperature profile, Nusselt number and concentration profile. Fig. 5.2 presents the variation in stretching velocity m on $f'(\eta)$ profile. Figure shows that the velocity distribution improves by incrementing the stretching velocity index m. The physical reason behind this is that on enhancing velocity, stretching rate m generates extra forces in the direction of flow, causing enhancement in velocity profile. Fig. 5.3 illustrates the variations in wall thickness parameter α on velocity distribution. It is found that by enhancing the values of α velocity profile reduces. Because for large values of wall thickness parameter α, the thickness of the sheet increases, so resistance is created between the fluid particles in the direction of flow causing reduction in velocity profile. It is found that the velocity close the sheet reduces as that is α enhances for $m < 1$ and opposite behavior is noticed for $m > 1$. Fig. 5.4 shows the impact of Ha^2 number on velocity profile. It is found that the velocity declines for large values of Ha^2 number. Because large values of Ha^2 number produces a drag-like force (Lorentz force) which converges the fluid motion in the direction of flow and velocity gradient. Fig. 5.5 represents the variation in thermal stratification St on horizontal velocity distribution. It is noticed that the horizontal velocity profile reduces for large values of thermal stratification St. Fig. 5.6 scrutinizes the influence of Weissenberg number of We^2 on velocity situation. It is clear that velocity gradient decreases by increasing the values of We^2. Because Weissenberg number We^2

enlarges the relaxation time of the material which produces resistance to flow, so reduction in velocity is noticed. Fig. 5.7 examines the variation in viscosity parameter ζ on velocity profile. It can be examined that enhancement in the magnitude of temperature dependent viscosity ζ causes reduction in velocity profile. Because due to increase in viscosity parameter the fluid become more thick causing reduction in velocity profile.
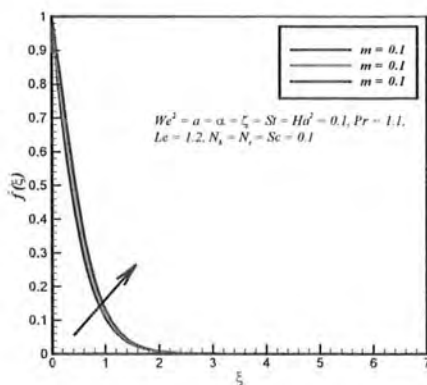

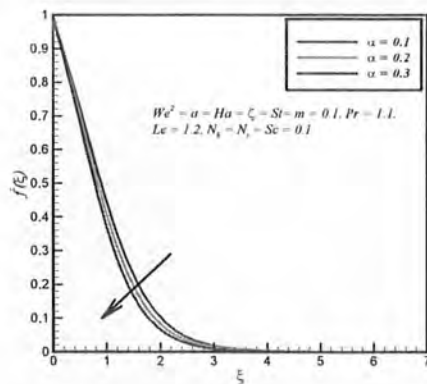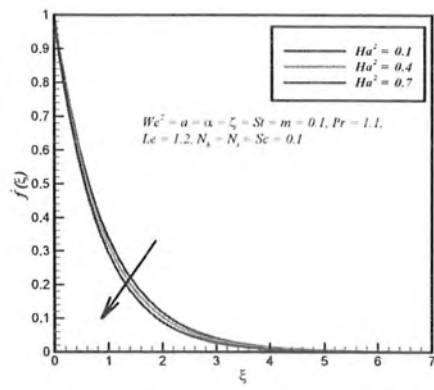Fig. 5.2. Influence of m on $f'(\xi)$.

Fig. 5.3. Influence of α on $f'(\xi)$.

Fig. 5.4. Influence of Ha^2 number on $f'(\xi)$.
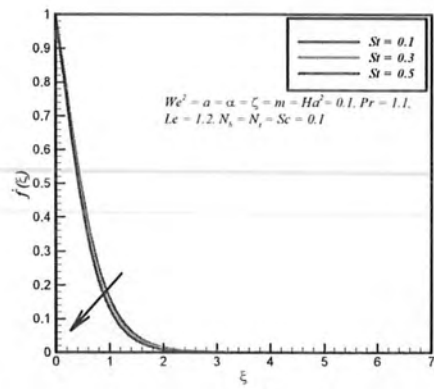
Fig. 5.5. Influence of St on $f'(\xi)$.

80
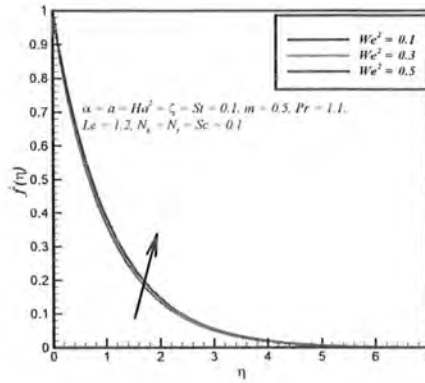
Fig. 5.6. Influence of We^2 number on $f'(\xi)$.
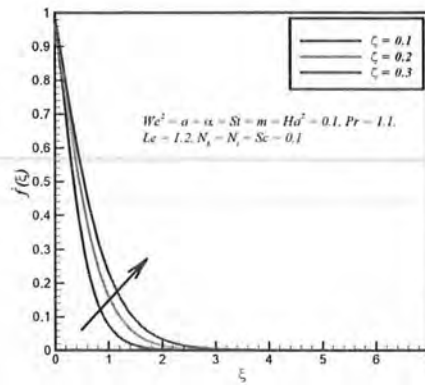
Fig. 5.7. Influence of ζ on $f'(\xi)$.

Fig. 5.8 is plotted to see the behavior of Prandtl number Pr on temperature profile. Prandtl number Pr relates momentum and thermal diffusions in the boundary layer region. The temperature and thermal boundary layer decreases due to reduction in thermal diffusion. Fig. 5.9 is plotted to see the nature of Brownian motion N_b on temperature profile. Temperature consistently increases by enhancing values of Brownian moment parameter N_b. It is due to the fact that increase in N_b accelerates collision among fluid particles and thus temperature enhances.

81

Fig. 5.10 is plotted to observe the nature of thermophoretic parameter N_t on temperature profile. It is clear that the thermophoretic parameter N_t rises the temperature distribution. Because nanoparticles transfer heat from hot to cold region causing temperature of the fluid to increase. Fig. 5.11 deliberates the impact of St on temperature profile. It is due to the fact that temperature is increasing function of thermal stratification St. Because thermal boundary diminishes for large values of the thermal stratification St.
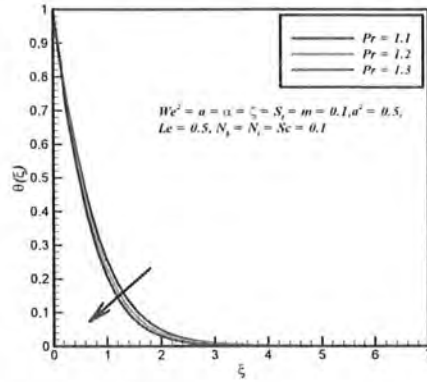
Fig. 5.8. Influence of Pr on $\theta(\xi)$.
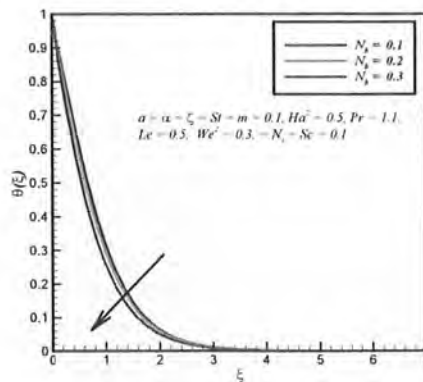
Fig. 5.9. Influence of N_b on $\theta(\xi)$.
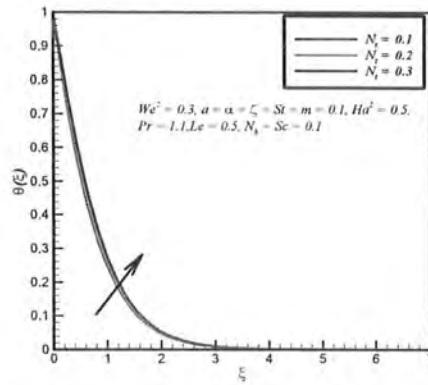
Fig. 5.10. Influence of N_t on $\theta(\xi)$.
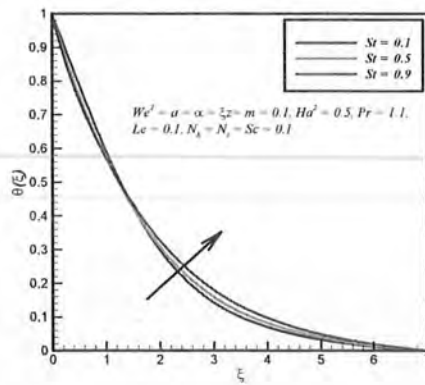
Fig. 5.11. Influence of St on $\theta(\xi)$.

The distinction on concentration for various values of Lewis number Le is seen in fig. 5.12. View in this case is that for large values of Le declines in concentration distribution. Because for large values of Lewis number Le mass diffusivity reduces near the boundary layer region causing reduction in concentration profile. Fig. 5.13 illustrates the fluid concentration distribution for changing values of stretching index m. It is found that stretching velocity m rises the concentration profile due to enhancement of fluid particles near the surface of plate. Fig. 5.14

shows the heat diffusion rate for unlike values of Pr. It is clear from this plot that the behavior of heat diffusion rate decays for higher values of Prandtl number Pr. **Tables 5.1-5.3** illustrate the local friction factor, heat and mass diffusion rates for unlike values of Weissenberg number We^2, Prandtl number Pr, thermophoretic parameter N_t, Hartmann number Ha^2, Lewis number Le and thermal stratification St.
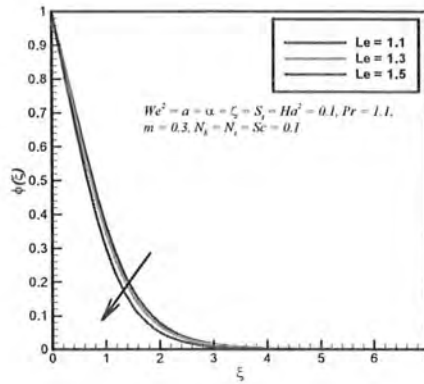
Fig. 5.12. Influence of Le on $\phi(\xi)$.
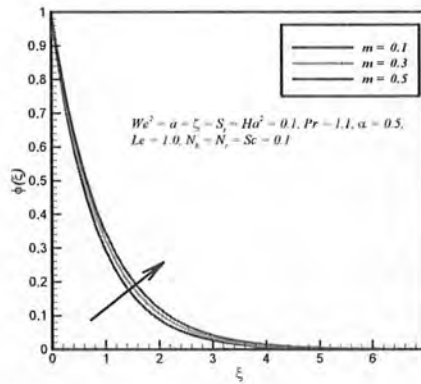
Fig. 5.13. Influence of St on $\phi(\xi)$.
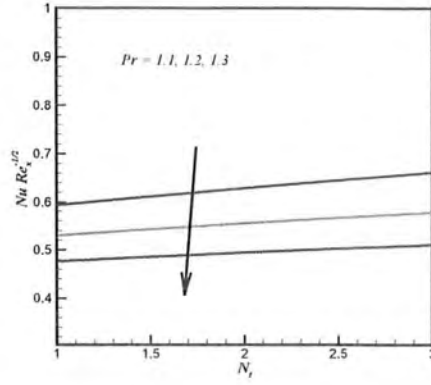
Fig. 5.14. Influence of N_t and Pr on $Nu\mathrm{Re}_x^{\frac{1}{2}}$.

Table 5.1: Computational results of wall friction factor for unlike values of ζ, δ_t, Ha^2 and α when $m = 0.5$, $N_t = N_b = Le = Sc = We^2 = 0.1$, Pr $= 0.1$ and $\alpha = 0.9$.

ζ	St	Ha^2	α	$C_f\,\mathrm{Re}_x^{\frac{1}{2}}$
0.1	0.1	0.1	0.9	1.2104
0.2				0.8276
0.3				0.5984
0.1	0.1	0.1	0.9	1.2104
	0.2			1.2569
	0.3			1.3064
0.1	0.1	0.1	0.9	1.2104
		0.2		1.1112
		0.1		0.9527
0.1	0.1	0.1	0.9	1.2104
			1.0	1.2769
			1.1	1.3163

85

Table 5.2: Numerical values of heat diffusion rate i.e. $\left(-Nu\,\mathrm{Re}_x^{\frac{-1}{2}}\right)$ for unlike values of Pr, N_t and St.

N_t	Pr	St	$-Nu\mathrm{Re}_x^{\frac{-1}{2}}$
0.1	1.1	0.1	0.5047
0.2			0.5536
0.3			0.7530
0.1	1.1	0.1	0.5047
	1.2		0.5336
	1.3		0.5615
0.1	1.1	0.1	0.5047
		0.2	0.5718
		0.3	0.5309

Table 5.3: Computational results of mass transfer rate i.e. $(-\phi'(0))$ for different values of Le, Pr and S_t

Le	Pr	St	$-Sh\mathrm{Re}_x^{\frac{1}{2}}$
0.1	1.1	0.1	1.1676
0.2			1.2013
0.3			1.2495
0.1	1.1	0.1	1.1676
	1.2		1.1701
	1.3		1.1727
0.1	1.1	0.1	1.1676
		0.2	1.1670
		0.3	1.1662

Chapter 6

Change in internal energy of thermal diffusion stagnation point with Maxwell nanofluid flow along with solar radiation and thermal conductivity

This chapter concerns the characteristics of heat and mass transfer in upper convected Maxwell fluid flow over a linear stretching sheet with solar radiation, viscous dissipation and temperature based viscosity. After boundary layer approximation, the governing equations are achieved (namely Maxwell, upper convected material derivative, thermal and concentration diffusions). By using the self-similarity transformations the governing PDEs are converted into nonlinear ODEs and solved by RK-4 method in combination with Newton Raphson (shooting technique). The effects of developed physical parameters on velocity, temperature, concentration, fraction factor, heat and mass diffusions are exemplified through graphs and tabular form and are deliberated in detail. Numerical values of fraction factor, heat and mass transfer rates with several parameters are computed and examined.

6.1 Mathematical formulation

Let us consider thermal radiation, thermal conductivity, viscous dissipation and chemical reaction on two dimensional laminar steady heat and mass transfer flow of an electrically conducting upper convected Maxwell nanofluid flow passed by a linear stretching surface placed in x-direction and y-axis is vertical to the sheet with stagnation point at the origin (as illustrated in Fig. 6.1). It is assumed that the sheet is stretching with linear velocity $u = U_w(x) = cx$ and the free stream velocity is $u = u_e(x) = ax$, here a and c are positive constants. The temperature at the surface is conserved at T_w and T_∞ for away from the plate, and same assumption for nanoparticle volume fraction C_w and C_∞. An external magnetic field H_0 normal to the stretching sheet is applied.
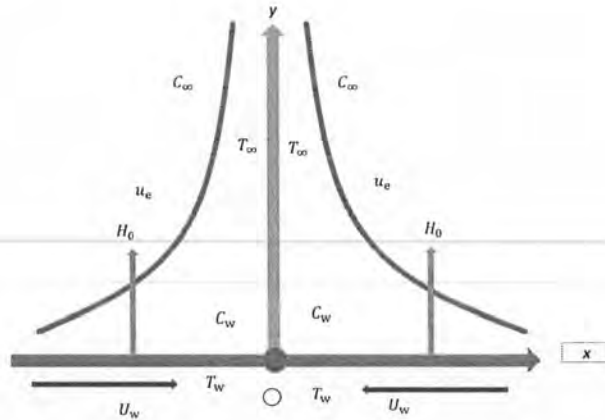
Fig. 6.1. Schematic representation of the problem.

From the above basic assumptions, the required governing equations are as follow:

$$\partial_x u + \partial_y v = 0, \tag{6.1}$$

$$u\partial_x u + v\partial_y u + \lambda \left[u^2 \partial_{xx} u + v^2 \partial_{yy} u + uv\partial_{xy} u \right] = -\frac{1}{\rho}\partial_x P + \partial_y\left(\mu \partial_y u\right) - \frac{\sigma \mu_e^2 H_0^2}{\rho}\left(u + \lambda v \partial_y u\right) - \frac{\mu F_s}{\rho K^*}u - \frac{\rho F_s}{\sqrt{K^*}}u^2, \tag{6.2}$$

88

due to hydrostatic and magnetic pressure gradient the force will be in equilibrium as given by

$$-\frac{1}{\rho}\partial_x P = u_e\frac{du_e}{dx} + \frac{\sigma\mu_e^2 H_0^2}{\rho}u_e.$$ (6.3)

Hence, eq. (6.2) becomes

$$u\partial_x u + v\partial_y u + \lambda\left[u^2\partial_{xx}u + v^2\partial_{yy}u + uv\partial_{xy}u\right] = u_e\frac{du_e}{dx} + \partial_y\left(\mu\partial_y u\right) - \frac{\sigma\mu_e^2 H_0^2}{\rho}\left(u - u_e + \lambda v\partial_y u\right) - \frac{\mu}{\rho K^*}u - \frac{\rho F_s}{\sqrt{K^*}}\iota$$ (6.4)

now energy and concentration equations are

$$u\partial_x T + v\partial_y T = \frac{1}{\rho c_p}\partial_y\left(k\partial_y T\right) - \frac{1}{\rho c_p}\partial_y q_r + \tau\left\{D_B\left(\partial_y T\partial_c C\right) + \frac{D_T}{T\infty}\left(\partial_y T\right)^2\right\} + \frac{\mu}{\rho c_p}\left(\partial_y u\right)^2,$$ (6.5)

$$u\partial_x C + v\partial_y C = D_B\partial_{yy}C + \frac{D_T}{T\infty}\partial_{yy}T - k_r(C - C_\infty),$$ (6.6)

the boundary condition are given as

$$
\begin{aligned}
u(x,y) &= U_w(x) = ax,\ v(x,y) = 0,\\
T(x,y) &= T_w(x) = T_\infty + bx,\ C(x,y) = C_w = C_\infty + bx,\ \text{at } y = 0,\\
u(x,y) &= u_e(x) = cx,\ T(x,y) = T_\infty,\ C(x,y) = C_\infty,\ \text{as } y \to \infty.
\end{aligned}
$$ (6.7)

The temperature based viscosity (see Ref. [87]) is

$$\mu(T) = \mu_0 e^{-m_0(T - T_\infty)},$$ (6.8)

and the temperature based thermal conductivity is given as

$$k = k_\infty\left(1 + \varepsilon\frac{T - T_\infty}{T_w - T_0}\right),$$ (6.9)

89

where q_r is the radiative heat flux, utilizing the Rosseland approximation for radiation (see Ref. [88]), we get

$$\mathbf{q}_r = -\frac{4\alpha^\circ}{3k^\circ}\partial_y T^4,$$

(6.10)

expressing T^4 by utilizing Taylor's series term about T_∞ and neglecting higher order terms

$$T^4 \approx 4TT_\infty^3 - 3T_\infty^4,$$

(6.11)

using Eq. (6.10) and Eq. (6.11)

$$\partial_y \mathbf{q}_r = -\frac{16\alpha^\circ T_\infty^3}{3k^\circ}\partial_{yy}T,$$

(6.12)

here μ_0 is the fluid viscosity, F_s is the inertial factor, K^* is the permeability, k_r is the rate of chemical reaction, m_0 is the variation viscosity, k° is the absopation constant, α° is the Stefan-Boltzman constant, (u, v) are the velocity components along the (x, y) directions, ρ is the density, μ_e is the magnetic permeability velocity, σ is the electrical conductivity, λ is the Maxwell fluid parameter, ν is the kinematic viscosity, k represents thermal conductivity, D_B is the Brownian motion, $\tau = \frac{(\rho c)_s}{(\rho c)_f}$ is the ratio of nanopartical heat capacity and base fluid thermal capacity, $\alpha_f = \frac{k}{(\rho C_p)_f}$ represents thermal diffusion, $T_w(x,y)$ is known as temperature at the wall, $C_w(x,y)$ is known as concentration at the wall, T and C are the temperature and concentration of the fluid respectively, C_p is the specific heat, T_∞ and C_∞ are the free stream temperature and concentration. Temperature of the sheet is $T_w = T_\infty + bx$, for heated surface $b > 0$ so $T_w > T_\infty$ and for cooled surface $b < 0$ and $T_w < T$, b is a constant and D_T is known as thermophoresis diffusivity

The similarity variables give the dimensionless quantities

$$\eta = y\sqrt{\frac{a}{\nu}}, \ \Psi = xf(\eta)\sqrt{a\nu}, \ \theta(\eta) = \frac{T - T_\infty}{T_w - T_\infty}, \ \phi(\eta) = \frac{C - C_\infty}{C_w - C_\infty}, \ u = \frac{\partial\psi}{\partial y}, \ v = -\frac{\partial\psi}{\partial x}. \ (6.13)$$

Incompressibility condition (6.1) is automatically satisfied and eqs. (6.4)-(6.6) takes the following nonlinear differential form

90

$$(1 + \zeta\theta) f''' + \zeta\theta' f'' + f'f'' - (f')^2 + \lambda_m \left(2f(\eta)f'f'' - (f(\eta))^2 f''' \right) + Ha^2 \left(1 - f' + \lambda_m f'f'' \right)$$

$$- (1 + \zeta\theta) \lambda f' - F_c (f')^2 + 1 = 0, \tag{6.14}$$

$$\left(1 + \zeta\theta + \frac{4}{3}R \right) \theta'' + \varepsilon (\theta')^2 + (1 + \zeta\theta)Ec (f'')^2 + \Pr \left[f(\eta)\theta' + N_b \phi'\theta' + N_t (\theta')^2 \right] = 0, \tag{6.15}$$

$$\phi'' + \frac{N_t}{N_b}\theta'' + \Pr Le \left(f(\eta)\phi' - K\phi(\eta) \right) = 0, \tag{6.16}$$

using (6.12), the associated boundary conditions are

$$
\begin{aligned}
f' &= 1, \ f(\eta) = 0, \ \theta(\eta) = 1, \ \phi(\eta) = 1, \ \text{at } \eta = 0, \\
f' &\to \frac{c}{a}, \ \theta \to 0, \ \phi \to 0, \ \text{as } \eta \to \infty.
\end{aligned}
\tag{6.17}
$$

where fluid relaxation parameter is $\lambda_m = \lambda a$, local inertia factor is $F_c = \frac{F_s x}{\sqrt{K^*}}$, Hartmann number is $Ha^2 = \mu_e H_0 \sqrt{\frac{\sigma}{\rho a}}$, porosity parameter is $\lambda = \frac{\nu}{aK^*}$, Prandtl number is $\Pr = \frac{\mu c_p}{k_\infty}$, radiation parameter is $R = \frac{16\alpha^\circ T_\infty^3}{k3k^\circ}$, $\zeta = e^{-(T_w - T_\infty)}$ variable viscosity parameter, thermophoresis parameter is $N_t = \frac{\tau D_t(T_w - T_0)}{T_\infty \nu}$, Eckert number is $Ec = \frac{u_e^2}{(T_w - T_\infty)c_p} = \frac{c^2 x}{bc_p}$, Lewis number is $Le = \frac{\alpha}{D_B}$, Brownian motion parameter is $N_b = \frac{\tau D_B(C_w - C_0)}{\nu}$ and chemical reactive species is $\frac{k_r}{a}$.

Friction factor coefficient (C_f) is defined as:

$$C_f = \frac{\tau_w}{\rho u_e^2} = \mathrm{Re}_x^{\frac{-1}{2}} \left[f''(0) + \lambda_m(f'(0) f''(0) + f(0) f'''(0)) \right], \tag{6.18}$$

here τ_w denotes the wall shear stress

91

$$\tau_w = \mu \partial_y \left(u + \lambda v \partial_y u \right)_{y=0}. \qquad (6.19)$$

The Nusselt number is defined as

$$q_w = -k \left(\partial_y T \right)_{y=0}, \implies Nu_x = \frac{-x q_w}{k \left(T_w - T_\infty \right)} = - \operatorname{Re}_x^{\frac{-1}{2}} \left(1 + \varepsilon \theta \left(0 \right) + \frac{4}{3} R \right) \theta' (0). \qquad (6.20)$$

The mass transfer rate is defined as

$$J_w = -D_B \left(\partial_y C \right)_{y=0}, \implies Sh_x = \frac{-J_w x}{D_B \left(T_w - T_\infty \right)} = - \operatorname{Re}_x^{\frac{-1}{2}} \phi' (0).$$

Where $\operatorname{Re}_x = u_e \left(x \right)$ is local Reynolds number.

6.2 Numerical Procedure

Nonlinear differential eqs. (6.14)-(6.16) with boundary condition (6.17) are solved by a convenient Runge-Kutta based shooting technique. Among some other numerical methods, shooting method (Cash and karp) is more flexible for the aim that the initial guesses control the convergent criteria. The main steps are as follows:

1.   Reduce differential eqs. (6.14)-(6.16) into a system of first order differential form.

2.   Insert the three unknown initial approximation.

3.   Finally, solved the converted system of 1st order equations by Runge-Kutta based shooting scheme.

4.   The unfamiliar unknown initial conditions have been approximated with Newton's method in such a way that the residuals are less than error i.e 10^{-6}.

5.   The computational solution is repeated until convergent criteria is not satisfied.

6.3 Results and discussion

In the current section, the governing phyical parameters and numerical results are illustrated through figures and tables. Figs. (6.2-6.6) describe the physical behavior of non-dimesnional

92

velocity subject to Hartmann number, porosity parameter, inertia factor, fluid relaxation parameter and temperature based fluid viscosity parameter. Fig. 6.2 represents the velocity profile for several values of Hartmann number Ha^2. It is analyzed from this figure that by enhancing values of Hartmann number Ha^2 decelerates the velocity profile. Fig. 6.3 illustrates the influence of velocity graph for various values of porosity parameter λ. It is seen that by rising the values of porosity parameter λ declines the velocity profile. Because the permeability enhances the resistance of the permeable sheet which tends to decrease the velocity profile. Fig. 6.4 illustrates the variation in inertia factor F_c on velocity profile. It is obvious that improvement in values of F_c sorts a resistive force which decelerates the velocity plot. Fig. 6.5 describes the variation on velocity profile for corresponding values of fluid relaxation parameter λ_m. It is clear from this figure that the momentum boundary layer thickness reduces by increasing the fluid relaxation parameter λ_m and consequently induces an intensifications in the absolute values of the velocity profile at the surface. Fig. 6.6 examines the effect of temperature based fluid viscosity ζ on velocity profile. It can be analyzed that the velocity profile enhances by enhancing the temperature based fluid viscosity parameter ζ.
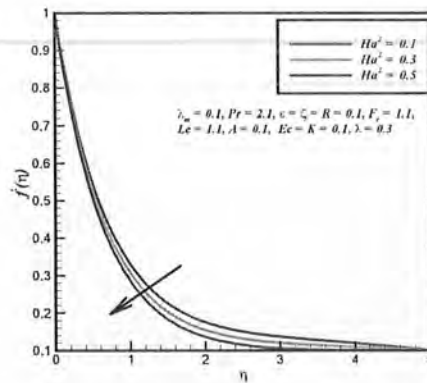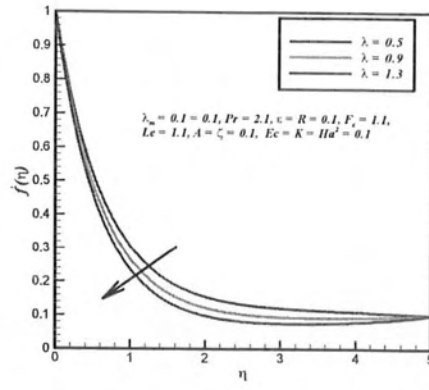

Fig. 6.2. Outcome of Ha^2 on $f'(\eta)$.

Fig. 6.3. Outcome of λ on $f'(\eta)$.
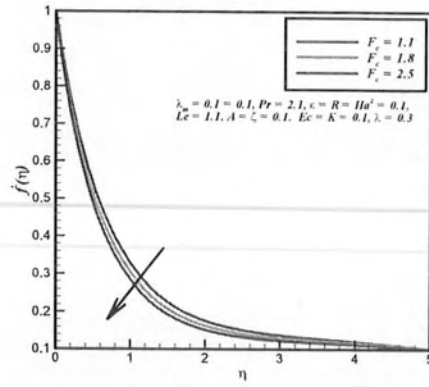

Fig. 6.4. Outcome of F_c on $f'(\eta)$.

94
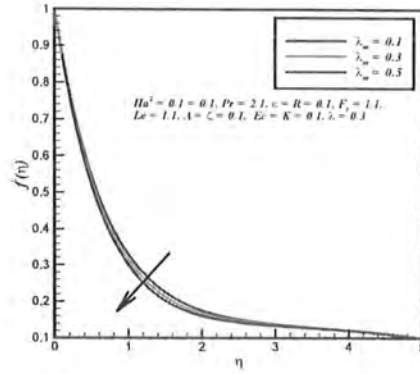
Fig. 6.5. Outcome of λ on $f'(\eta)$.
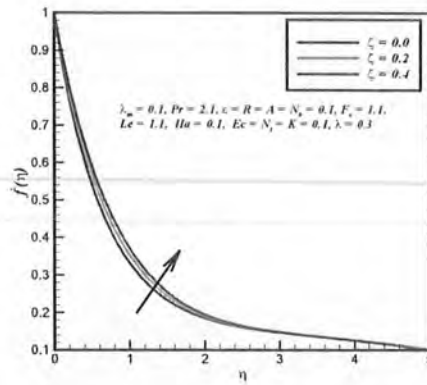
Fig. 6.6. Outcome of ζ on $f'(\eta)$.

The disparity in temperature distribution with reference to similarity variables such as Prandtl number , Brownian motion factor , thermophoresis constraint, thermal radiation parameter, Eckert number and small parameter are presented in Figs. (6.7-6.12). It is perceived that Fig. 6.7 represents the temperature distribution for corresponding values of Pr. By enhancing the values of Pr reduces the temperature profile and also reduces thermal boundary layer thickness. Fig. 6.8 illustrates the deviation on temperature for different values of N_b. It can be seen as N_b enhances the mass diffusivity rises which leads to increase the temperature

profile in the boundary layer segment. Fig. 6.9 shows the variation of N_t on temperature profile. It is found that for improved values of N_t temperature distribution also top ups. Because increase in the values of N_t, generates the rise in the thermophoresis force which has trend to move nanomaterials from hot surface to the cold surface. Fig. 6.10 establishes the effect of Eckert number Ec on temperature profile. It is clear that the kinetic motion increases by increasing the energy enthalpy which enhances the temperature profile. Fig. 6.11 displays the influence of thermal radiation R on temperature distribution. It is seen that the temperature profile rises due to fact that the conduction effects of the nanoliquid enhances in the occurrence of thermal radiation R. Therefore for large values of radiation parameter R surface becomes more heated, which causes heat transfer rate within boundary layer region to increase. It is also clear that the thermal boundary layer rises by increasing the radiation parameter R. Fig. 6.12 examines the influence of small parameter ε on temperature distribution. It is noticed that enhance in small parameter ε corresponding to improve the kinetic energy of the fluid material which enhances variation of thermal characteristics.

Fig. 6.7. Outcome of Pr on $\theta(\eta)$.

Fig. 6.8. Outcome of N_b on $\theta(\eta)$.

Fig. 6.9. Outcome of N_t on $\theta(\eta)$.

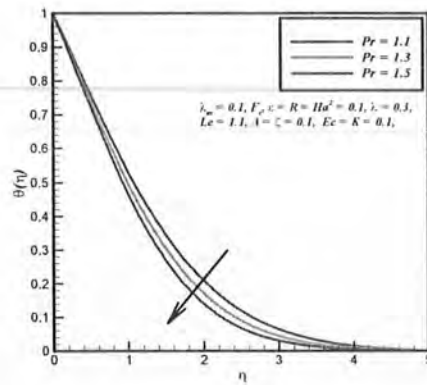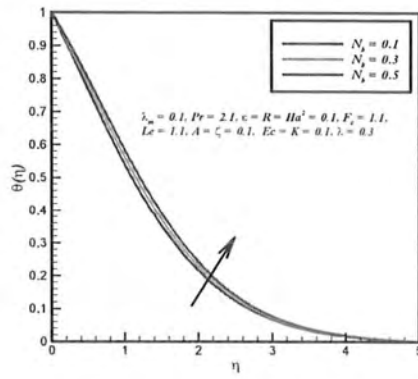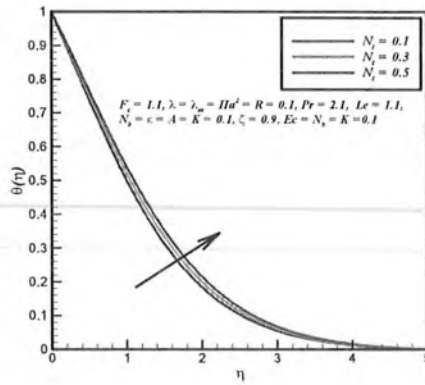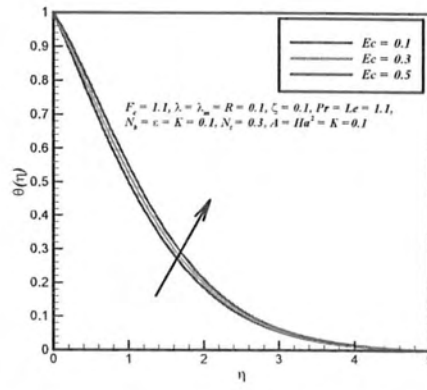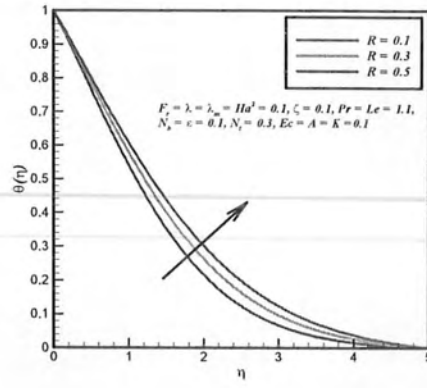Fig. 6.10. Outcome of Ec on $\theta(\eta)$.

Fig. 6.11. Outcome of R on $\theta(\eta)$.

98
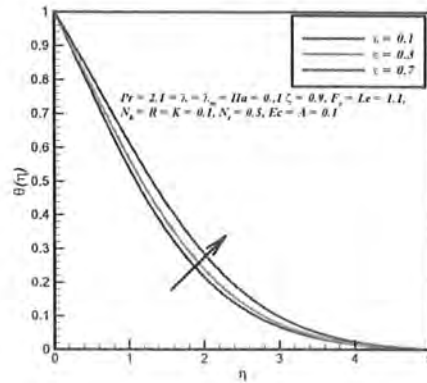
Fig. 6.12. Outcome of ε on $\theta(\eta)$.

The behavior of nanoparticles concentration against Lewis number and chemical reaction are discussed in figs. 6.13-6.14. It is apparent that fig. 6.13 scrutinizes the influence of Lewis number Le on concentration profile. It can be examined that the concentration profile reduces significantly for developing values of Lewis number Le. Fig. 6.14 reveals the influence of chemical reactive species K on concentration profile. It is seen that for extensive values of K, concentration profile reduces.

Figs. 6.15 and 6.16 show skin friction coefficient and heat transfer rate for different values of variable viscosity parameter ζ and Eckert number Ec along Ha^2 and Pr. It is clear that the reduction in fraction factor and heat transfer rate is noticed for enhanced values of ζ and Ec. Fig. 5.17 represents the nature of mass transfer rate for several values of chemical reaction K along Le. It is found that the mass transfer rate increases for increasing values of chemical reaction K.

Tables 6.1 and 6.2 demonstrate the deviation in several physical parameters for friction factor $C_f \operatorname{Re}_x^{\frac{1}{2}}$ and heat transfer rate $\operatorname{NuRe}_x^{\frac{-1}{2}}$. It is found that reduction is noticed for rising values of variable viscosity parameter ζ, inertia factor F_c, porosity parameter λ, Eckert number Ec and thermophoresis parameter N_b and increase is noticed for Ha^2 and Pr. Table 6.3 designates the numerical results on the mass transfer rate $\operatorname{ShRe}_x^{\frac{-1}{2}}$ for several physical parameter. It can be analyzed that the mass transfer rate $\operatorname{ShRe}_x^{\frac{-1}{2}}$ is enhancing function for increasing parameters Le,

K and N_b. For the justification of current numerical scheme, the results are compared with Afify and Elgazery [89] in a limiting case for $Ec = R = \varepsilon = Ga = F_R = 0.1$, $N_b = 0.1$, $N_t = 0.5$, and $\Pr = Le = 1.0$. The numerical results show good agreement as demonstrated in **Table 6.4**. Further the numerical outcomes are also compared with Khan and Pop [81] in **Table 6.5**.
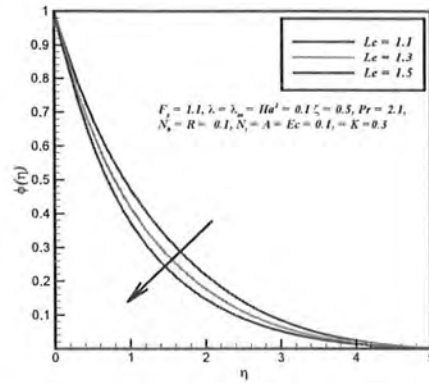
Fig. 6.13. Outcome of Le on $\phi(\eta)$.
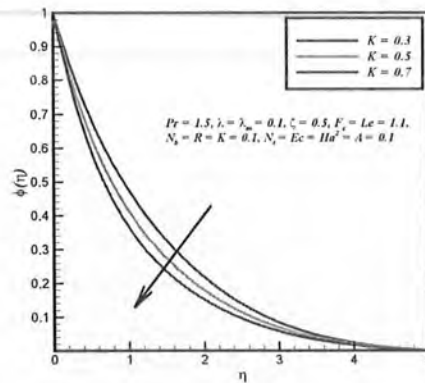
Fig. 6.14. Outcome of K on $\phi(\eta)$.

100
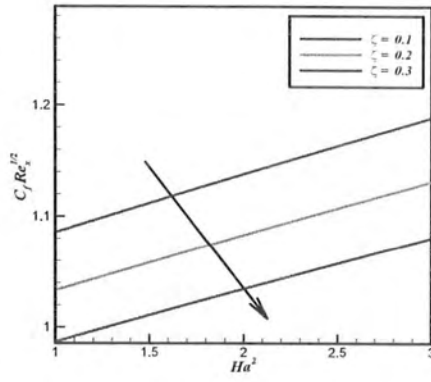
Fig. 6.15. Outcome of ζ and Ha^2 on skin friction coefficient.
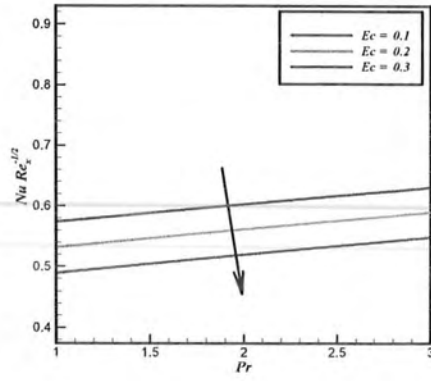
Fig. 6.16. Outcome of Ec and Pr on Nusselt number.
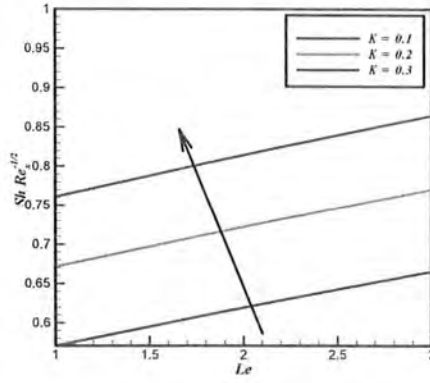
Fig. 6.17. Outcome of K and Le on Nusselt number.

Table 6.1: Numerical results of $[f''(0) + \lambda_m(f'(0) f''(0) + f(0) f'''(0))]$ for different values of Ha^2, ζ, F_r and λ when $\lambda_m = 0.1$, $N_t = 0.5$, $N_b = Ec = \varepsilon = K = 0.1$, $\Pr = 2.1$ and $Le = 1.5$.

Ha	ζ	F_c	λ	$-C_f \operatorname{Re}_x^{\frac{1}{2}}$
0.1	0.1	1.1	0.1	1.2473
0.2				1.2862
0.3				1.3243
0.1	0.1	1.1	1.1	1.2473
	0.2			1.3278
	0.3			1.1314
0.1	0.1	1.1	1.1	1.2473
		1.2		1.2709
		1.3		1.2941
0.1	0.1	1.1	0.1	1.2473
			0.2	1.2835
			0.3	1.3189

102

Table 6.2: Computational results of $-(1+\varepsilon\theta(0)+\frac{4}{3}R)\theta'(0)$ for unlike values of Pr, Ec, and N_t when $\lambda_m = N_b = Ec = Ha^2 = \zeta = \lambda = K = F_r = 0.1$, $\zeta = 0.9$ and $Le = 1.1$.

Pr	Ec	N_t	$-Nu\,Re_x^{\frac{1}{2}}$
1.1	0.1	0.1	0.5734
1.2			0.6024
1.3			0.6299
0.1	0.1	0.1	0.5734
	0.2		0.5311
	0.3		0.4886
0.1	0.1	0.1	0.5734
		0.2	0.5541
		0.3	0.5354

Table 6.3: Numerical results of $-\phi'(0)$ for corresponding values of Le, K and N_b.

Le	K	N_b	$-ShRe_x^{\frac{1}{2}}$
1.1	0.1	0.1	0.5707
1.2			0.6189
1.3			0.6651
0.1	0.1	0.1	0.5707
	0.2		0.6711
	0.3		0.7610
0.1	0.1	0.1	0.5707
		0.2	0.6090
		0.3	0.6815

Table 6.4: Comparison of the friction factor $C_f \ \text{Re}_x^{\frac{1}{2}}$ for various values λ_m and Ha^2 when $N_b = 0.1$.

λ_m	Ha^2	Afify et al. [89]	Prsent Results
0.5	0.0	-1.68935	-1.4593
0.5	0.1	-1.69715	-1.5516
0.5	0.2	-1.72034	-1.7131
0.5	0.3	-1.75830	-1.7403
0.0	0.1	-1.00499	-1.0112
0.1	0.2	-2.49440	-2.4326

Table 6.5: Numerical comparison of heat transfer rate $-\theta'(0)$ and mass transfer rate $-\phi'(0)$ when $Pr = 10$ and $N_b = 0.1$

N_t	Khan and Pop [81] $-\theta'(0)$	Khan and Pop [81] $-\phi'(0)$	Presnt Results $-\theta'(0)$	Presnt Results $-\phi'(0)$
0.1	0.9524	2.1294	0.9834	2.0184
0.2	0.6932	2.2732	0.7821	2.1531
0.3	0.5201	2.5286	0.5789	2.4871
0.4	0.4026	2.7952	0.4001	2.7831
0.5	0.3211	3.0351	0.3301	3.0021

Chapter 7

Arrhenius activation in MHD radiative Maxwell nanoliquid flow along with transformed internal energy

In this chapter, theoretical study is performed to analysis the behavior of transformed internal energy in magnetohydrodynamic Maxwell nanofluid flow over a stretching sheet along with Arrhenius activation energy and chemical reaction. The suitable similarity transformations are used to convert the constitute governing nonlinear PDEs into ODEs. Runge-Kutta based shooting approach is used in order to yield the numerical solution of the differential system. The effects of involved physical parameters are explored through graphical investigations. The numerical results of skin friction coefficient, rate of heat and mass transport are analyzed through graphs and tables. The temperature distribution is explored with the variation in Eckert number, small parameter, Brownian parameter, thermophoresis parameter and thermal radiation parameter, and Prandtl number. Moreover, the concentration profile also studied with the increase in Lewis number. Achieved numerical results will be compared with the obtaied results in limiting cases.

7.1 Mathematical analysis

7.1.1 Preservation of mass, momentum, energy and concentration

Let us consider Arrhenius activation energy and viscous dissipation on two dimensional, laminar heat and mass transfer flow in an electrical conducting upper convected Maxwell nanofluid flow passed by a linear stretched surface. Stagnation point occurs at the origin as shown in Fig. 7.1. It is assumed that the stretching velocity at the surface is $u = U_w(x) = cx$ and the free stream velocity is $u = u_e(x) = ax$, here a and c are positive constants. The temperature at the surface is T_w and T_∞ for away from the plate and same assumptions for nanoparticle volume fractions (C_w and C_∞). An external magnetic field H_0 is applied normal to the sheet.
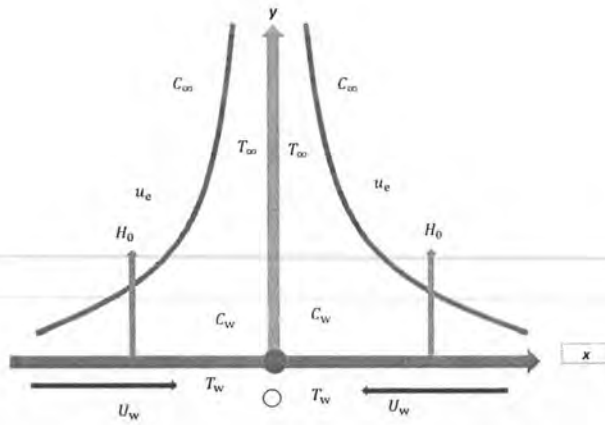

Fig. 7.1. Geometry of the problem.

Under these approximations the required equations are:

Continuity:

$$\text{div } \mathbf{V} = 0, \tag{7.1}$$

Momentum:

$$\rho \frac{d\mathbf{V}}{dt} = -\nabla P + \text{div } \mathbf{S} + \mathbf{J} \times H_0, \tag{7.2}$$

The upper-convected Maxwell (UCM) fluid Cauchy stress tensor is given by

$$\boldsymbol{\tau} = -P\mathbf{I} + \mathbf{S}, \text{ where } \mathbf{S} + \lambda\frac{D\mathbf{S}}{Dt} = \mu\mathbf{A}_1, \tag{7.3}$$

in which $\boldsymbol{\tau}$ is the Cauchy tensor, $\mathbf{S}$ is the extra tensor, μ is the dynamic viscosity, $\mathbf{J}$ is the current density, λ is the relaxation parameter, $\mathbf{A}_1 = (\boldsymbol{\nabla}\mathbf{V}) + (\boldsymbol{\nabla}\mathbf{V})^t$ is the first Rivlin-Ericksen tensor, $\mathbf{V} = [u(x,y), v(x,y), 0]$ is the velocity, $H = [0, H_0, 0]$ is the external magnetic field, P is the Hydrostatic pressures and $\frac{D}{Dt}$ is the contravariant convected derivative and is denoted by

$$\frac{D\mathbf{S}}{Dt} = \frac{d\mathbf{S}}{dt} - (\boldsymbol{\nabla}\mathbf{V})\,\mathbf{S} - \mathbf{S}(\boldsymbol{\nabla}\mathbf{V})^t, \tag{7.4}$$

Eq. (7.2) can be written as

$$\left(1 + \lambda\frac{D}{Dt}\right)\frac{d\mathbf{V}}{dt} = \left(1 + \lambda\frac{D}{Dt}\right)(-\boldsymbol{\nabla}P) + \left(1 + \lambda\frac{D}{Dt}\right)\boldsymbol{\nabla}.\mathbf{S} + \left(1 + \lambda\frac{D}{Dt}\right)\mathbf{J}\times H, \tag{7.5}$$

$$\left(1 + \lambda\frac{D}{Dt}\right)\frac{d\mathbf{V}}{dt} = -\left(1 + \lambda\frac{D}{Dt}\right)(\boldsymbol{\nabla}P) + \boldsymbol{\nabla}.\left(1 + \lambda\frac{D}{Dt}\right)\mathbf{S} + \left(1 + \lambda\frac{D}{Dt}\right)\mathbf{J}\times H, \tag{7.6}$$

$$\left(1 + \lambda\frac{D}{Dt}\right)\frac{d\mathbf{V}}{dt} = -\left(1 + \lambda\frac{D}{Dt}\right)(\boldsymbol{\nabla}P) + \mu\boldsymbol{\nabla}.\mathbf{A}_1 + \left(1 + \lambda\frac{D}{Dt}\right)\mathbf{J}\times H, \tag{7.7}$$

after these assumptions the governing Maxwell model becomes

$$u\partial_x u + v\partial_y u + \lambda\left[u^2\partial_{xx}u + v^2\partial_{yy}u + uv\partial_{xy}u\right] = -\frac{1}{\rho}\partial_x P + \nu\partial_{yy}u - \frac{\sigma\mu_e^2 H_0^2}{\rho}\left(u + \lambda v\partial_y u\right), \tag{7.8}$$

due to hydrostatic and magnetic pressure gradient, the forces will be in equilibrium, as given by

$$-\frac{1}{\rho}\partial_x P = u_e\frac{du_e}{dx} + \frac{\sigma\mu_e^2 H_0^2}{\rho}u_e, \tag{7.9}$$

hence, eq. (7.8) becomes

107

$$u\partial_x u + v\partial_y u + \lambda \left[u^2\partial_{xx}u + v^2\partial_{yy}u + uv\partial_{xy}u\right] = -u_e\frac{du_e}{dx} + \nu\partial_{yy}u - \frac{\sigma\mu_e^2 H_0^2}{\rho}\left(u - u_e + \lambda v\partial_y u\right). \tag{7.10}$$

Energy:

Temperature based thermal conductivity is (see Ref. [34])

$$k = k_\infty\left(1 + \varepsilon\frac{T - T_\infty}{T_w - T_0}\right), \tag{7.11}$$

where q_r is the radiative heat flux, utilizing the Rosseland approximation for radiation term we get

$$\mathbf{q}_r = -\frac{4\alpha^\circ}{3k^\circ}\partial_y T^4. \tag{7.12}$$

By expanding T^4 after utilizing Taylor's series about T_∞ and by taking higher order terms negligible, we get

$$T^4 \approx 4TT_\infty^3 - 3T_\infty^4. \tag{7.13}$$

Using eqs. (7.12) and (7.13) one can write

$$\partial_y \mathbf{q}_r = -\frac{16\alpha^\circ T_\infty^3}{3k^\circ}\partial_{yy}T, \tag{7.14}$$

and the energy equation becomes

$$u\partial_x T + v\partial_y T = \frac{1}{\rho c_p}\partial_y\left(k\partial_y T\right) - \frac{1}{\rho c_p}\partial_y q_r + \tau\left\{D_B\left(\partial_y T\partial_y C\right) + \frac{D_T}{T\infty}\left(\partial_y T\right)^2\right\} + \frac{\mu}{\rho c_p}\left(\partial_y u\right)^2. \tag{7.15}$$

Concentration:

Arrhenius law in general form is (see Ref. [51]):

$$K_A = (T - T_\infty)^w \exp[\frac{-E_a}{k(T - T_\infty)}]K_B. \tag{7.16}$$

The balanced nanoconcentration equation is

$$u\partial_x C + v\partial_y C = D_B \partial_{yy} C + \frac{D_T}{T\infty}\partial_{yy}T - (T - T_\infty)^w \exp[\frac{-E_a}{k(T - T_\infty)}]K_B(C - C_\infty). \tag{7.17}$$

The boundary conditions are

$$
\begin{aligned}
u(x,y) &= U_w(x) = ax + k\partial_y u, \ v(x,y) = 0, \\
T(x,y) &= T_w(x) = T_\infty + bx, \ C(x,y) = C_w = C_\infty + bx, \text{at } y = 0. \\
u(x,y) &= u_e(x) = cx, \ T(x,y) = T_\infty, \ C(x,y) = C_\infty \text{ as } y \to \infty. \tag{7.18}
\end{aligned}
$$

Here $A = \frac{c}{a}$ is the ratio parameter, μ is the fluid viscosity, $k = 8.61 \times 10^{-5}$ is the boltzmann constant, K_B is the pre-exponential constant $(\frac{K^{-w}}{\sec})$, K_A is the rate constant of chemical reaction$(\frac{1}{\sec})$, k° is the absopation constant, α° is the Stefan-Boltzman constant (u, v) are the velocity components along the (x, y) directions, E_a is the activation energy (eV), ρ is the density, μ_e is the magnetic permeability velocity, σ is the electrical conductivity, λ is the Maxwell fluid parameter, ν is the kinematic viscosity, k represents thermal conductivity, D_B is the Brownian motion, $\tau = \frac{(\rho c)_s}{(\rho c)_f}$ is the ratio of nanoparticals heat capacity and base fluid thermal capacity, $\alpha_f = \frac{k_\infty}{(\rho C_p)_f}$ represents thermal diffusion, $T_w(x,y)$ is known as temperature at the wall, $C_w(x,y)$ is known as concentration at the wall, T and C are the temperature and concentration of the fluid respectively, C_p is the specific heat, T_∞ and C_∞ is the temperature and concentration at free stream. Temperature of the sheet is $T_w = T_\infty + bx$, for heated surface $b > 0$ that is $T_w > T_\infty$ and for cooled surface $b < 0$ and $T_w < T_\infty$, b is a constant and D_T is known as thermophoresis diffusivity.

The following variables reduce the above equations into dimensionless quantities:

$$\eta = y\sqrt{\frac{a}{\nu}}, \ \Psi = xf(\eta)\sqrt{a\nu}, \ \Theta(\eta) = \frac{T - T_\infty}{T_w - T_\infty}, \ \phi(\eta) = \frac{C - C_\infty}{C_w - C_\infty}, \ u = \frac{\partial \psi}{\partial y}, \ v = -\frac{\partial \psi}{\partial x}. \quad (7.19)$$

Incompressibility condition (7.1) is automatically satisfied and eqs. (7.10), (7.15) and (7.17) take the following form:

$$f''' + f'f'' - (f')^2 + \lambda_m \left(2f(\eta)f'f'' - (f(\eta))^2 f''' \right) + Ha^2 \left(1 - f' + \lambda_m f'f'' \right) + 1 = 0, \quad (7.20)$$

$$\left(1 + \varepsilon\theta + \frac{4}{3}R \right) \theta'' + \varepsilon (\theta')^2 + Ec (f'')^2 + \Pr \left[f(\eta)\theta' + N_b\phi'\theta' + N_t (\theta')^2 \right] = 0, \quad (7.21)$$

$$\phi'' + \frac{N_t}{N_b}\theta'' + \Pr Le \left(f(\eta)\phi' - K\phi(\eta) (\theta(\eta))^w \exp(\frac{-E}{\theta}) \right) = 0, \quad (7.22)$$

using (7.18), the associated boundary conditions become

$$\begin{aligned}
f' &= 1 + \lambda_1 f'', \ f(\eta) = 0, \ \theta(\eta) = 1, \ \phi(\eta) = 1, \ \text{at } \eta = 0, \\
f' &\to A, \ \theta \to 0, \ \phi \to 0, \ \text{as } \eta \to \infty.
\end{aligned} \quad (7.23)$$

Where, fluid relaxation parameter is $\lambda_m = \lambda a$, chemical reaction rate of constant is $K = \frac{K_B}{c}(T_w - T_\infty)^w$, Hartmann number is $Ha^2 = \mu_e H_0 \sqrt{\frac{\sigma}{\rho a}}$, Prandtl number is $\Pr = \frac{\mu c_p}{k_\infty}$, radiation parameter is $R = \frac{4\alpha^\circ T_\infty^3}{k^\circ}$, thermophoresis parameter is $N_t = \frac{\tau D_t (T_w - T_\infty)}{T_\infty \nu}$, dimensionless activation energy parameter is $E = \frac{E_a}{k(T_w - T_\infty)}$, Eckert number is $Ec = \frac{u_c^2}{(T_w - T_\infty)c_p}$, Lewis number is $Le = \frac{\alpha}{D_B}$ and Brownian motion parameter is $N_b = \frac{\tau D_B (C_w - C_\infty)}{\nu}$.

7.1.2 Declaration of curiosity

Skin friction coefficient

Mathematically, it is defined as:

$$C_f = \frac{\tau_w}{\rho u_e^2} = \mathrm{Re}_x^{\frac{-1}{2}} \left[f''(0) + \lambda_m (f'(0) f''(0) + f(0) f'''(0)) \right], \qquad (7.24)$$

where τ_w denotes the wall shear stress, given as:

$$\tau_w = \mu \partial_y \left(u + \lambda v \partial_y u \right)_{y=0}. \qquad (7.25)$$

Nusselt number

The Nusselt number is defined as:

$$q_w = -k \left(\partial_y T \right)_{y=0} + q_r, \implies Nu_x = \frac{-x q_w}{k_\infty \left(T_w - T_\infty \right)} = -\mathrm{Re}_x^{\frac{-1}{2}} \left(1 + \varepsilon\theta + \frac{4}{3} R \right) \theta'(0). \qquad (7.26)$$

Sherwood number

The average mass transfer rate is defined as:

$$J_w = -D_B \left(\partial_y C \right)_{y=0}, \implies Sh_x = \frac{-J_w x}{D_B \left(T_w - T_\infty \right)} = -\mathrm{Re}_x^{\frac{-1}{2}} \phi'(0).$$

Where $\mathrm{Re}_x = u_e(x)$ is local Reynolds number.

7.2 Numerical Procedure

Shooting method is implemented for current problem and nonlinear differential eqs. (7.20)-(7.22) along with boundary conditions (7.23) are solved through Runge-Kutta Fehlberg approach. The boundary value problem is converted into a system of initial value problems. Guess the missing initial conditions and than by using Newton's method the required boundary conditions are achieved. The procedure is repeated until the required accuracy 10^{-6} is achieved.

7.3 Results and discussion

The reduced ordinary differential eqs. (7.20)-(7.22) with boundary conditions (7.23) are solved by using Runge-Kutta-Fehlberg method known as Cash and Karp. The results are achieved for fluid relaxation parameter, Hartmann number and slip parameter on velocity, temperature and concentration profiles. Fig. 7.2 illustrates the behavior of nanoliquid velocity on λ_1. It can be illustrated from this figure that intensification in slip parameter λ_1 correspondes to the reduction in velocity. Fig. 7.3 illuminates a very significant effect of Hartmann number Ha^2 on velocity profile. For each value of Hartmann number Ha^2, the velocity profile reduces. In fact the transverse magnetic field generates the Lorentz force which causes reduction in velocity profile. Fig. 7.4 illustrates the fluid relaxation parameter λ_m on flow velocity. It can be investigated that the velocity profile reduces for increasing values of fluid relaxation parameter λ_m.
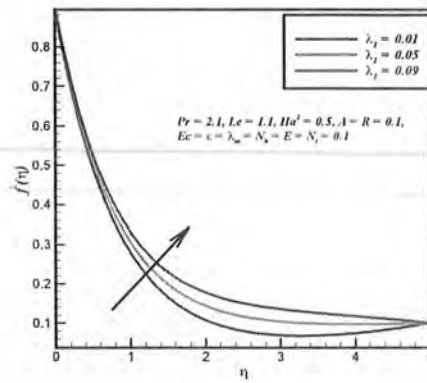

Fig. 7.2. Outcome of λ_1 on $f'(\eta)$.

112
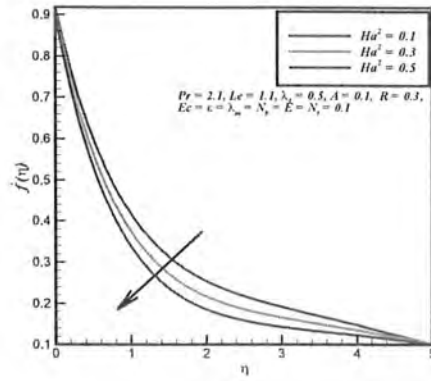
Fig. 7.3. Outcome of Ha^2 number on $f'(\eta)$.
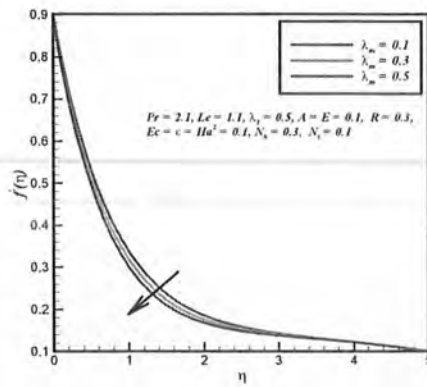
Fig. 7.4. Outcome of λ_m on $f'(\eta)$.

Fig. 7.5 represents the behavior of Prandtl number Pr on temperature graph. It is obvious that the rising values of Prandtl number Pr on the temperature profile is reducing. Clearly illustrated from this figure that the thermal boundary layer weakens, as on increasing the values of Prandtl number Pr. The lower values of Prandtl number Pr are corresponding to enhance the thermal conductivity. Therefore thermal region layer becomes thicker and rate heat transport reduces the Prandtl number Pr. Fig. 7.6 describes the variation of thermal radiation R on

113

temperature graph. It shows that the temperature enhances by enhancing thermal radiation parameter R. The temperature profile reduces with increase of thermal radiation R. Fig. 7.7 shows the temperature profile for several values of Eckert number Ec. It is seen that for large values of Ec the temperature profile reduces. Fig. 7.8 depicts the variation of small parameter ε on temperature profile. Layer thickness and temperature are improved by large values of ε. Figs. 7.9 and 7.10 illuminate a very important effect of N_b and N_t on temperature profile. It is observed that the temperature profiles increases by increasing the values of N_b and N_t. Physically, with rise in the values of N_t generates the thermophoresis force, helping nanomaterials to move from the hot surface to cold one.
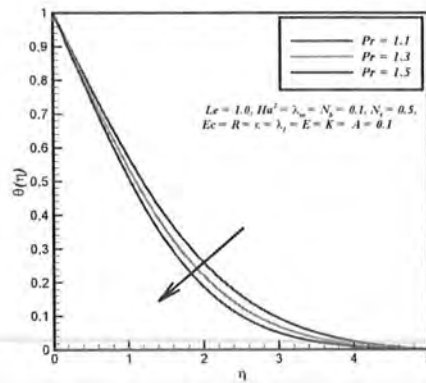

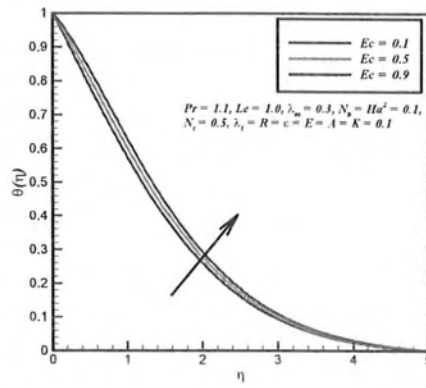Fig. 7.5. Outcome of Pr on $\theta(\eta)$.
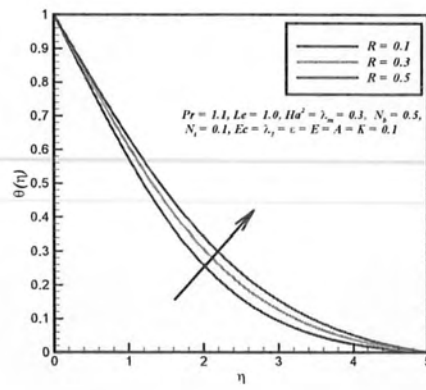
Fig. 7.6. Outcome of Ec on $\theta(\eta)$.

Fig. 7.7. Outcome of R on $\theta(\eta)$.

115

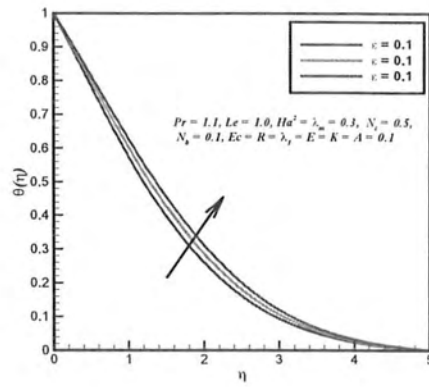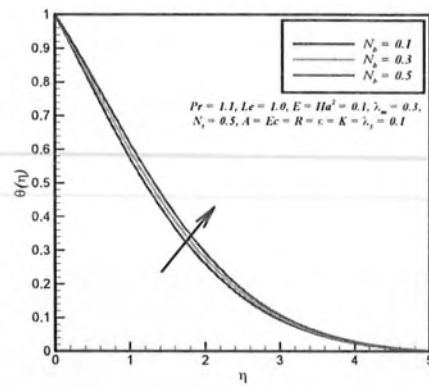Fig. 7.8. Outcome of ε on $\theta(\eta)$.

Fig. 7.9. Outcome of N_b on $\theta(\eta)$.

116
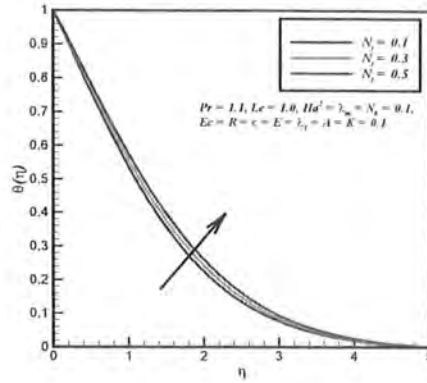
Fig. 7.10. Outcome of N_t on $\theta(\eta)$.

The influence of Lewis number Le on concentration profile is shown in Fig. 7.11. Lewis number Le mostly depends on the coefficient of concentration diffusion. Large values of Lewis number Le reduces the concentration diffusion. Figs. 7.12 and 7.13 describe the nature of concertation profiles for various values of chemical reaction and non-dimensional activation energy. Activation energy is insignificant amount of molecules or atoms in a system in order to initiate the chemical reaction. For chemical reaction to continue at a reasonable rate, there must exist a considerable number of atoms with energy equal to activation energy or greater than activation energy. From eq. (7.17) it is apparant that the reduction in concentration profile is noticed for large values of non-dimensional activation parameter E. Also the concentration profile reduces on improving values of chemical reaction parameter K (see in Fig. 7.13). Physically the ingesting reactive species increases on increasing the chemical reactor parameter K. The concentration profile reduces by enhancing the chemical reaction. Fig. 7.14 exhibits the behavior on friction factor for corresponding values of slip parameter λ_1. It can be analyzed that higher values of slip parameter λ_1 causes decline in the Hartmann number Ha^2. The Eckert number Ec is plotted against the Prandtl number Pr (as displayed in Fig. 7.15). It can be observed that Eckert number Ec is an enhancing function of the Prandtl number.

117

Fig. 7.11. Outcome of Le on $\phi(\eta)$.

Fig. 7.12. Outcome of K on $\phi(\eta)$.
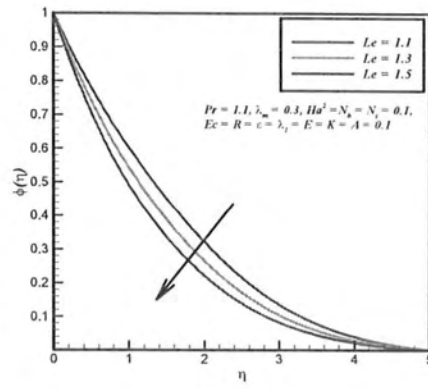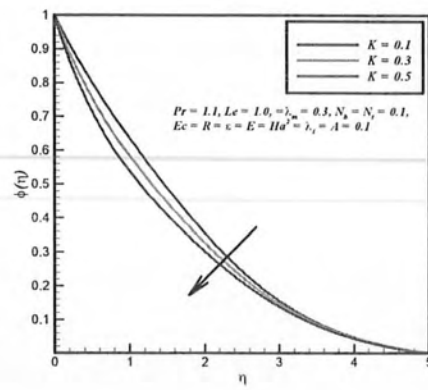
118
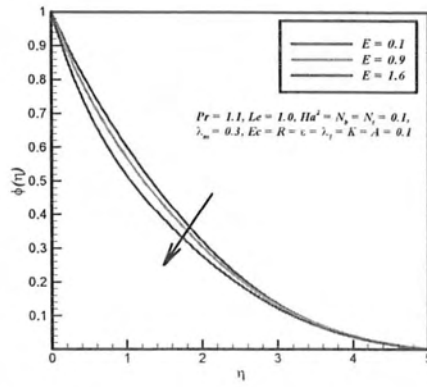
Fig. 7.13. Outcome of E on $\phi(\eta)$.
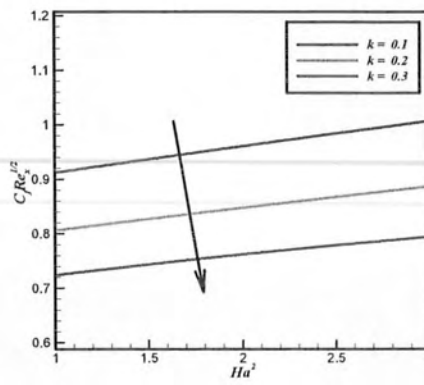
Fig. 7.14. Outcome of K and Ha^2 number on skin friction coefficient.

119
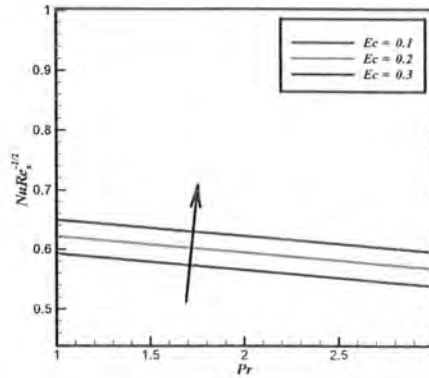
Fig. 7.15. Outcome of Ec and Pr number on Nusselt number.

Table 7.1 calculates the numerical values of friction factor coefficient $[f''(0) + \lambda_m(f'(0) f''(0) + f(0) f'''$
for different values of involving physical parameters λ_m, Ha and λ_1. This table validates that Ha^2 and λ_m i.e. both parameters enhance the friction factor $[f''(0) + \lambda_m(f'(0) f''(0) + f(0) f'''(0))])$, on the other hand enhancing the slip parameter k causes the reduction in friction factor $[f''(0) + \lambda_m(f'(0) f''(0) + f(0) f'''(0))]$. **Table 7.2** shows the numerical values of heat transfer rate $(1 + \varepsilon\theta + \frac{4}{3}R)\theta'(0)$ for several values of included physical parameters Pr, R, Ec and ε. This table analyzed that increasing the values of three parameters Pr, R and ε, enhances the friction factor coefficient in the absolute sense, but by increasing the values of Eckert number, the heat transfer rate $(1 + \lambda_m) f''(0)$ reduces. **Table. 7.3** shows the mass transfer rate $Sh \; Re_x^{\frac{-1}{2}}$ for unlike values of Le, K, N_t and N_b. It can be examined from this table that the mass transfer rate $Sh \; Re_x^{\frac{-1}{2}}$ increases at the surface for the corresponding values of $Le = 1.1$, 1.2, 1.3 and $K = N_b = 0.1$, 0.2, 0.3, on the other hand, the mass transfer rate $Sh \; Re_x^{\frac{-1}{2}}$ decreases for corresponding values of $N_t = 0.1$, 0.2, .0.3. To check the accuracy of our current study we have computed the numerical values of $-\theta'(0)$ and $\phi(0)$ for unlike values of N_t fixing $N_b = 0.1$, Pr $= 1.0$, $\varepsilon = \lambda_m = Ha = R = Ec = K = \lambda_1 = E = Le = 0.0$. These values are recruited in **Table 7.4** and compared these numerical values with Acharya et al. [80].

120

Table 7.1: Numerical results of $[f''(0) + \lambda_m(f'(0)f''(0) + f(0)f'''(0))]$ for unlike values of Ha, $\lambda_m = 0.1$, $N_t = 0.5$, $N_b = Ec = \varepsilon = K = 0.1$, and $Pr = Le = 1.1$.

Ha^2	λ_1	λ_m	$-C_f Re_x^{\frac{1}{2}}$
0.1	0.1	0.1	0.9120
0.2			0.9606
0.3			1.0069
0.1	0.1	0.1	0.9120
	0.2		0.8606
	0.3		0.7240
0.1	0.1	0.1	0.9120

Table 7.2: Compositional results of $-(1 + \varepsilon\theta + \frac{4}{3}R)\theta'(0)$ with pervious literature when $\lambda_m = N_b = Ec = Ha = \varepsilon = K = 0.1$ and $Le = 1.1$.

Pr	Ec	R	ε	$NuRe_x^{\frac{-1}{2}}$
1.1	0.1	0.1	0.1	0.5928
1.2				0.6216
1.3				0.6490
1.1	0.1	0.1	0.1	0.5928
	0.2			0.5656
	0.3			0.5383
1.1	0.1	0.1	0.1	0.5928
		0.2		0.6234
		0.3		0.6557
1.1	0.1	0.1	0.1	0.5928
			0.2	0.6079
			0.3	0.5790

121

Table 7.3: Numerical results of $-\phi'(0)$ for corresponding values of Le, K, N_t and N_b.

Le	K	N_t	N_b	$ShRe_x^{\frac{-1}{2}}$
1.1	0.1	0.1	0.1	0.4971
1.2				0.5428
1.3				0.5867
1.1	0.1	0.1	0.1	0.4971
	0.2			0.5760
	0.3			0.6510
1.1	0.1	0.1	0.1	0.4971
		0.2		0.2879
		0.3		0.1025
1.1	0.1	0.1	0.1	0.4971
			0.2	0.6260
			0.3	0.6692

Table. 7.4: Comparison of the numerical results by utilizing the current technique with Acharya et al. [80].

N_t	Acharya et al. [80] $-\theta'(0)$	Acharya et al. [80] $-\phi'(0)$	Presnt Results $-\theta'(0)$	Presnt Results $-\phi'(0)$
0.1	0.9524	2.1294	0.9634	2.0153
0.2	0.6932	2.2740	0.7721	2.1421
0.3	0.5201	2.5287	0.5685	2.4561
0.4	0.4026	2.7952	0.4032	2.7620
0.5	0.3211	3.0352	0.3201	3.0135

Chapter 8

Generalized diffusion effects on Maxwell nanofluid stagnation point flow over a stretchable sheet with slip conditions and chemical reaction

This chapter expands the previous work by adding the heat and mass diffusion (Cattanco–Christov model) of the upper convected Maxwell nanomaterial passed by a linear stretched surface (slip surface) near the stagnation point region. Conventional Fourier's and Fick's laws are employed to investigate heat and mass diffusion phenomena. Using the similarity transformations the governing PDEs are rendered into ODEs along with boundary conditions. The obtained boundary value problem is solved numerically by using Runge-Kutta method along with shooting technique (Cash and Karp). Effects of embedded parameters, namely, fluid relaxation parameter, Hartmann number, Brownian moment, thermophoresis parameter, thermal relaxation parameter, Lewis number, chemical reaction, concentration relaxation parameter and slip parameter on velocity, temperature and concentration distributions are deliberated through graphs. The skin friction coefficient is deliberated and their numerically values are accessible through graphs and table. Also the comparison between present and published values is made at the end.

8.1 Mathematical formulation

Let us consider two dimensional laminar steady heat and mass transfer flow of an electrically conducting Maxwell nanofluid passing by a linear stretched surface placed along x-axis and y-axis, vertical to the sheet with stagnation point at the origin (as illustrated in Fig. 8.1). The free stream velocity is $u = u_e(x) = cx$ and the stretched velocity $u = U_w(x) = ax$, here a and c are positive constants. The temperature at the surface is conserved at T_w and T_∞ far away from the plate. In a similar manner, the nanoparticle volume fractions are C_w and C_∞. An external magnetic field H_0 is applied normal to the sheet.
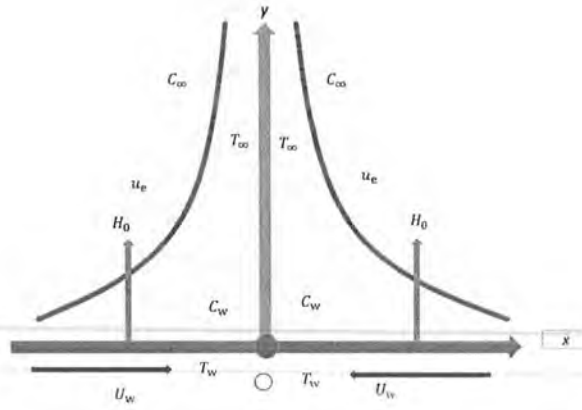
Fig. 8.1. Geometry of the problem.

Under the above assumptions the required equations are as follows:

$$\partial_x u + \partial_y v = 0, \tag{8.1}$$

$$u\partial_x u + v\partial_y u + \lambda \left[u^2 \partial_{xx} u + v^2 \partial_{yy} u + uv\partial_{xy} u \right] = -\frac{1}{\rho}\partial_x P + \nu\partial_{yy} u - \frac{\sigma\mu_e^2 H_0^2}{\rho}\left(u + \lambda v\partial_y u \right). \tag{8.2}$$

Here ρ is the density, μ_e is the magnetic permeability velocity, σ is the electrical conductivity, λ is the Maxwell fluid parameter and ν is the kinematic viscosity. Due to hydrostatic and

magnetic pressure gradient the force will be in equilibrium as given by

$$-\frac{1}{\rho}\partial_x P = u_e \frac{du_e}{dx} + \frac{\sigma \mu_e^2 H_0^2}{\rho} u_e \qquad (8.3)$$

Hence, eq. (8.2) becomes

$$u\partial_x u + v\partial_y u + \lambda \left[u^2\partial_{xx}u + v^2\partial_{yy}u + uv\partial_{xy}u\right] = u_e \frac{du_e}{dx} + \nu\partial_{yy}u - \frac{\sigma \mu_e^2 H_0^2}{\rho}\left(u - u_e + \lambda v\partial_y u\right).$$

The classical form of Fourier's and Fick's laws with the Cattaneo-Christove equations takes the following form:

$$\mathbf{q} + \lambda_T \left[\partial_t \mathbf{q} + \mathbf{V}.(\nabla \mathbf{q}) - \mathbf{q}.(\nabla \mathbf{V}) + (\nabla.\mathbf{V})\mathbf{q}\right] = -k_f \nabla T, \qquad (8.4)$$

$$\mathbf{J} + \lambda_c \left[\partial_t \mathbf{J} + \mathbf{V}.(\nabla \mathbf{J}) - \mathbf{J}.(\nabla \mathbf{V}) + (\nabla.\mathbf{V})\mathbf{J}\right] = -D_B \nabla C. \qquad (8.5)$$

By assuming that $\nabla.\mathbf{q} = 0$, $\nabla.\mathbf{J} = 0$, and for steady state $\frac{\partial \mathbf{q}}{\partial t} = 0$, $\frac{\partial \mathbf{J}}{\partial t} = 0$, the revised equations are:

$$\mathbf{q} + \lambda_T \left[\mathbf{V}.\nabla \mathbf{q} - \mathbf{q}.\nabla \mathbf{V}\right] = -k_f \nabla T, \qquad (8.6)$$

$$\mathbf{J} + \lambda_C \left[\mathbf{V}.\nabla \mathbf{J} - \mathbf{q}.\nabla \mathbf{J}\right] = -D_B \nabla C. \qquad (8.7)$$

Now in component form, energy and concentration equations (eqs. (8.7) and (8.8)) take the following form

$$u\partial_x T + v\partial_y T + \lambda_T \left[\partial_x T u\left(\partial_x u\right) + \partial_x T v\left(\partial_y u\right) + u\left(\partial_x v\right)\partial_y T + v\left(\partial_y v\right)\partial_y T\right]$$

$$+\lambda_T \left[2uv\partial_{xy}T + v^2\partial_{yy}T + u^2\partial_{xx}T\right] = \alpha\partial_{yy}T + \tau\left\{D_B\left(\partial_y T\partial_y C\right) + \frac{D_T}{T\infty}\left(\partial_y T\right)^2\right\}, \qquad (8.8)$$

125

$$u\left(\partial_x C\right) + v\left(\partial_y C\right) + \lambda_c\left[u\partial_x u\left(\partial_x C\right) + v\partial_y u\left(\partial_x C\right) + u\left(\partial_x v\right)\partial_y C + v\left(\partial_y v\right)\partial_y C\right]$$

$$\lambda_c\left[+2uv\partial_{xy}C + v^2\partial_{yy}C + u^2\partial_{xx}C\right] = D_B\partial_{yy}C + \frac{D_T}{T\infty}\partial_{yy}T - k_r(C - C_\infty), \quad (8.9)$$

where $\partial_x = \frac{\partial}{\partial x}$ and $\partial_y = \frac{\partial}{\partial y}$.

The specified boundary conditions of the current problem takes the form

$$
\begin{aligned}
u(x,y) &= U_w(x) = ax + g\partial_y u, \ v(x,y) = 0, \\
T(x,y) &= T_w = T_\infty + bx, \ C(x,y) = C_w = C_\infty + bx, \text{at } y = 0, \\
u(x,y) &= u_e(x) = cx, \ T(x,y) = T_\infty, \ C(x,y) = C_\infty \text{ as } y \to \infty. \quad (8.10)
\end{aligned}
$$

Here $(u, \ v)$ are the velocity components along the $(x, \ y)$ directions. q and J are the normal heat and mass flux respectively, k_f represents the thermal conductivity, D_B is the Brownian motion, λ_T, λ_C are the relaxation parameters for thermal and concentration, $\alpha_f = \frac{(\rho c)_s}{(\rho c)_f}$ is the ratio of nanopartical heat capacity and base fluid thermal capacity, $\alpha_f = \frac{k_f}{(\rho C_p)_f}$ represents thermal diffusion, $T_w(x,y)$ is known as temperature at the wall, $C_w(x,y)$ is known as concentration at the wall, T and C are the temperature and concentration of the fluid respectively, C_p is the specific heat, C_∞ and T_∞ are the concentration and temperature at free streams. Temperature of the sheet is $T_w = T_\infty + bx$, for heated surface $b > 0$ so, $T_w > T_\infty$ and for cooled surface $b < 0$ and $T_w < T_\infty$, where b is a constant.

The similarity variables are used to transform these PDEs into dimensionless form:

$$\eta = y\sqrt{\frac{a}{\nu}}, \ \theta\left(\eta\right) = \frac{T - T_\infty}{T_w - T_\infty}, \ \phi\left(\eta\right) = \frac{C - C_\infty}{C_w - C_\infty}, u = \frac{\partial\psi}{\partial y}, \ v = -\frac{\partial\psi}{\partial x}. \quad (8.11)$$

substituting Eq. (8.11) into Eqs. (8.1), (8.4), (8.8) and (8.9), we get:

$$f''' + f'f'' - \left(f'\right)^2 + \lambda_m\left(2f(\eta)f'f'' - \left(f(\eta)\right)^2 f'''\right) + Ha^2\left(1 - f' + \lambda_m f'f''\right) + 1 = 0, \quad (8.12)$$

126

$$\theta'' + \Pr\left[f(\eta)\theta' + N_b\phi'\theta' + N_t\left(\theta'\right)^2 + \delta_t\left(f(\eta)f'\theta' - \theta''\left(f(\eta)\right)^2\right)\right] = 0, \qquad (8.13)$$

$$\phi'' + \frac{N_t}{N_b}\theta'' + \Pr Le\left[f(\eta)\phi' - K\phi(\eta) + \delta_c\left(f(\eta)f'\phi' - \phi''\left(f(\eta)^2\right)\right)\right] = 0. \qquad (8.14)$$

and the associated boundary conditions are modified to:

$$f' = 1 + \lambda_1 f'', \ f(\eta) = 0, \ \theta(\eta) = 1, \ \phi(\eta) = 1, \ \text{at } \eta = 0,$$
$$f' \to A, \ \theta \to 0, \ \phi \to 0, \ \text{as } \eta \to \infty. \qquad (8.15)$$

Here fluid relaxation parameter is $\lambda_m = \lambda a$, Hartmann number is $Ha^2 = \mu_e H_0\sqrt{\frac{\sigma}{\rho a}}$, concentration relaxation parameter is $\delta_c = a\lambda_C$, ratio parameter is $A = \frac{c}{a}$, Lewis number is $Le = \frac{\alpha}{D_B}$, thermal relaxation parameter is $\delta_t = a\lambda_T$, thermophoresis parameter is $N_t = \frac{\tau D_t(T_w - T_\infty)}{T_\infty \nu}$, Prandtl number is $Pr = \frac{\mu c_p}{k}$, Brownian motion parameter is $N_b = \frac{\tau D_B(C_w - C_\infty)}{\nu}$, slip parameter is $\lambda_1 = g\sqrt{\frac{a}{\upsilon}}$ and chemical reactive species is $K = \frac{k_r}{a}$.

Friction factor coefficient (C_f) is defined as:

$$C_f = \frac{\tau_w}{\rho u_e^2} = \text{Re}_x^{\frac{-1}{2}}\left[f''(0) + \lambda_m(f'(0)f''(0) + f(0)f'''(0))\right]. \qquad (8.16)$$

Here τ_w denotes the wall shear stress, which is:

$$\tau_w = \mu\partial_y\left(u + \lambda\upsilon\partial_y u\right)_{y=0}, \qquad (8.17)$$

$Re_x = u_e(x)$ is local Reynolds number.

8.2 Numerical procedure

Numerical solution of the nonlinear differential eqs. (8.12)-(8.14) along with Neumann boundary conditions (8.15) is achieved by applying the shooting method with Runge-Kutta integration technique for various values of parameters. Let $y_1 = f$, $y_2 = f'$, $y_3 = f''$, $y_4 = \theta$, $y_5 = \theta'$, $y_6 = \phi$ and $y_7 = \phi'$.

127

Hence the leading equations become

$$y_1 = y_2',\tag{8.18}$$

$$y_2' = y_3,\tag{8.19}$$

$$y_3' = \frac{y_2^2 - y_2 y_3 - \lambda_m\left(y_1 y_2 y_3\right) - Ha^2\left(1 - y_2 + \lambda_m y_2 y_3\right) - 1}{\left(1 - \lambda_m y_1\right)},\tag{8.20}$$

$$y_4' = y_5,\tag{8.21}$$

$$y_5' = \frac{-\Pr\left(y_1 y_5 + N_b y_7 y_5 + N_t\left(y_5\right)^2 + \delta_t\left(y_2 y_1 y_5\right)\right)}{\left(1 - \delta_t\left(y_1\right)^2\right)},\tag{8.22}$$

$$y_6' = y_7,\tag{8.23}$$

$$y_7' = \frac{-\Pr Le\left(y_1 y_6 - K y_6 + \delta_c\left(y_2 y_1 y_6\right)\right) - \frac{N_t}{N_b} y_5'}{\left(1 - \delta_c\left(y_1\right)^2\right)},\tag{8.24}$$

and subsequent initial conditions are:

$$
\begin{aligned}
y_1\left(0\right) &= 0,\ y_2\left(0\right) = 1 + \lambda_1 y_2,\ y_4\left(0\right) = 1,\ y_6\left(0\right) = 1,\\
y_2\left(\eta\right) &\rightarrow A,\ y_4\left(\eta\right) \rightarrow 0,\ y_6\left(\eta\right) \rightarrow 0\ \text{when}\ \eta \rightarrow \infty.
\end{aligned}\tag{8.25}
$$

This technique is successfully used to solve different problems related to the boundary layer flow. The boundary conditions at $f'(\eta)$, $\theta(\eta)$ and $\phi(\eta)$ as $\eta \rightarrow \infty$ are converted into finite interval length (here it is $\eta = 5$). Insert three initial guesses to $f''(0)$, $\theta'(0)$ and $\phi'(0)$ for approximate solutions. Here the step size and convergence criteria are chosen to be 0.001 and 10^{-6} (in all cases).

128

8.3   Results and discussion

Main efforts of this work are to examine the influence of magnetic field and stagnation point Maxwell nanofluid flow due to a linear stretching surface with slip conditions. The governing differential eqs. (8.12)-(8.15) along with corresponding boundary conditions (8.16) are solved numerical by implying shooting procedure (Cash and Karp). Fig. 8.2 represents the change in velocity profile for distinct values of Hartmann number Ha^2. From this figure, enhancement in Ha^2 results to decrease in velocity profile. Since the Hartmann number Ha represents the ratio of MHD force to viscous force, hence enhancement in Ha^2 leads to stronger the MHD force, which declarants the velocity motion. Fig. 8.3 depicts the variation of slip parameter λ_1 on velocity profile. The influence of slip parameter λ_1 significantly enhances the velocity profile. Fig. 8.4 illustrates the variation of fluid relaxation parameter λ_m on velocity profile. It can be analyzed that the velocity of the fluid reduces by enhancing the fluid relaxation parameter λ_m.
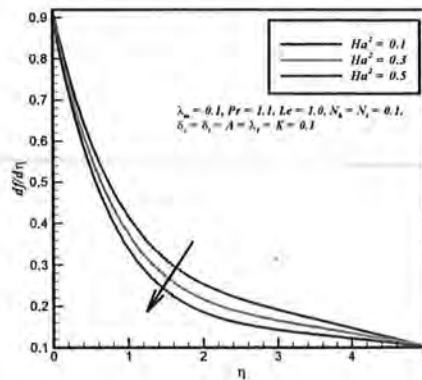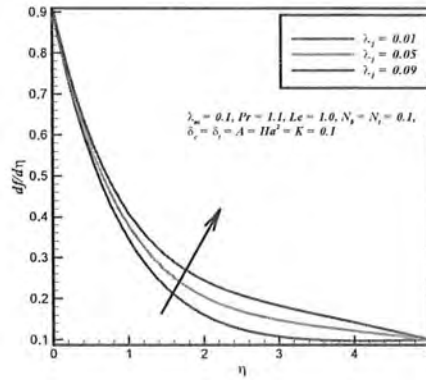

Fig. 8.2. Outcome of Ha^2 on $f'(\eta)$ .Fig.

8.3. Outcome of λ_1 on $f'(\eta)$.
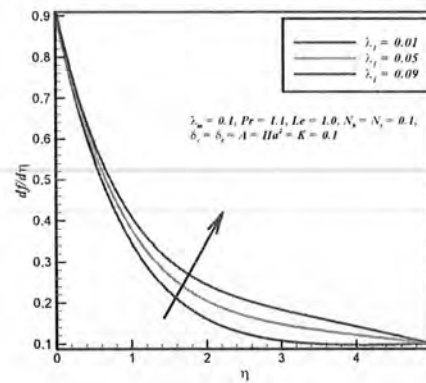
Fig. 8.4. Outcome of λ_m on $f'(\eta)$.

Fig. 8.5 represents the change in temperature distribution for distinct values of N_t. It is found that by enhancing N_t, the temperature distribution also increases. Fig. 8.6 depicts the variation of Brownian motion parameter N_b on temperature distribution. It can be analyzed that by increasing N_b, the mass diffusivity trek up which leads to enhance the temperature and the boundary layer thickness. Fig. 8.7 shows the behavior of Prandtl number Pr on temperature profile. It is found that the temperature profile reduces on rising values of Prandtl number Pr.

130

Fig. 8.5. Outcome of N_t on $\theta(\eta)$.

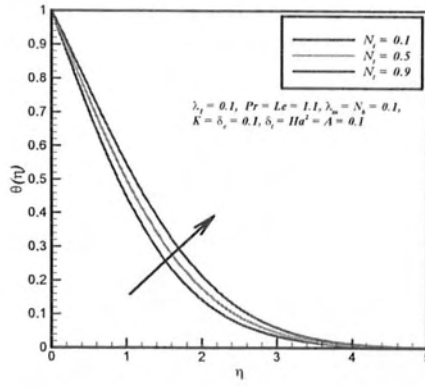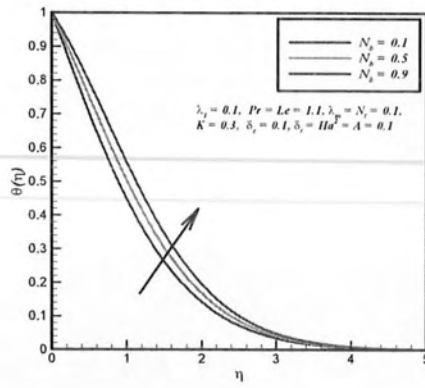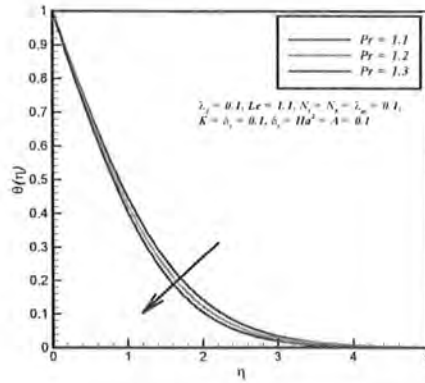Fig. 8.6. Outcome of N_b on $\theta(\eta)$.

131

Fig. 8.7. Outcome of Pr on $\theta(\eta)$.

Fig. 8.8 presents the deviation of temperature profile for distinct values of δ_t. It is seen that by enhancing thermal relaxation parameter δ_t fluid particles require more time to heat the boundary layer region, as a result temperature profile reduces. Fig. 8.9 displays the effect of relaxation parameter δ_t on concentration distribution. From this figure it is observed that by increasing the relaxation parameter δ_t the concentration profile reduces. Fig. 8.10 represents the variation on concentration profile for different values of chemical reaction K. It is found that for large values of chemical reaction parameter K the concentration profile reduces. Fig. 8.11 represents the influence of Lewis number Le on nanoconcentration profile. It is found that the higher values of Lewis number Le leads to reduce the mass diffusivity, so the concentration profile reduces. Figs. 8.12 and 8.13 validate the distribution of skin friction coefficient $C_f \, \mathrm{Re}_x^{\frac{1}{2}}$ with respect to Hartmann number Ha^2 and for several values of slip parameter k and fluid relaxation parameter λ_m. It is very important to see that the skin friction coefficient $C_f \, \mathrm{Re}_x^{\frac{1}{2}}$ enhances by enhancing the values of slip parameter k but decreases by increasing the fluid relaxation parameter λ_m. **Table 8.1** shows that the fraction factor rise due to increase in Hartmann number Ha^2 and fluid relaxation parameter λ_m and opposite behavior is noticed for slip parameter k. The achieved results are in good agreement with Afify and Elgazery [89] for different values of Ha^2 and λ_m as shown in **Table. 8.2**. To detention accuracy of our present analysis we have calculated the numerical values for different values of N_t fixing $N_b = 0.1$, $Le = \mathrm{Pr} = 10$ and $\lambda_m = Ha^2 = k = St = \delta t = \delta c = K = A = 0.0$. We have recruited

132

the values in **Table 8.3** and compared those numerical values with Hsiao [90].
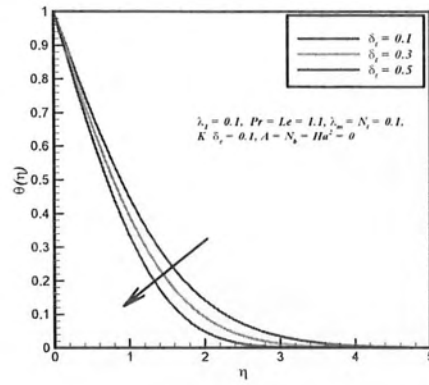
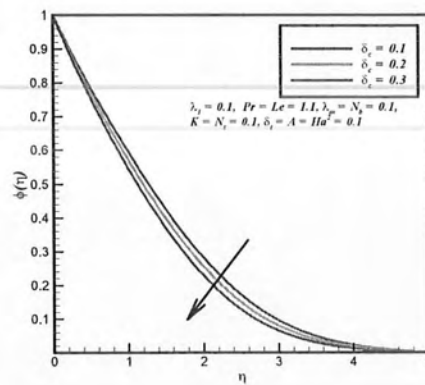Fig. 8.8. Outcome of δ_t on $\theta(\eta)$.

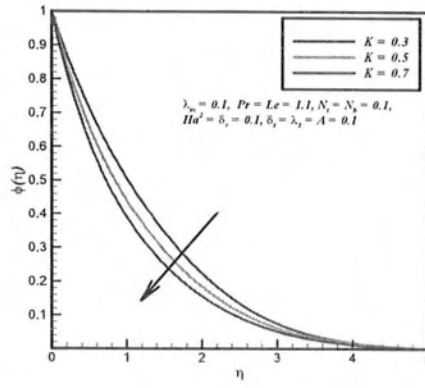Fig. 8.9. Outcome of δ_c on $\phi(\eta)$.

133

Fig. 8.10. Outcome of K on $\phi(\eta)$.
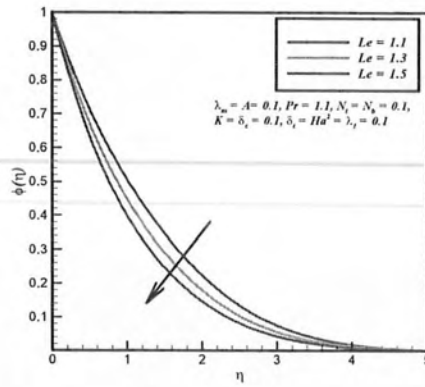
Fig. 8.11. Outcome of Le on $\phi(\eta)$.

134
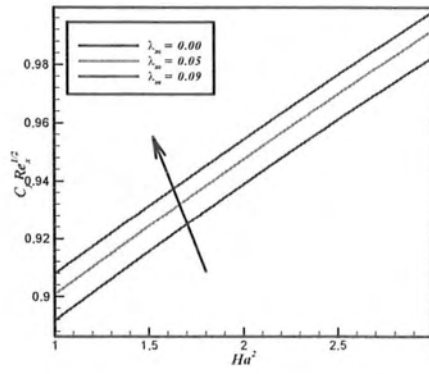
Fig. 8.12. Skin friction coefficinent for various values of Ha^2 and λ_m.
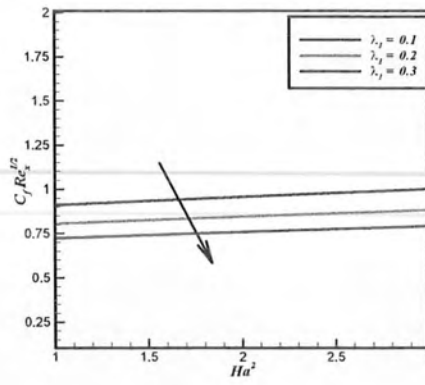
Fig. 8.13. Skin friction coefficinent for various values of Ha^2 and λ_1.

135

Table 8.1: Computational results of $C_f \, \mathrm{Re}_x^{\frac{1}{2}}$ for different values of Ha^2, λ_1 and λ_m when $K = A = N_b = 0.1$, $Le = 1.0$, $\delta_c = \delta_t = 0.0$, $N_t = 0.5$, and $\mathrm{Pr} = 1.1$.

Ha	λ_1	λ_m	$-C_f \, \mathrm{Re}_x^{\frac{1}{2}}$
0.1	0.1	0.1	0.9097
0.2			0.9559
0.3			0.9999
0.1	0.1	0.1	0.9097
	0.2		0.8042
	0.3		0.7225
0.1	0.1	0.00	0.8918
		0.05	0.9008
		0.09	0.9097

Table 8.2: Comparison of $[f''(0) + \lambda_m(f'(0) \, f''(0) + f(0) \, f'''(0))]$ with pervious literature when $N_b = \lambda_1 = St = 0.1$, $\delta t = \delta c = K = A = 0.0$, $N_t = 0.5$ and $Le = \mathrm{Pr} = 1.0$.

λ_m	Ha^2	Afify et al. [89]	Present results
0.5	0.0	-1.68935	-1.6752
0.5	0.1	-1.69715	-1.6821
0.5	0.2	-1.72034	-1.7000
0.5	0.3	-1.75830	-1.7321
0.0	0.1	-1.00499	-1.0001
0.1	0.1	-2.49440	-2.1898

Table 8.3: Comparison of $-\theta'(0)$ and $-\phi'(0)$ with pervious literature when $\lambda_m = Ha^2 = \lambda_1 = St = \delta t = \delta c = K = A = 0.0$, $N_t = 0.1$ and $Le = \Pr = 10$.

N_t	Hsiao [90] $-\theta'(0)$	Hsiao [90] $-\phi'(0)$	Present Outcome $-\theta'(0)$	Present Outcome $-\phi'(0)$
0.1	-0.9524	-2.1294	-0.9131	-2.1526
0.2	-0.6932	-2.2740	-0.6922	-2.2945
0.3	-0.5201	-2.5287	-0.5018	-2.5002
0.4	-0.4026	-2.7952	-0.4022	-2.7590
0.5	-0.3211	-3.0352	-0.3462	-3.0617

Chapter 9

Conclusions

In this thesis boundary layer flow of non-Newtonian fluids having complex geometries are considered, we have presented the base flow solutions for different non-Newtonina fluid models. In each case, we non-dimensionlised the governing continuity, Navier-Stokes, energy and mass equations by using suitable transformations and boundary-layer approximation in order to determine the main governing equations. The solutions of the modelled differential equations are computed by using moderate and well-known numerical technique namely shooting method. The different governing physical parameters are utilized to control the motion of fluid. Skin friction coefficient, Nusselt number and Sherwood number are calculated in order to examine the flow behavior near the surface. A comparison has been made with the previous published literature in order to check the accuracy of the method. The following conclusions are drawn based on entire study:

- Velocity profile enhances for large values of Wall thickness (α), Weissenberg number (We^2), plastic dynamic viscosity (ξ) and power law index (n).

- Velocity profile reduces for large values of Hartman number (Ha^2).

- Velocity profile enhances by enhancing fluid parameter (d), Weissenberg number (We^d), tangential slip condition (λ_1) and nonlinear stretching index (n).

- It is clear that the impact of inclined angle γ, wall thickness parameter α, variable viscosity θ_r and Hartmann number Ha^2 decelerates the velocity.

- For large values of mixed convection parameter λ and Weissenberg number We^2, the velocity profile increases.

- It is clear that the wall thickness parameter α and Hartmann number Ha^2 decreases the velocity profile.

- For large values of Weissenberg number We^2 and temperature dependent viscosity ζ, the velocity profile decreases.

- Due to increase in variable viscosity ζ and fluid relaxation parameter λ_m, the velocity profile enhances.

- Velocity profiles reduces for $\lambda_1 = Ha^2 = 0.1,\ 0.3,\ 0.5$, and $\lambda_m = 0.1,\ 0.4,\ 0.6$.

- An intensification in the Hartmann number Ha^2, porosity parameter λ and inertia factor F_c is noticed.

- Temperature profile reduces by increasing thermal stratification (St) and Prandtl number (Pr).

- High temperature is obtained for large values of thermophoretic parameter (N_t) and Brownian motion (N_b).

- For numerous values of thermal buoyance parameter (δ_c) and Prandtl number (Pr), the temperature distribution reduces.

- By using generalized Fourier's law, favorable decrease in temperature profile is observed.

- For numerous values of Prandtl number (Pr) and relaxation parameter (δ_t) temperature profile reduces.

- The influence of variable thermal conductivity (ε) increases causes by increase in temperature profile.

- By using classical Fourier's law, significant reduction in temperature profile is observed.

- Temperature profile increases by increasing the values of Eckert number Ec, radiation parameter R, Brownian motion N_b, thermal conductivity parameter ε and thermophoresis parameter N_t.

- Large values of Lewis number (Le) and solutal stratification (Sc) causes decay in concentration.

- Higher values of chemical reactive species (K), concentration buoyancy parameter (δ_c) and Lewis number (Le) causes decay in concentration.

- Using generalized Fick's law, reduction in concentration profile is noticed.

- Concentration profiles reduce for increasing values of chemical reactive species K and Lewis number Le.

- Concentration profile shows favorable reduction due to rise in Lewis number Le, chemical reaction K and activation energy Ea.

- For increasing values of chemical reaction K, Prandtl number Pr, thermal relaxation parameter δ_t, concentration relaxation parameter δ_c and Lewis number Le reduces the concentration and temperature profiles.

- The local friction coefficient $\left(C_f \ \mathrm{Re}_x^{\frac{1}{2}} \right)$ increases for large values of Hartmann number (Ha^2).

- Wall friction factor coefficient increases for large values of Hartmann number Ha^2.

- Skin friction coefficient enhances for large values of Ha^2.

- Reduction in friction factor is noticed for enhancing values of slip parameter λ.

- Skin friction coefficient $C_f \, \mathrm{Re}_x^{\frac{1}{2}}$ reduces for large values of slip parameter λ_1 but opposing behavior is noticed for fluid relaxation parameter λ_m.

- For large values of Prandtl number Pr the heat transport rate reduces.

- For large values of variable viscosity parameter ζ and Eckert number Ec the friction factor and heat transfer rate reduces. But the opposite behavior is noticed in mass transfer rate.

- Heat transfer rate rises by increasing the values of Eckert number Ec.

140

Bibliography

[1] P.J. Carreau, Rheological equations for molecular network theories, Transactions of the Society of Rheology, 16(1972)99-127.

[2] M.B. Bush and N. Phan-Thien, Drag force on a sphere in creeping motion through a Carreau model fluid, Journal of Non-Newtonian Fluid Mechanics, 16(1984)301-313.

[3] Chhapra and Uhlherr, Creeping motion of spheres through shear-thinning elastic fluids described by the Carreau viscosity equation, Rheologica Acta, 19(1980)187-195.

[4] K. Vajravelu, S. Sreenadh and R. Saravana, Combined influence of velocity slip, temperature and concentration jump conditions on MHD peristaltic transport of a Carreau fluid in a non-uniform channel, Applied Mathematics and Computation, 225(2013)656-676.

[5] N.S. Akbar and S. Nadeem, Carreau fluid model for blood flow through a tapered artery with a stenosis, Engineering Physics and Mathematics, 5(2014)1307-1316.

[6] S. Tabakova, S. Kutev and S. Radev, Application of the Carreau viscosity model to the oscillatory flow in blood vessels, AIP Conference Proceedings, (2015). doi.org/10.1063/1.4936726.

[7] T. Hayat, S. Qayyum, M. Waqas and B. Ahmed, Influence of thermal radiation and chemical reaction in mixed convection stagnation point flow of Carreau fluid, Results in Physics, 7(2017)4058-4064.

[8] M. Khan, A. Hussain, M.Y. Malik and T. Salahuddin, Biconvection flow of Carreau fluid over an upper paraboloid surface: A computational study, Results in Physics, 7(2017)4050-4057.

[9] S.T. Chaffin and J.M. Rees, Carreau fluid in wall driven corner flow, Journal of non-Newtonian Fluid Mechanics, 253(2018)16-26.

[10] Hashim, M. Khan, N.U. Kuda and A. Hamid, Non-linear radiative heat transfer analysis during the flow of Carreau nanofluid due to wedge-geometry: A revised model, International Journal of Heat and Mass Transfer, 131(2019)1022-1031.

[11] K. Yasuda, Investigation of the analogies between the viscometric and linear viscoelastic properties of polystyrene fluid. Ph.D, Massachusette Institutes of Technology, Department of chemical engineering, Boston, (1979).

[12] J. Boyd and J.M. Buick, Analysis of the Casson and Carreau-Yasuda non-Newtonian blood models in steady and oscillatory flows using the lattice Boltzmann method. Phyiscs of Fluid, 19(2007) 093103.

[13] A. Shamekhi and K. Sadeghy, Cavity flow simulation of Carreau–Yasuda non-Newtonian fluids using PIM meshfree method, Applied Mathematical Modelling, 33(2009)4131-4145.

[14] T. Hayat, F.H. Abbasi, B. Ahmad and A. Alsaedi, Peristaltic transport of Carreau-Yasuda fluid in a curved channel with slip effects, PLOSE ONE, 9(4)(2014)e95070.

[15] Z. Alloui and P. Vasseur, Natural convection of Carreau–Yasuda non-Newtonian fluids in a vertical cavity heated from the sides, International Journal of Heat and Mass Transfer, 84(2015)912-924.

[16] K. Khechiba, M. Mamou, M. Hachemi , N. Delenda, and R. Rebhi, Effect of Carreau-Yasuda rheological parameters on subcritical Lapwood convection in horizontal porous cavity saturated by shear-thinning fluid, Physics of Fluids, 29(2017)063101.

[17] T. Salauddin, M.Y. Malik, A. Hussain, S. Bilal, M. Awais and I. Khan, MHD squeezed flow of Carreau-Yasuda fluid over a sensor surface, Alexandria Engineering Journal, 56(2017)27-34.

[18] A. Tanveer, T. Hayat, A. Alsaedi and B. Ahmad, Numerical simulation for peristalsis of Carreau-Yasuda nanofluid in curved channel with mixed convection and porous space, PLOSE ONE, 12(2)(2017)e0170029.

[19] M. Khan, A. Shahid, M.Y. Malik and T. Salahuddin, Chemical reaction for Carreau-Yasuda nanofluid flow past a nonlinear stretching sheet considering Joule heating, Results in Physics, 8(2017)1124-1130.

[20] G.R. Kefayati and H. Tang, Three-dimensional Lattice Boltzmann simulation on thermosolutal convection and entropy generation of Carreau-Yasuda fluids, International Journal of Heat and Mass Transfer, 131(2019)346-364.

[21] R.V. Williamson, The flow of pseudoplastic materials, Industrial and Engineering Chemistry Research, 21(1929)1108-1111.

[22] D.V. Lyubimov and A.V. Perminov, Motion of a thin oblique layer of a pseudoplastic fluid, Journal of Engineering Physics and Thermophysics, 75 (200)920-924.

[23] S. Nadeem, T. Hussain and Changhoon Lee, Flow of a Williamson fluid over a stretching sheet, Brazilian Journal of Chemical Engineering, 30(2013)619-625.

[24] M. Kothandapani and J. Prakash, Effects of thermal radiation parameter and magnetic field on the peristaltic motion of Williamson nanofluids in a tapered asymmetric channel, International Journal of Heat and Mass Transfer, 81(2015)234-2245.

[25] P. Prakash and D. Tripathi, Electroosmotic flow of Williamson ionic nanoliquids in a tapered microfluidic channel in presence of thermal radiation and peristalsis, Journal of Molecular Liquids, 256(2018)352-371.

[26] M. Khan, T. Salahuddin, M.Y. Malik and F. O. Mallawi, Change in viscosity of Williamson nanofluid flow due to thermal and solutal stratification, International Journal of Heat and Mass Transfer, 126(2018)941-948.

[27] T.P. Lyubimova, A.V. Perminov and M.G. Kazimardanov, Stability of quasi-equilibrium states and supercritical regimes of thermal vibrational convection of a Williamson fluid in zero gravity conditions, International Journal of Heat and Mass Transfer, 129(2019)406-414.

[28] M.I. Khan, S. Qayyum, T. Hayat, M.I. Khan and A. Alsaedi, Entropy optimization in flow of Williamson nanofluid in the presence of chemical reaction and Joule heating, International Journal of Heat and Mass Transfer, 133(2019)959-967.

[29] W.M. Christopher, Rheology: Principles, Measurements and Applications, Wiley-VCH Publisher, Weinheim, (1993).

[30] K. S. Adegbie, A.J. Omowaye, A.B. Disu and I.L. Animasaun, Heat and mass transfer of upper convected Maxwell fluid flow with variable thermo-physical properties over a horizontal melting surface, Applied Mathematics, 6(2015)1362-1379.

[31] Y. Mahsud, N. Ali Shah and D. Vieru, Influence of time-fractional derivatives on the boundary layer flow of Maxwell fluids, Chinese Journal of Physics, 55(2017)1340-1351.

[32] L. Liu and F. Liu, Boundary layer flow of fractional Maxwell fluid over a stretching sheet with variable thickness, Applied Mathematics Letters, 79(2018)92-99.

[33] P. Poungthong, A.J. Giacomin, C. Saengow and C. Kolitawong, Exact solution for intrinsic nonlinearity in oscillatory shear from the corotational Maxwell fluid, Journal of Non-Newtonian Fluid Mechanics, 265(2019)53-65.

[34] M. Khan, T. Salahuddin, A. Tanveer, M.Y. Malik and A. Hussain, Change in internal energy of thermal diffusion stagnation point Maxwell nanofluid flow along with solar radiation and thermal conductivity, Chinese Journal of Chemical Engineering, (2019) doi.org/10.1016/j.cjche.2018.12.023.

[35] D.Y. Na, B.H.V. Borges and F.L. Teixeira, Finite element time-domain body-of-revolution Maxwell solver based on discrete exterior calculus, Journal of Computational Physics, 376(2019)249-275.

[36] J.B.J. Fourier, Theorie analytique de la chaleur, Paris: Chez Firmin Didot, Pere et Fils, (1822).

[37] C. Cattaneo, Sulla Conduzionedelcalore, Atti del Seminario Matematico e Fisico dell' Universita di Modena e Reggio Emilia, 3(1948)83-101.

[38] C.I. Christov, On frame in different formulation of the Maxwell-Cattaneo model of finite speed heat conduction, Mechanics Research Communications, 36(2009)481-486.

[39] M. Khan, A. Shahid, M.Y. Malik and T. Salahuddin, Thermal and concentration diffusion in Jeffery nanofluid flow over an inclined stretching sheet: A generalized Fourier's and Fick's perspective, Journal of Molecular Liquids, 251(258)7-14.

[40] W. Ibrahim, Three dimensional rotating flow of Powell-Eyring nanofluid with non-Fourier's heat flux and non-Fick's mass flux theory, Results and Physics, 8(2018)569-577.

[41] M. Khan, T. Salahuddin and M.Y. Malik, An immediate change in viscosity of Carreau nanofluid due to double stratified medium: Application of Fourier's and Fick's Laws, Journal of the Brazilian Society of Mechanical Sciences and Engineering 40(9)(2018)457.

[42] Choi SUS. Enhancing thermal conductivity of fluids with nanoparticles. In: Proceedings of the ASME international mechanical engineering congress and exposition, San Francisco, Calif, USA, 66(1995)99-105.

[43] H. Masuda, A. Ebata, K. Teramae and N. Hishinuma, Alteration of thermal conductivity and viscosity of liquid by dispersing ultra-fine particles, Netsu Bussei, 7(1993)227-233.

[44] Y. Bai, X. Liu, Y. Zhang and M. Zhang, Stagnation-point heat and mass transfer of MHD Maxwell nanofluids over a stretching surface in the presence of thermophoresis, Journal of Molecular Liquids, 224(2016)1172-1180.

[45] M.K. Nayak, MHD 3D flow and heat transfer analysis of nanofluid by shrinking surface inspired by thermal radiation and viscous dissipation, International Journal of Mechanical Sciences, 124-125(2017)185-193.

[46] M. Shen, S. Chen, F. Liu, Unsteady MHD flow and heat transfer of fractional Maxwell viscoelastic nanofluid with Cattaneo heat flux and different particle shapes, Chinese Journal of Physics, 56(2018)119-121.

[47] Q. Li, J. Wang, J. Wang, J. Baleta, C. Min and B.Sundén, Effects of gravity and variable thermal properties on nanofluid convective heat transfer using connected and unconnected walls, Energy Conversion and Management, 171(2018)1440-1448.

[48] A.R. Bestman, Natural convection boundary layer with suction and masstransfer in a porous medium, International Journal of Energy Research, 14(1990)389-396.

[49] F.G. Awad, S. Motsa and M. Khumalo, Heat and mass transfer in unsteady rotating fluid flow with binary chemical reaction and activation energy, PLOS ONE, PLoS ONE 9(9)(2014)e107622.

[50] K.L. Hsiao, To promote radiation electrical MHD activation energy thermal extrusion manufacturing system efficiency by using Carreau-Nanofluid with parameters control method, energy, 130(2017)486-499.

[51] A. Hamid, Hashim and M. Khan, Impacts of binary chemical reaction with activation energy on unsteady flow of magneto-Williamson nanofluid, Journal of Molecular Liquids, 262(2018)435-442.

[52] K. Hiemenz, Die Grenzschicht an einem in den gleichförmingen Flussigkeitsstrom eingetauchten geraden Kreiszylinder, Dinglers Polytechn Journal, 326(1911)321-410.

[53] F. Homann, Der Einfluss grosser Zähigkeit bei der Strömung um den Zylinder und um die Kugel Zeitschrift fur angewandte, Mathematik und Mechanik, 16(1936)153-164.

[54] T.R. Mahapatra and A.S. Gupta, Heat transfer in stagnation point flow toward a stretching sheet, Heat and Mass Transfer, 38(2002)517-521.

[55] J.H. Merkin and I. Pop, Stagnation point flow past a stretching/shrinking sheet driven by Arrhenius kinetics, Applied Mathematics and Computation, 337(2018)583-590

[56] T.R. Mahapatra and S. Sidui Unsteady heat transfer in non-axisymmetric Homann stagnation-point flows towards a stretching /shrinking sheet, European Journal of Mechanics-B/Fluids, (2018)doi.org/10.1016/j.euromechflu.2018.10.001.

[57] M.R. Turner and P.D. Weidman, Impinging Howarth stagnation-point flows, European Journal of Mechanics-B/Fluids, 74(2019)241-251.

[58] M.W. Anyakoha, New School Physics. 3rd Edition, Africana First Publisher, Enugu, (2010)36-51.

[59] S. Xun, J. Zhao, L. Zheng and X. Zhang, Bioconvection in rotating system immersed in nanofluid with temperature dependent viscosity and thermal conductivity, International Journal of Heat and Mass Transfer, 111(2017)1001-1006.

[60] T. Hayat, M.I. Khan, M. Farooq, N. Gull and A. Alsaedi, Unsteady three-dimensional mixed convection flow with variable viscosity and thermal conductivity, Journal of Molecular Liquids, 223(2016)1297-1310.

[61] M. Kameyama and M. Yamamoto, Numerical experiments on thermal convection of highly compressible fluids with variable viscosity and thermal conductivity: Implications for mantle convection of super-Earths, Physics of The Earth and Planetary Interiors, 274(2018)23-36.

[62] F. Sedaghat and F. Yousefi, Synthesizes, characterization, measurements and modeling thermal conductivity and viscosity of graphene quantum dots nanofluids, Journal of Molecular Liquids, 278(2019)200-308.

[63] Sunil, S. Choudhary and A. Mahajan, Stability analysis of a couple-stress fluid saturating a porous medium with temperature and pressure dependent viscosity using a thermal non-equilibrium model, Applied Mathematics and Computation, 340(2019)15-30.

[64] T. Robert and Lackey, A technique for eliminating for thermal stratification in Lake, Journal of the American Water Association, 8(1972)46-49.

[65] N.F.H.M. Sohut, A.M.A. Aziz and Z.M. Ali, Double stratification effects on boundary layer over a stretching cylinder with chemical reaction and heat generation, Journal of Physics: Conference Series, 890(2017)012019.

[66] Y.S. Daniel, Z.A. Aziz, Z. Ismail and F. Salah, Thermal stratification effects on MHD radiative flow of nanofluid over nonlinear stretching sheet with variable thicknes, Journal of Computational Design and Engineering, 5(2018)232-242.

[67] R. Kandasamy, R. Dharmalingam and K.K.S. Prabhu, Thermal and solutal stratification on MHD nanofluid flow over a porous vertical plate, Alexandria Engineering Journal, 57(2018)121-130.

147

[68] M. Khan, M.Y. Malik, T. Salahuddin and A. Hussian, Heat and mass transfer of Williamson nanofluid flow yield by an inclined Lorentz force over a nonlinear stretching sheet, Results in Physics, 8(2018)862-868.

[69] P. Rana, N. Shukla, Y. Gupta and I. Pop, Analytical prediction of multiple solutions for MHD Jeffery–Hamel flow and heat transfer utilizing KKL nanofluid mode, Physics Letters A, 383(2019)176-185.

[70] M. Sheikholeslami, New computational approach for exergy and entropy analysis of nanofluid under the impact of Lorentz force through a porous media, Computer Methods in Applied Mechanics and Engineering, 334(2019)319-333.

[71] S.Z. Alamri, A.A. Khan, M. Azeez and R. Ellahi, Effects of mass transfer on MHD second grade fluid towards stretching cylinder: A novel perspective of Cattaneo–Christov heat flux model, Physics Letters A, 383(2019)276-281.

[72] S.R. Hosseini, M. Ghasemian, M. Sheikholeslami, A. Shafee and Z. Li, Entropy analysis of nanofluid convection in a heated porous microchannel under MHD field considering solid heat generation, Powder Technology, 344(2019)914-925.

[73] M.K. Nayak, MHD 3D flow and heat transfer analysis of nanofluid by shrinking surface the inspired by thermal radiation and viscous dissipation, international Journal of Mechanical Sciences, 124-125(2017)185-193.

[74] A.K. Pandey and M. Kumar, Chemical reaction and thermal radiation effects on boundary layer flow of nanofluid over a wedge with viscous and Ohmic dissipation, St. Petersburg Polytechnical University Journal: Physics and Mathematics, 3(2017)322-332.

[75] S.P.A. Devi and D.V. kumara, Thermal radiation, viscous dissipation, ohmic dissipation and mass transfer effects on unsteady hydromagnetic flow over a stretching surface, Engineering Physics and Mathematics, 9(2018)1168-1163.

[76] K.G. Kumra, G.K. Ramesh, B.J. Gireesha and R.S.R. Gorla, Characteristics of Joule heating and viscous dissipation on three-dimensional flow of Oldroyd B nanofluid with thermal radiation, Alexandria Engineering Journal, 57(2018)2139-2140.

[77] T. Salahuddinn, M.Y. Malik, A. Hussain, S. Bilal, M. Awais, MHD flow Cattaneo-Christov heat flulx model for Williamson fluid over a stretching sheet with variable thickness: Using numerical approach, Journal of Magnetism and Magnetic Materials, 401(2016)991-997.

[78] T.M. Ajayi, A.J. Omowaye and I.L. Animasaun, Effects of viscous dissipation and double stratification on MHD Casson fluid flow over a surface with variable thickness: boundary Layer analysis, International Journal of Engineering Research in Africa, 28(2017)73-89.

[79] T. M. Ajayi, A.J. Omowaye and I. L. Animasaun, Viscous dissipationeEffects on the motion of Casson fluid over an upper horizontal thermally stratified melting surface of a paraboloid of revolution: boundary layer analysis, Journal of Applied Mathematics, doi.org/10.1155/2017/1697135.

[80] N. Acharyaa, K. Das and P.K. Kundua, Cattaneo–Christov intensity of magnetised upper-convected Maxwell nanofluid flow over an inclined stretching sheet: A generalised Fourier and Fick's perspective, International Journal of Mechanical Sciences, 130(2017)167-173.

[81] W.A. Khan and I. Pop, Boundary layer flow of a nanofluid past a stretching sheet, International Journal of Heat and Mass Transfer, 53(2010)2477-2483.

[82] R.H.S. Winterton, Early study of heat transfer: Newton and Fourier, Heat Transfer Engineering, 22(2001)3-11.

[83] Fang and H. Tao, Unsteady viscous flow over a rotating stretchable disk with deceleration, Communications in Nonlinear Science and Numerical Simulation, 17(2012)5064-5072.

[84] H. .T. Lin, L.K. Lin, Heat transfer from a rotating cone or disk to fluids of any Prandtl number, International Communications in Heat and Mass Transfer, 14(1987)323-332.

[85] Y.S. Daniel, Z.A. Aziz, Z. Ismail and Faisal Salah, Effects of thermal radiation, viscous and Joule heating on electrical MHD nanofluid with double stratification, Chinese Journal of Physics, 55(217)630-651.

[86] M. Khan, M.Y. Malik and T. Salahuddin, Heat generation and solar radiation effects on Carreau nanofluid over a stretching sheet with variable thickness: Using coefficients improved by Cash and Carp, Results in Physics, 7(2017)2512-2519.

149

sources:

1   1% match (Internet from 03-Jan-2015)
http://www.ebiblewords.com/05_English_Word_Concordances/BOOKCON3L__con.txt

2   1% match (student papers from 28-Sep-2018)
Submitted to Universiti Putra Malaysia on 2018-09-28

3   1% match (student papers from 07-Feb-2020)
Submitted to University of Venda on 2020-02-07

4   1% match (student papers from 01-Oct-2019)
Submitted to Higher Education Commission Pakistan on 2019-10-01

5   1% match (student papers from 24-Jun-2019)
Submitted to Higher Education Commission Pakistan on 2019-06-24

6   1% match (publications)
M. Wahiduzzaman, Md. Shakhaoath Khan, P. Biswas, Ifsana Karim, M. S. Uddin. "Viscous Dissipation and Radiation Effects on MHD Boundary Layer Flow of a Nanofluid Past a Rotating Stretching Sheet", Applied Mathematics, 2015

7   1% match (student papers from 24-Jan-2017)
Submitted to Jawaharlal Nehru Technological University on 2017-01-24

8   < 1% match (student papers from 05-Mar-2019)
Submitted to Higher Education Commission Pakistan on 2019-03-05

9